AWARD NUMBER: W81XWH-10-1-0864

TITLE: A Clinically Realistic Large Animal Model of Intra-Articular Fracture

PRINCIPAL INVESTIGATOR: Jessica E. Goetz, PhD

CONTRACTING ORGANIZATION: The University of Iowa
Iowa City, IA 52242

REPORT DATE: December 2014

TYPE OF REPORT: Final

PREPARED FOR: U.S. Army Medical Research and Materiel Command
Fort Detrick, Maryland 21702-5012

DISTRIBUTION STATEMENT: Approved for Public Release;
Distribution Unlimited

REPORT DOCUMENTATION PAGE

Form Approved
OMB No. 0704-0188

1. REPORT DATE
December 2014

2. REPORT TYPE
Final

3. DATES COVERED
15 Sept 2010-14 Sept 2014

4. TITLE AND SUBTITLE
A Clinically Realistic Large Animal Model of Intra-Articular Fracture

5a. CONTRACT NUMBER

5b. GRANT NUMBER
W81XWH-10-1-0864

5c. PROGRAM ELEMENT NUMBER

6. AUTHOR(S)
Jessica E. Goetz, PhD

E-Mail: jessica-goetz@uiowa.edu

5d. PROJECT NUMBER

5e. TASK NUMBER

5f. WORK UNIT NUMBER

7. PERFORMING ORGANIZATION NAME(S) AND ADDRESS(ES)

University of Iowa
Iowa City, Iowa 52242-1100

8. PERFORMING ORGANIZATION REPORT NUMBER

9. SPONSORING / MONITORING AGENCY NAME(S) AND ADDRESS(ES)

U.S. Army Medical Research and Materiel Command
Fort Detrick, Maryland 21702-5012

10. SPONSOR/MONITOR'S ACRONYM(S)

11. SPONSOR/MONITOR'S REPORT NUMBER(S)

12. DISTRIBUTION / AVAILABILITY STATEMENT

Approved for Public Release; Distribution Unlimited

13. SUPPLEMENTARY NOTES

14. ABSTRACT
The primary objective of this project is to develop a novel large animal survival model of intra-articular fracture (IAF) in which all major pathophysiological attributes corresponding to human injuries are realistically replicated, and in which post-traumatic osteoarthritis (PTOA) predictably develops. This final report summarizes all project activities. Initial work included development of hardware to reliably induce a highly repeatable fracture of the Yucatan minipig hock and development of a definitive post-operative treatment protocol. These methods were used in a series of 22 animals to document the natural history of the fractured and repaired joint over a 12 week survival period, focusing on limb loading, joint inflammatory response, bone healing, and cartilage degeneration. After the natural history was established, a short-term study was performed for the purpose of demonstrating that a promising biological treatment could be meaningfully investigated in this new model. In that work an antioxidant/anti-inflammatory cocktail was given immediately after fracture and 24 hours later. Specific measures of whole joint and chondrocyte health were made using direct biological measures and histology. Over the course of this project, the model was fully developed, the natural history (including joint degeneration) was documented, and the model was shown to be an appropriate vehicle for investigation of promising treatments to prevent PTOA.

15. SUBJECT TERMS
post-traumatic osteoarthritis, joint injuries, intra-articular fracture, survival animal model, cartilage degeneration, oxidative stress, inflammation

16. SECURITY CLASSIFICATION OF:			17. LIMITATION OF ABSTRACT	18. NUMBER OF PAGES	19a. NAME OF RESPONSIBLE PERSON
a. REPORT	b. ABSTRACT	c. THIS PAGE			USAMRMC
U	U	U	UU	76	19b. TELEPHONE NUMBER *(include area code)*

Standard Form 298 (Rev. 8-98)
Prescribed by ANSI Std. Z39.18

Table of Contents

Appendices (53 pages):

1. Tochigi Y, Buckwalter JA, Martin JA, Hillis SL, Zhang P, Vaseenon T, Lehman AD, Brown TD. *Distribution and progression of chondrocyte damage in a whole-organ model of human intra-articular fracture.* J Bone Joint Surg Am. 2011 Mar;93(6):533-9. PMID:21411703, PMC3052703.
2. Tochigi, Y; Zhang, P; Rudert, MJ; Baer, TE; Martin, JA; Hillis, SL; Brown, TD. *A novel impaction technique for modeling intra-articular fracture in large animal joints.* Osteoarthritis Cartilage 2013; 21(1): 200-8. PMID:23069855, PMC3538937.
3. Diestelmeier BW, Rudert MJ, Tochigi Y, Baer TE, Fredericks DC, Brown TD. *An instrumented pendulum system for measuring energy absorption during fracture insult to large animal joints in vivo.* J Biomech Eng. 2014 Jun;136(6):064502. PMID:24760051.
4. Goetz JE, Fredericks DC, Petersen E, Rudert MJ, Baer TE, Swanson E, Roberts NH, Martin JA, Tochigi Y. *A clinically realistic large animal model of intra-articular fracture that progresses to post-traumatic osteoarthritis.* Osteoarthritis Cartilage (In revision).
5. Coleman MC, Martin JA, Fredericks DC, Bergh MS, Goetz JE. *Intraarticular administration of n-acetylcysteine and glycyrrhizin alleviates acute oxidative stress following intraarticular fracture.* 2015 Annual Meeting of the Orthopaedic Research Society, March 25-31, 2015, Las Vegas NV. (submitted)

1. INTRODUCTION

The primary objective of this project was to develop a novel large animal survival model of intra-articular fracture (IAF) in which all major pathophysiological attributes of corresponding human clinical injuries were realistically replicated, and in which post-traumatic osteoarthritis (PTOA) predictably developed. Specifically, work was proposed to thoroughly validate a fracture insult technique/system developed for introducing pathophysiologically realistic IAFs in the porcine hock *in vivo* (Aim 1), to establish post-insult management methodology (Aim 2), and to validate the capability of the animal model as a research tool for piloting new treatment methods (Aim 3). Over the course of this project, we have established a definitive methodology to create a clinically realistic large animal survival model of IAF, and we have begun to demonstrate the value of the animal model as a powerful new translational research tool. It is our aim that this animal model will facilitate translational research of orthopaedic treatment for IAFs, specifically by providing opportunities to test efficacy and safety of new treatment strategies prior to clinical trial, thereby advancing orthopaedic treatment to mitigate the risk of PTOA following IAFs.

2. KEYWORDS

1. Post-traumatic osteoarthritis
2. Intra-articular fracture
3. Animal Model
4. Yucatan Minipig
5. Impact
6. Pendulum
7. Mankin Scoring
8. Inflammatory Cytokines
9. Gait Analysis
10. Incongruity

3. OVERALL PROJECT SUMMARY

3.1 Administrative & Personnel Changes

During Project Year 3, Dr. Yuki Tochigi, the principal investigator leading this project left the University of Iowa to return to his family in Japan. Dr. Jessica Goetz assumed the role of Principal Investigator on this project effective 8/1/2013. Dr. Todd McKinley also left the University of Iowa during Project Year 3 to pursue a new job in Indiana. As a result of these key departures, several project activities were delayed, and a one-year no-cost extension of the project was granted to complete the activities outlined in the SOW.

Over the course of the project, the following individuals were paid from this grant:

Full Name	Pay Period Begin Dt	Pay Period End Dt
Baer, Thomas E	09/01/2010	12/31/2013
Bogner, Ashley M	03/01/2013	12/31/2013
Bornmann, Samantha L	04/14/2013	05/24/2014
Brow n, Thomas D	09/01/2010	12/31/2013
Burnes, Tony T	05/01/2011	02/28/2013
Cannistraro,David	03/01/2012	03/31/2012
Diestelmeier,Bryce	01/01/2011	10/13/2012
Fredericks, Douglas C	09/01/2010	12/31/2013
Goetz, Jessica E	10/01/2010	08/31/2014
Kurriger, Gail L	07/01/2012	08/31/2014
Martin, James A	09/01/2010	12/31/2013
McKinley, Todd O	09/01/2010	01/31/2013
Roberts, Jacob T	01/06/2013	01/18/2014
Roberts, Nathaniel H	02/01/2013	07/31/2014
Rudert, Melvin J	09/01/2010	12/31/2013
Smith, Abigail D	05/01/2011	10/31/2013
Tochigi, Yuki	09/01/2010	03/31/2013

3.2 Summary of Task 1

As specified in the statement of work, Task 1 was to fine tune the techniques for impaction fracture insult and subsequent surgical fixation. This was the first step in addressing Specific Aims 1 & 2 of the project, which were to validate the fracture insult methodology (SA1) and to establish the post-insult management methodology (SA2). Task 1 was primarily hardware upgrades and ex-vivo experimentation of the pendulum.

3.2.a Device Upgrades

The primary hardware upgrade was to instrument the impaction pendulum device to enable accurate measurement of the energy that was consumed in the creation of the intra-articular fracture. As reported in the PY1 progress report, the pendulum was equipped with a rotary potentiometer at the fulcrum of the pendulum. This rotary potentiometer measures the angular velocity of the swing arm, permitting measurement of the kinetic energy of the pendulum head immediately before impaction. A system consisting of a minimum-friction sled on linear bearings, a stiff compression spring, and a linear potentiometer is mounted on the specimen anchorage system. In this "sled" system, the linear potentiometer transduces the linear position of the sled. With the linear displacement and spring constant being known, measurement of the energy required to stop the sled after impaction is enabled. The difference between the kinetic energy of the pendulum head and the energy required to stop the sled yields the energy that was absorbed during the creation of the fracture. A Matlab program was written to calculate the fracture energy from all of the pendulum geometric parameters and the energy measures.

3.2.b Device Validation

To validate this energy measurement instrumentation, an *ex-vivo* experiment was performed using polyurethane foam blocks as stand-ins for the pig hocks. Five impactions were performed at nine different drop angles (Figure 1). For each drop angle, the theoretical potential energy was compared with the experimentally measured kinetic energy. As reported in the progress report for PY1, the potential energy correlated very closely with the kinetic energy. This strong correlation indicated very little energy was lost to the pendulum system and validated the use of the rotary potentiometer data for pendulum head kinetic energy measurement.

A second validation experiment was performed in which similar impaction trials were repeated while varying both the magnitude of the pendulum potential energy and the sled mass. In these trials, the depth of polyurethane foam indentation after each impaction was measured to quantify energy absorption during impact. It was assumed that all damage to the polyurethane foam blocks

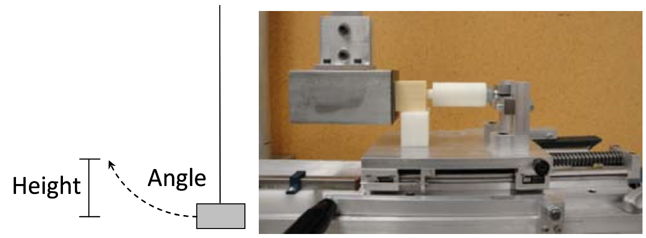

Figure 1: *Ex-vivo* surrogate model setup, which uses polyurethane foam blocks (white arrow) as stand-ins for the pig hocks.

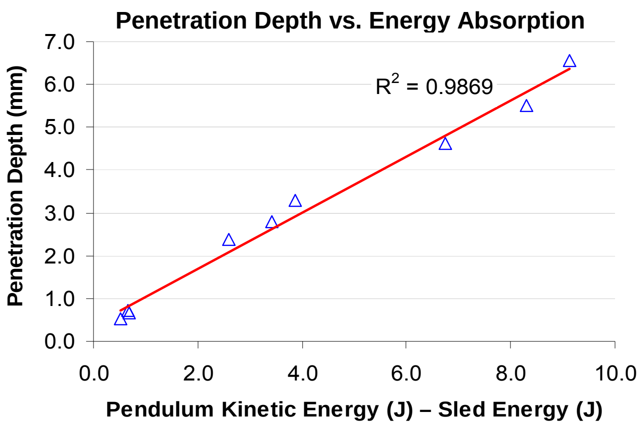

Figure 2: Relationship of the depth of polyurethane foam penetration vs. the energy absorption measure (difference between the pendulum kinetic energy and sled energy values).

occurred from the time the pendulum came in contact with the specimen until the time when the sled-spring was fully compressed. The relationship between penetration depth and the energy absorbed by the material demonstrated a highly linear correlation ($R^2 = 0.99$, Figure 2), validating this approach as a measure of energy absorption during the impaction fracture insult. This work was published in the Journal of Biomechanical Engineering in June 2014 (Appendix).

3.3 Summary of Task 2

Task 2 described in the statement of work was to establish the definitive impaction and treatment protocol in a series of survival animal experiments. The first group of animals in this work was a pilot series in which an articular fragment was created without impaction insult and surgical stabilization constructs were investigated. The second pilot series of animals in this task were subjected to the impaction insult and a fixation methodology based upon the pilot sham series. All data collection and analysis procedures were also piloted as a part of completing this task. These analysis methods will be discussed in detail as a part of Task 3.

3.3.a Fracture Insult Methodology

Under general anesthesia, each animal is subjected to a fracture insult of the left hock using a purpose-designed "offset" impaction technique (Figure 3).[1,2] First, the distal impact "tripod" is anchored to the talus through the calcaneus using three cortical pins. This device facilitates direct delivery of a fracture force pulse through the tibiotalar joint without energy loss associated with soft tissue absorption or compression of the subtalar joint. Next, a transverse stress-rising saw cut is placed across the anterior cortex of the tibia (leaving a 2 mm-thick zone of juxta-articular bone intact) to guide the location and orientation of fracture line. The distal tibial shaft of the experimental leg is secured to the pendulum impaction apparatus in a posteriorly tilted "offset" position (Figure 3). The fracturing force pulse is then delivered using a 5.8 kg pendulum mass released from a user-controlled height of 79 cm, which generates 45 joules of kinetic energy. The energy absorbed during the impaction insult (causing the fracture) is determined by measuring the difference between energy delivered (the pendulum's kinetic energy immediately before impaction) and energy passed through the specimen (energy transmitted to the sled-spring instrument to which the tibia holder is mounted).[1]

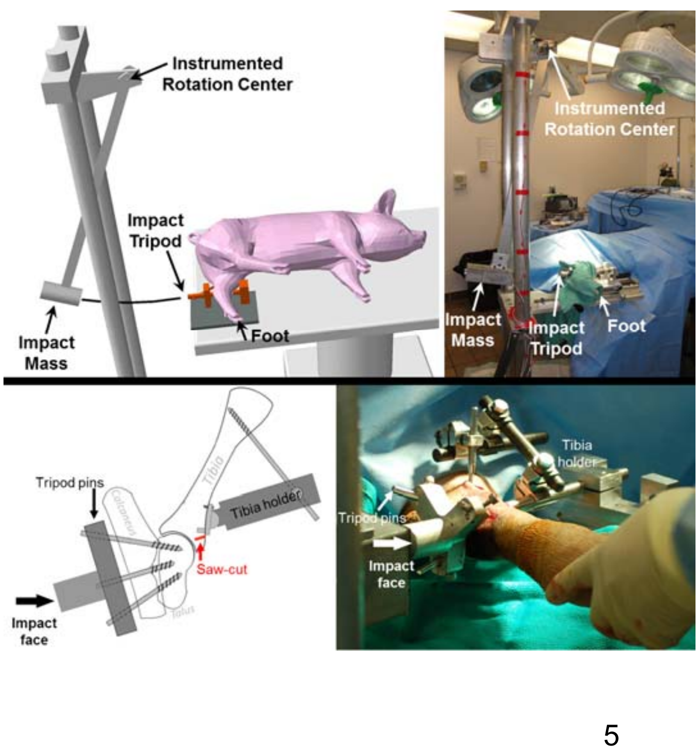

Figure 3. A schematic representation of the animal orientation during surgical impact (top left) illustrates the position of the animal beneath the drape during surgery (top right). A schematic of the tripod impaction device applied to the bones of the pig hock (lower left) and a corresponding intra-operative application of the tripod impaction device are shown (lower right). The impact mass of the pendulum swings down and contacts the impact face of the tripod, which passes the energy through the calcaneus to the talus via the tripod pins. The talus is driven into the anterior portion of the tibia causing an intra-articular fracture extending through the saw cut.

3.3.b Post-Insult Management

Immediately following the impact insult, the tripod and pendulum attachment hardware devices are removed and the experimental fractures are surgically stabilized. In the sham pilot series (no impact), the hocks were surgically treated by means of internal fixation using a standard-of-care buttress plating technique, followed by joint-spanning external fixation for post-operative load protection. For internal fixation, several types of veterinary fracture implants were tested, including the originally proposed low-profile (1.5-mm thick) mini T-plate and a bulkier locking plate (Veterinary Orthopedic Implants Inc., South Burlington, VT). The post-operative external fixation was performed using a system designed for human pediatric surgery (EBI® Dynafix® Small, Biomet Inc., Parsippany, NJ).

Post-operative external fixation times ranged from 1-3 weeks. During that period, animals managed modestly good three-legged load protective gait, however, all animals had loosening of external fixator pins, particularly at the distal (calcaneal, talar, or metatarsal) insertion sites. One of these animals had mild infection at the distal pin sites, but it did not lead to deep infection. After ex-fix removal, animals gradually started to use the experimental legs, and load protective gait patterns disappeared by the end of the study period (4 to 8 weeks post-surgery).

Based upon the knowledge gained from the non-impact sham series, a treatment protocol was selected for the second pilot series in this Task. As originally intended, the internal fixation technique chosen was very consistent with "standard-of-care" techniques for human clinical intraarticular fractures. The primary fixation implant was a clover-shaped locking plate designed for canine proximal tibial osteotomy (SYNTHES® Vet 2.7 mm TPLO plate, Synthes GmbH, Solothurn, Switzerland). This plate is placed on the anterior aspect of the distal tibial shaft using three bi-cortical screws, so as to provide a "buttress" effect for the anterior malleolar fragment. Through the central hole of the clover-shaped head, a distal locking screw is placed for fragment stabilization. To provide additional rotational stability, a combination of additional screws through the cloverleaf and/or an antero-medial screw outside of the clover plate may be added at the discretion of the surgeon. Rather than using the external fixator to stabilize the joint during the immediate healing phase, the repaired limb was provided supplemental external stabilization with a fiberglass cast.

The details of each of the four animals included in this pilot group are included in the PY1 progress report. Briefly, Animal #1 required 4 progressively stronger impacts, and Animal #4 required a second stronger impact to achieve a fracture. Animals #2 and #3 fractured on the first impact. Animal #4 was fixed with an intentional 2 mm step-off. Animal #1 suffered an accidental fall and had to be euthanized early. The remaining 3 animals survived the full 12-week study period with no complications.

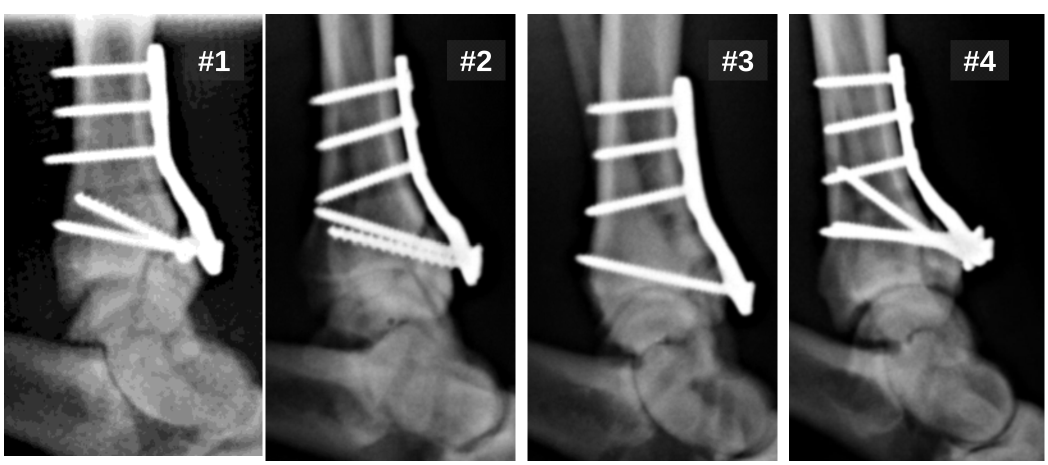

Figure 4. Sagittal radiographs of Animals #1 - #4 one day after surgery.

3.3.c Preliminary Results

Complete details of the analysis performed on the animals in this 12-week survival pilot series are included in the progress report for PY1. There was no radiographic evidence of fixation loosening or fragment subsidence over the 12 week period, and upon tissue harvest at the time of animal sacrifice, the fracture fragment had healed firmly. There was a spectrum of macroscopic cartilage damage, ranging from minimal pathologic changes in the joint with a single impact, anatomic reduction, and rigid fixation (Animal #2), to obvious cartilage erosion and discoloration in the joint with the 2 mm step-off (Animal #4). Based on limb loading analysis, the animals in this pilot series demonstrated substantial load protection for 1-2 weeks following the fracture and fixation surgery. After 4 weeks, limb loading appeared to return to near pre-operative levels.

3.4 Summary of Task 3

Task 3 in the statement of work was to document the natural course of the fractured joint. The purpose of this task was to expand upon the second pilot series in Task 2. Originally, this task was scheduled to be accomplished with 7 animals. With the additional animals that had been planned an not utilized for pilot work in Tasks 1 and 2, we were able to expand the number of animals in this series to 9 per group, and add a group with an intentional 2 mm step-off. To treat the step-off fracture, an extra T-plate on the medial side of the joint was utilized to provide additional stability. The fracture and treatment protocols used in these animals were the same as those established in Task 2, and the survival time was also 12 weeks. The outcome measures of interest were the same as those piloted in the Task 2 pilot group. This included plain radiographs of the fracture, pre- and post-operative CT scans of the joint, synovial fluid cytokine analysis, limb loading, and cartilage histology. Radiographs, synovial fluid draws, and limb loading data were collected pre-operatively, and post-operatively at 3 days, 1, 2, 4, 8, and 12 weeks.

An additional 18 animals were operated on for completion of Task 3. Including the 4 animals from the pilot series in Task 2, brings the total number of animals available to complete this task to 22. Four animals had to be sacrificed earlier than the 12 week time point due to fracture/dislocations. An additional 2 animals were excluded from analysis because the fixation hardware extended into the joint. The details of each animal used in this task are shown in Table 1. The animals in the May 2011 series are the pilot animals from Task 2.

Table 1. Details of the animals used in Tasks 2 & 3 to address Specific Aims 1 & 2 (Tasks 2 & 3). The number of impacts used to create the fracture and any complications are listed.

	Test	Reduction	Impact Count	Complication	Action/Outcome
May 2011 Series	1	Anatomical	4	Hip dislocation	Early Sacrifice (4 days post-op)
	2	Anatomical	1		
	3	Anatomical	1	Delayed union	
	4	Step-Off	2		
April 2012 Series	5	Anatomical	1	Screw exposure	
	6	Anatomical	2		
	7	Step-Off	1	Fracture dislocation	Early Sacrifice (2 weeks post-op)
	8	Anatomical	1		
	9	Step-Off	1	Spontaneous reduction	
	10	Anatomical	2		
	11	Step-Off	1	Fracture dislocation	Early Sacrifice (1 week post-op)
July 2012 Series	12	Step-Off	1		
	13	Anatomical	1		
	14	Step-Off	1		
	15	Step-Off	1		
	16	Step-Off	1		
	17	Anatomical	1	Screw exposure	
November 2012 Series	18	Step-Off	1	Infection + Talus Fracture	Early Sacrifice (8 weeks post-op)
	19	Anatomical	1		
	20	Step-Off	1		
	21	Anatomical	1		
	22	Anatomical	1		

3.4.a Fracture Morphology & Morphological Residuals

Fracture fixation stability and bone healing were monitored radiographically at 3 days and at 1, 2, 4, 8, and 12 weeks after index surgery. Stable fracture healing was achieved in all 18 animals at 12 weeks. The only complication related to healing was in experimental Animal #3, in which a delayed union was apparent on radiograph, specifically widening of the fracture gap (from week 2), which in turn resulted in decreasing density of the anterior malleolar fragment. However, when this experimental joint was dissected 12 weeks post-surgery, stable bone healing was apparent upon manual inspection. While there were three fracture dislocations in the early two series of experiments, this complication did not occur in the later series of animals, leading us to conclude that those early failures can be attributed to technique development.

3.4.a.1 Radiographic Evaluation: Radiographs were primarily used in this work to evaluate suitable progression of fracture healing. The fragment was seen to remain in its original immediate post-operative location (Figure 5), indicating the surgical fixation was adequate to maintain the initial reduction (anatomic or step-off) until bony union was achieved.

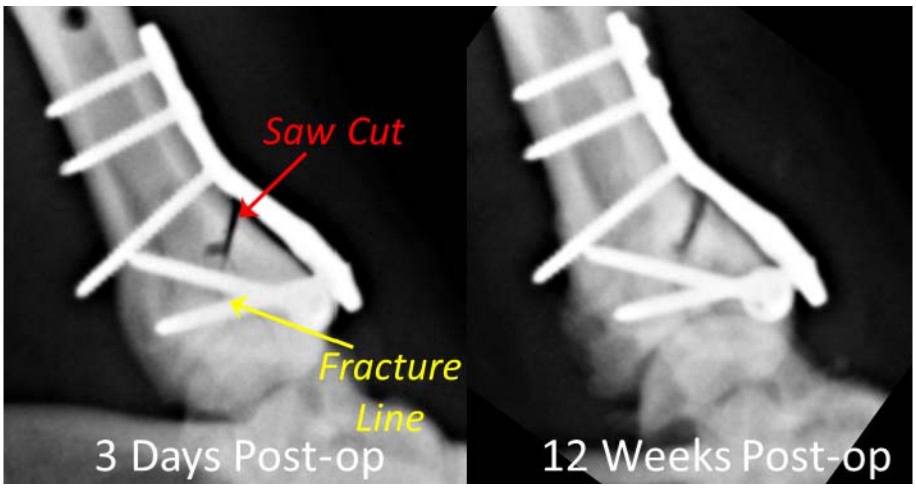

Figure 5. Radiographs of a fracture created in Series 4. The saw cut is clear and the fracture line closed early post-operatively (right). At the time of sacrifice, the fragment has healed in the proper location, with an indistinct fracture line and a less defined saw cut visible.

3.4.a.2 Evaluation of Joint Surface Incongruity: For every experimental joint, CT scans (0.3mm x 0.3mm x 1mm voxels) were acquired prior to fracture (baseline) and 12 weeks after index surgery. The outer cortex of the distal tibia was segmented manually and theses segmentations were smoothed into continuous 3D surfaces and registered to their respective pre-surgery surfaces using an iterative closest-point technique in Geomagic Studio software (Geomagic, Morrisville, NC, USA).

The maximum distance and the average distance between the intact and the registered fracture surfaces was calculated as a measure of joint surface incongruity. The percentage of the articular surface depressed more than 1, 2, 3, 4, and 5 millimeters was also quantified to determine the extent to which the entire joint surface was affected. As expected, animals that were intentionally reduced with a 2mm step-off had a greater amount of the total joint surface that was more depressed from the normal surface at the time of sacrifice (Figure 6). However, the maximum depth of depression seen in animals with an intentional step-off was not appreciably different from animals with an anatomic fracture reduction. This is likely a result of a small area of focal surface depression or non-mineralized repair tissue in the fracture line not demonstrating CT signal that was intense enough to be identified as bone.

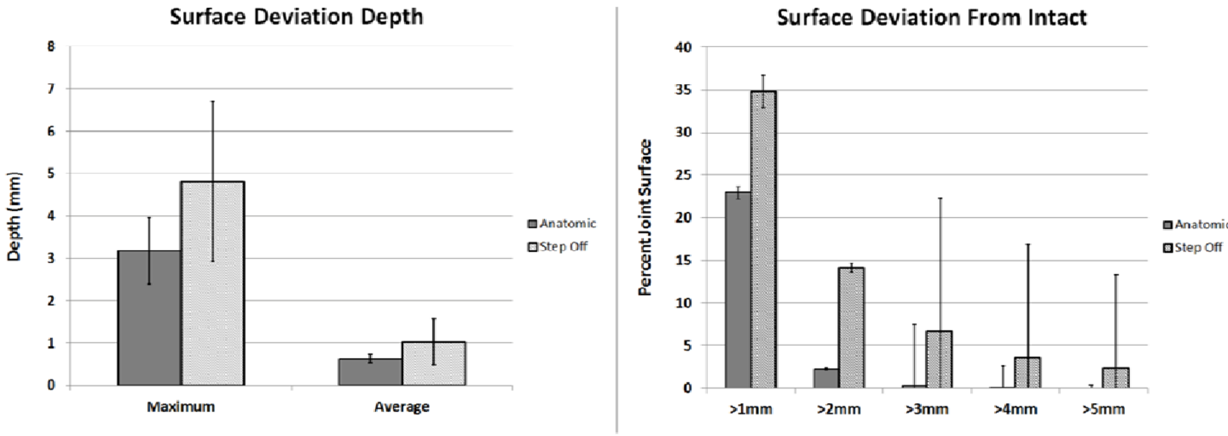

Figure 6. Both the maximum and the average surface depression were higher in animals that were fixed with a 2mm step-off. The step-off animals also demonstrated a much higher amount of total joint surface that was substantially depressed from the intact case, as indicated by the larger bars at the >3mm, >4mm, and >5mm conditions.

3.4.b Experimental Limb Usage

<u>3.4.b.1 Weightbearing Symmetry</u>: A pressure sensing walkway system (Tekscan Inc., North Boston, MA) was utilized to evaluate hind-leg usage during walking. Each animal underwent footprint contact stress measurement prior to the fracture insult (baseline), as well as at 1, 2, 4, 8, and 12 weeks after index surgery. Peak contact stress and vertical impulse was extracted for both the operated left hind-leg and the uninjured right hind-leg. All post-operative data were normalized to the pre-operative values.

The leg usage status in all 18 of the 12-week survival animals was characterized by significant load protection of the experimental leg at 1 and 2 weeks after surgery which recovered to near pre-operative levels at 4 weeks. The peak vertical force was significantly lower ($p<0.001$) at 1 and 2 weeks post-operatively, and recovered to pre-operative levels by 12 weeks post-operatively. The vertical force impulse demonstrated a similar trend with a significant decrease at the early post-operative time points which began to recover by 4 weeks postoperatively.

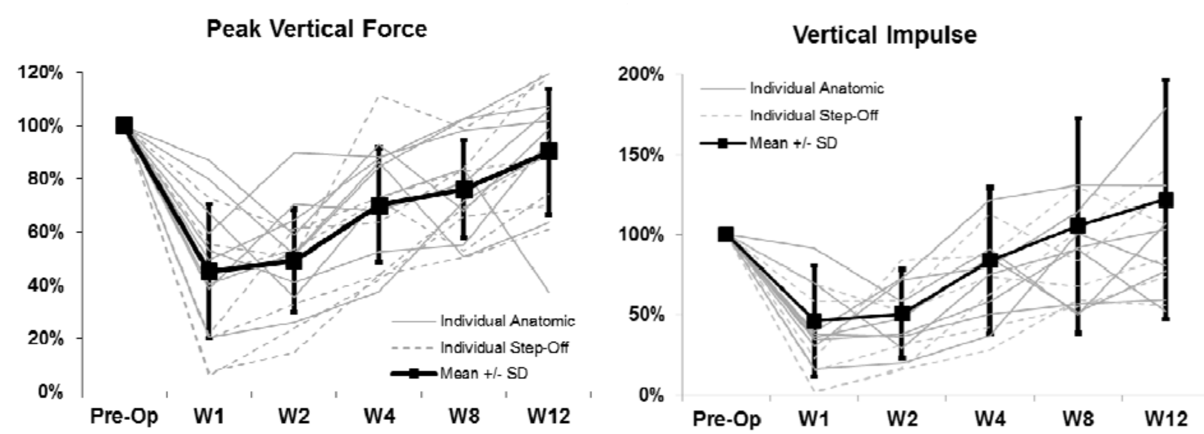

Figure 7. Hind-leg loading after experimental intra-articular fracture. Values are expressed relative to the individual animal's pre-operative levels.

3.4.b.2 Animal Activity Analysis: The overall activity of each animal was measured using a light-weight (48g) wireless accelerometer device developed for monitoring human limb activity (DigiTrac®, IM Systems, Inc. Baltimore, MD). This device reports tri-axial acceleration at the site to which the device is attached. The accelerometer was worn by each of the 12-week survival animals for 6 hours pre-op to establish a baseline activity level, and then again at 1, 2, 4, 8, and 12 weeks to track changes in animal activity. Video recordings were collected at the same time as the accelerometer data. Acceleration data indicated that most animals decreased their overall activity level in the early pre-operative time points, but recovered to higher activity levels by 12 weeks post-operatively (Figure 8). It was not possible to link specific animal activities such as individual steps to specific acceleration signals, therefore this analysis method was de-emphasized in favor of the quantitative Tekscan gait analysis.

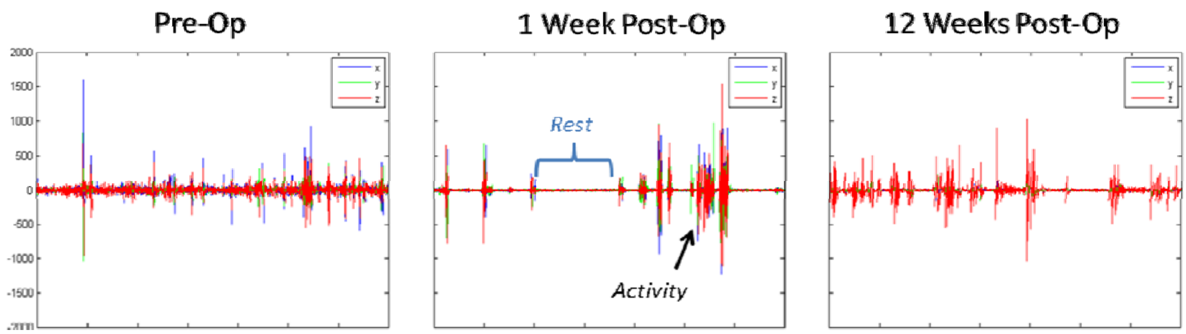

Figure 8. Accelerometer data collected from a single animal at three different time points. There was more activity during the pre-op data collection period than 1 week after intra-articular fracture. 12 weeks post-op, the activity levels were increased, but not yet returned to the pre-op values.

3.4.c Inflammatory Cytokine Response to Intra-articular Fracture

A porcine-specific multiplex cytokine array (Raybiotech, Norcross GA) was used to measure concentrations of ten cytokines (IL1β, IL4, IL6, IL8, IL10, IL12, GMCSF, INFγ, TNF and TGFβ) from the synovial fluid drawn from the fractured and surgically repaired hock and from the non-injured contralateral hock. Synovial fluid, being of a much smaller volume and in closest proximity to the joint injury would be expected to have the most dramatic fluctuations in cytokine concentrations after a joint injury. While blood was also harvested at the same time points as the synovial fluid, we elected to focus on the synovial fluid because it would be less confounded by systemic effects than the whole blood.

Interleukin 6 (IL6) and interleukin 8 (IL8) concentrations increased significantly (Figure 9) in the injured hock at the Day-3 and Week-1 time points ($p<0.001$ for both IL6 and IL8 at both time points). IL6 is an important factor for immune cell signaling during an acute inflammatory response and can function as either a pro- or as an anti-inflammatory factor. IL8 is a pro-inflammatory cytokine that promotes neutrophil chemotaxis and activation, thereby propagating an inflammatory response. Both IL6 and IL8 have been measured at significantly higher levels in synovial fluids of OA patients[3] and in patients with an acute ACL tear.[4] The similar increase in IL6 and IL8 levels in the mini-pig model indicate that there is an equivalent biological response (namely cytokine mediated inflammation) occurring in the acute post-fracture period. Increased levels of IL6 and IL8 have been attributed to an increased concentration of IL1β,[3] which we found to be elevated relative to the contralateral early after IAF. However, while there was a trend for IL1β to be elevated, that trend only reached statistical significance at one week.

The concentrations of the other cytokines measured were also not statistically significantly different from pre-operative values at any post-operative time points. However, these non-significant results did show trends toward injury-related increases in TGFβ, IL4, and TNF, and injury-related decreases in IL10. As IL1β and TNF are the primary cytokines that have been associated with cartilage catabolism in the development of OA, the slight increases in mini-pig synovial cytokine concentrations lend further support to a human-like biological response leading to PTOA occurring in the mini-pig hock after joint injury. Details about the analysis and a full table of all cytokine concentrations analyzed in this project are included in the full-length manuscript detailing the natural history of this model after an IAF (Appendix 2).

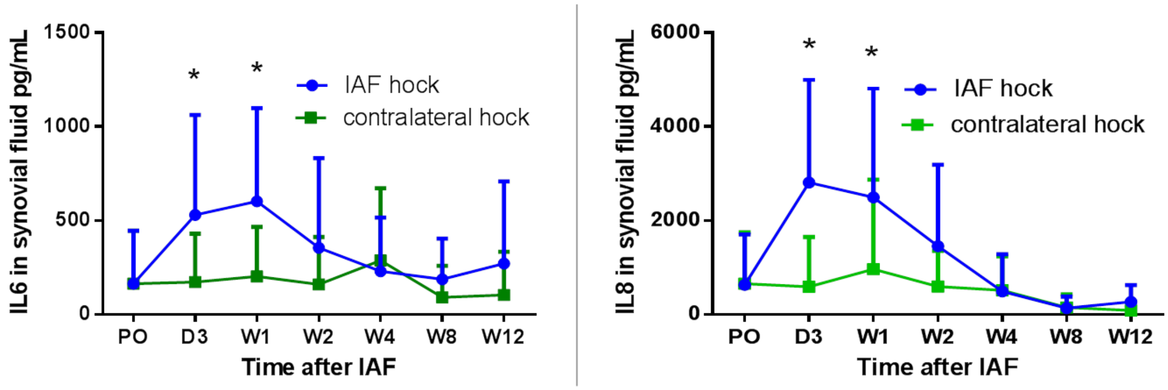

Figure 9. Variation in IL6 and IL8 concentrations with post-operative time. Both IL6 and IL8 concentrations increased significantly from pre-op values (PO) at 3 days (D3) and 1 week (W1) post-operatively. While the IL8 values returned to normal values at the end of the 12-week survival period, IL6 values remained slightly elevated. Asterisks indicate significant differences from baseline values at $p<0.05$.

3.4.d Histological Outcomes

At the end of testing period (12 weeks after index surgery), the experimental joints were dissected and prepared for histological evaluation of articular cartilage condition. The specimens were processed following the OARSI guidelines,[5] and sagittal sections from both the medial and lateral tibial and talar surfaces were stained with Safranin-O/Fast Green.

All sections were digitized using an Olympus VS110 digital histology system at a resolution of 383 nm/pixel (through the 20x objective). In order to facilitate analysis using an automated Mankin analysis[6] that is site and species specific, normal values of Yucatan minipig cartilage were obtained from the hock joints of 6 animals with no surgery to the hock. Zonal thickness was measured as a percentage of the total cartilage thickness at 4 locations along each joint surface and averaged. Zones were based primarily on chondrocyte organization. Flattened chondrocytes parallel to the articular surface defined the superficial zone, pairs of chondrocytes were characteristic of the transitional zone, organized chondrons were used to define the radial zone, and proteoglycan (PG) concentration plus paired or singular chondrocytes was used to identify the deep zone. After zonal definition, hand counts of the number of chondrocytes in each zone were obtained. These counts were converted to a zonal cell density value, and the standard deviation of cell density in each zone was used to define the range of normal cell density for each cartilage zone. These data were compared to the existing values for human, bovine, and rabbit carilage. It was found that zonal cell density in the minipig was most similar to that of a rabbit, and minipig cartilage was much more cellular than human or bovine cartilage (Figure 10).

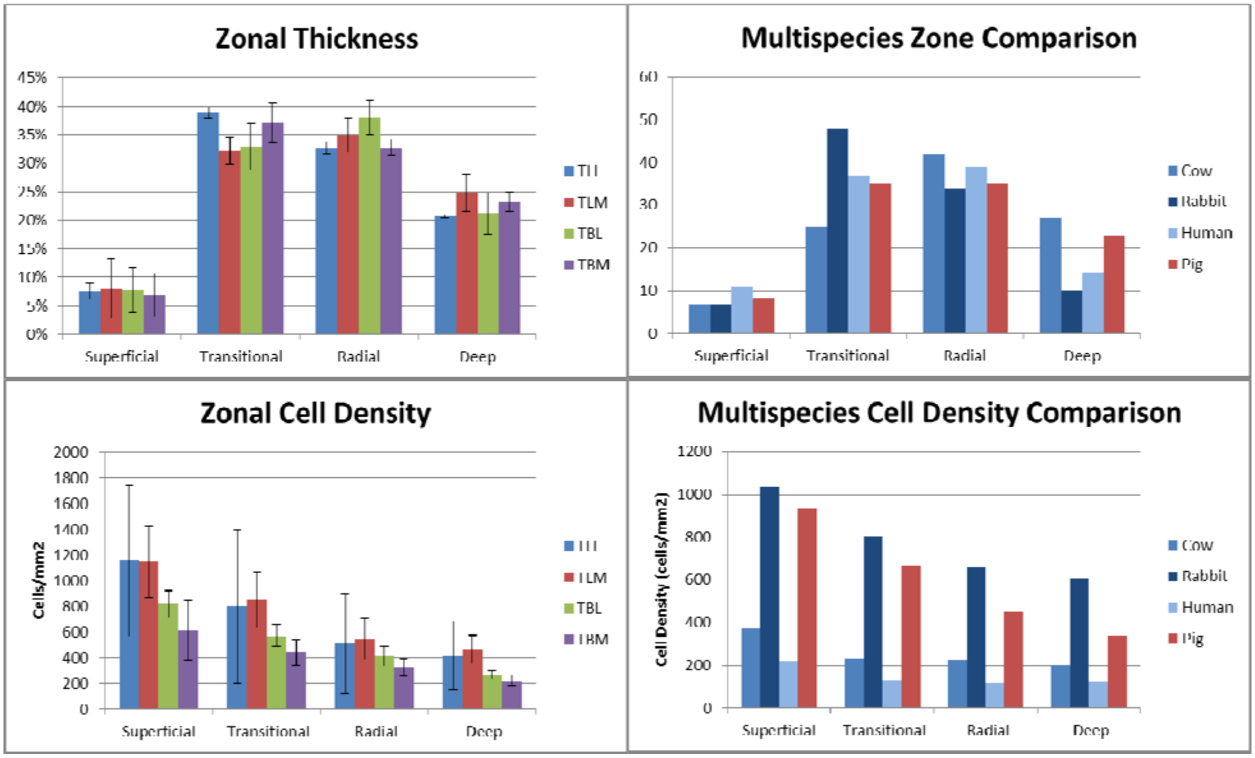

Figure 10. Normal Yucatan minipig histological cartilage data. The zonal thickness varies slightly with joint surface (top left), however the zonal definitions are very similar to other species (top right). As expected, the superficial zone cartilage had a higher cell density than the deeper zones (lower left), and the overall cell density was relatively high compared to humans (lower right).

These normative, site- and species-specific data were incorporated into the automated Mankin scoring program, which was then applied to all histological sections. In that program, Mankin scores are assigned every 0.5 mm to identify locations of focal cartilage damage. To obtain a single Mankin score for each joint surface, the scores were averaged.

Compared to normal cartilage, there were statistically significantly higher Mankin scores on both the medial and lateral talus in hocks that had sustained a fracture (Figure 11). As expected, the group of animals with an intentional step off on the tibial surface had more significant degeneration than the group that was anatomically reduced. Interestingly, the talar cartilage in the contralateral hocks had higher Mankin scores than the normal talar cartilage. This would imply that either the sequential synovial fluid draws over the course of the study, or the overloading of the contralateral that would have occurred soon after IAF while the pig load-protected its injured limb, was responsible for some slight cartilage degeneration.

Histological evaluation of the tibial surfaces (both medial and lateral) was complicated by the presence of the fracture line and the synovial fossa. The cartilage that grew into the gap between the fracture fragment and the remaining hock was poorly organized fibrocartilage that the Mankin score cannot adequately evaluate. The synovial fossa is a normal developmental feature in many quadruped joints, and while the cartilage in that area appears thin and low in PG content, it is not to be confused with OA.[7,8] When the average Mankin score was calculated for each tibial surface, the spans of tissue associated with the fracture line or the synovial fossa were not included. This left much more peripheral spans of cartilage that were away from the fracture line as tissue to be analyzed. Because the tissue included in the calculation of the average Mankin score was relatively remote to the zone of injury, it was not surprising to see that average Mankin scores were not statistically significantly higher than in normal tibial cartilage. However, there was still a clear trend of cartilage from the fractured joints appearing more degenerated in the fractured hocks than in the normal hocks, especially among those that were fixed with a 2-mm step-off. Again, the cartilage from the contralateral hocks had slightly higher Mankin scores than normal cartilage, indicating that the sequential synovial fluid draws and period of overloaded may have affected those joints.

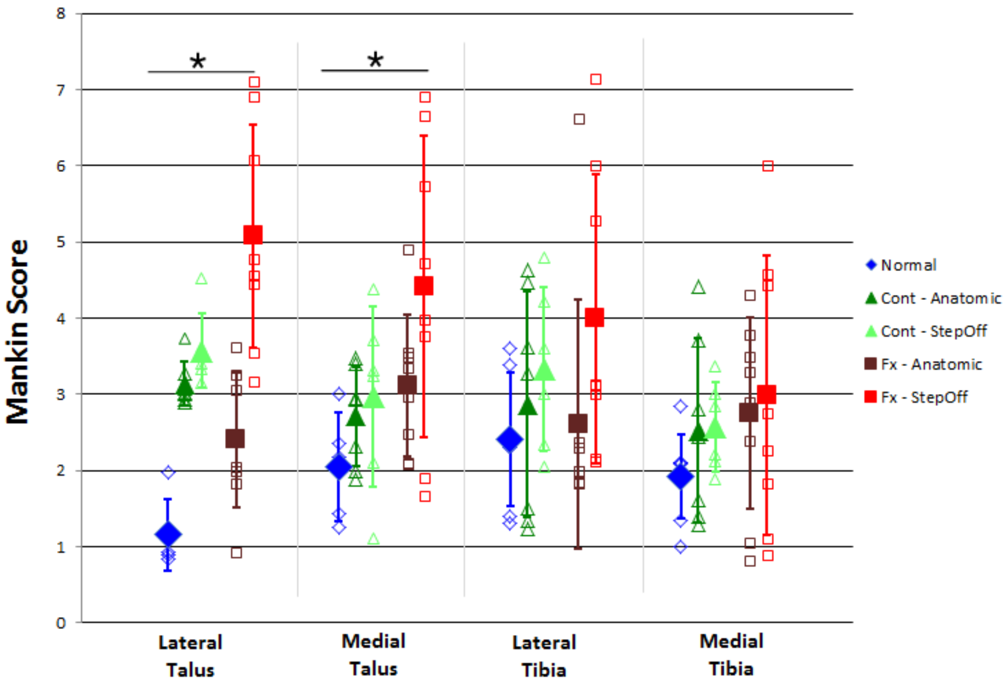

Figure 11. Average Mankin score by site. * indicates statistically significant differences of $p<0.05$. Empty shapes represent individual animals, and the filled shapes with error bars are averages and standard deviations.

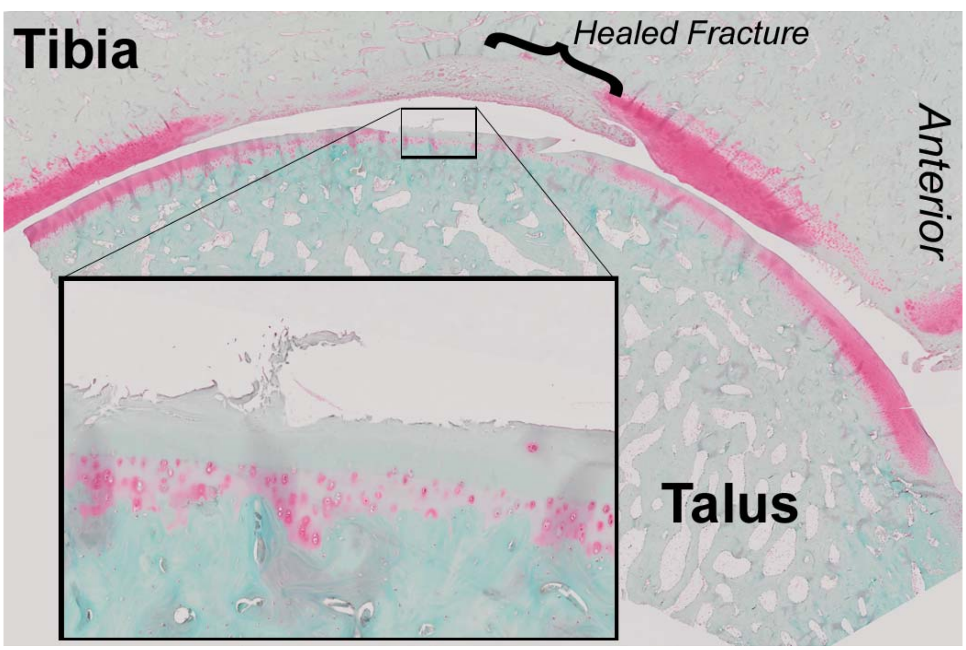

Figure 12. A representative pair of tibial (top) and talar (bottom) histology sections. There is clear PG loss, surface fibrillation, and extreme hypocellularity on the talar surface articulating with the healed fracture. On the tibia, the fracture is noted, and the low PG region posterior to that is the synovial fossa.

The full details of each aspect of the data analysis are included in the full length manuscript that is currently in revision at *Osteoarthritis and Cartilage* (Appendix 2). The data collected as part of Task 3 supports the use of the Yucatan minipig as an animal model for PTOA after an IAF. The minipig demonstrated healing rates that were reasonable in the context of human healing rates. The initial decrease in limb loading was to be expected; however, the animals were sufficiently treated to use their limb immediately post-operatively, and they regained full functionality of the injured limb in the 12-week study period. This behavior is indicative of a successful treatment protocol that allowed for recovery of full function with minimal pain that would discourage limb use. The inflammatory cytokine response in the joint fluid was very similar to that seen in human patients after a joint injury, indicating that the model was able to replicate a human-like biological response to an IAF. And finally, 12 weeks after an IAF, there was obvious cartilage degeneration on both the tibial and talar surfaces of the hock joint. While cartilage damage does not equate with late stage PTOA, which would include massive cartilage eburnation and bony changes, the cartilage damage seen in these experimental joints show clear cartilage thinning and major degenerative changes. This speed of joint degeneration is a positive of this model, since it indicates a much more human-realistic progression from joint injury to PTOA. While development of PTOA in the human ankle is often reported to occur very quickly (approximately 2 years after injury), even this speed of PTOA development would be poorly modeled by an animal that progressed to PTOA in 3 months. Therefore, the early-stage PTOA that is represented by this cartilage degeneration is a positive feature of the minipig model.

3.5 Task 4 – Demonstration of Model Utility

Aim 3 of this project was to demonstrate the utility of the mini-pig model as a pre-clinical tool in which to evaluate promising treatments to prevent PTOA following intra-articular fracture. In the original statement of work, OP-1/BMP-7 was proposed as the treatment that would be used to reduce inflammation in the acute period following intra-articular fracture. In the revised statement of work associated with the change in PI, OP-1/BMP-7 was replaced with a cocktail of glycyrrihizin (GZ) and n-acetyl-cysteine (NAC). The NAC/GZ compound is administered as intra-articular injection with the treatments suspended in a hyaluronic acid hydrogel which becomes more viscous at body temperature and prevents the therapeutics from leaking out of the injured joint. Glycyrrihizin is an anti-inflammatory, and NAC is an antioxidant. The cocktail has shown great promise for reducing inflammation in smaller animal models, and like OP-1/BMP-7, both NAC and GZ are approved for use in humans. This cocktail served the same purpose in the minipig model of reducing inflammation subsequent to IAF, and presented a more interesting research target as this pairing is a novel combination of therapeutics.

A total of 30 animals were used to complete this task. All surgeries were completed by Dr. Mary Bergh, who was initially the veterinary consultant on this project, and who became the operating surgeon upon Dr. Tochigi's departure in PY3. Six animals served as surgical control shams. All steps of the surgery were completed with the exception of the impact. Animals in this group were administered the hydrogel vehicle immediately after surgery and again 24 hours later. The remaining 24 animals in this group were fractured and repaired as described above. Twelve animals received the NAC/GZ cocktail (10 mM NAC and 100 μM GZ) in the hydrogel delivery vehicle immediately after surgery and again 24 hours later. The remaining 12 animals were administered the hydrogel delivery vehicle only at the same time points.

All animals were sacrificed one week after index surgery. Both the fractured and the intact contralateral hocks were harvested for analysis. The joint was opened anteriorly and evaluated for any surgical abnormalities. The 1 week post-operative time was insufficient for bone healing to have occurred, and the fracture fragment was stabilized only by the fixation hardware. Synovial fluid was drawn from the joints by pipetting before the joint was fully disarticulated. The posterior synovium was pinned flat on a piece of cork board for histological processing. A dermal punch was used to harvest specimens of fresh cartilage for analysis by glutathione assay and for mitochondrial metabolic function. The remaining joint was then processed for histological analysis using methods identical to those used in Task 3.

3.5.a Histological Analysis of Inflammation

The purpose of this aim was to investigate the effects of an anti-inflammatory treatment on the biology of the fractured minipig hock joint. In the short 1-week survival time of the animals associated with this Aim, there is not enough time for dramatic changes to occur in the cartilage. Because inflammation typically appears in the soft tissues surrounding the joints earlier than in the cartilage matrix, the main histological outcome of this work was a measure of inflammation of H&E-stained histological sections of the posterior synovium.

All sections were digitized on the VS110 virtual histology system and evaluated automatically using a custom routine developed in Visiomorph software (Visiopharm Inc., Hoersholm, Denmark). Increased monocyte density and increased fibrous tissue area are hallmarks of inflammation, and therefore the characteristics quantified by this program. In the analysis, cell nuclei, fibrous tissue, and fat cell areas are automatically identified based on staining color (Figure 13). After a series of morphological evaluations to differentiate between tissue and cell types, the density of monocytes in the fatty tissue and the ratio of fibrous tissue to the total tissue area are calculated.

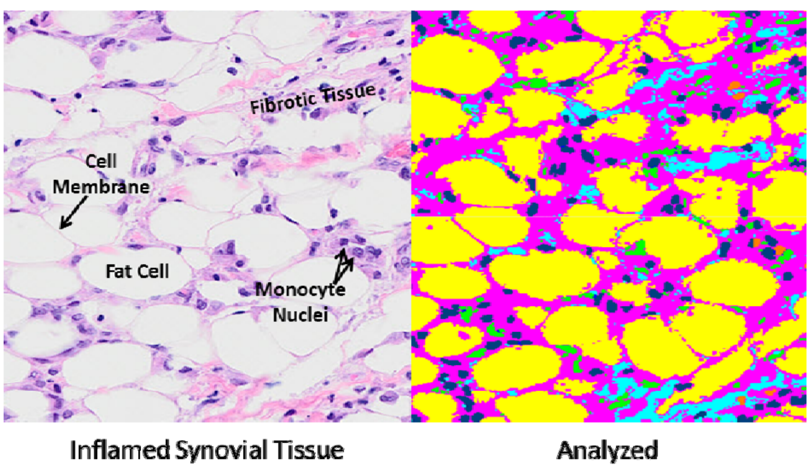

Figure 13. Hematoxylin and eosin-stained synovial tissue from a rabbit (left) and the corresponding analysis performed in Visiomorph (right). Cell nuclei (blue), fat cell area (yellow), fibrous tissue (cyan) and membranous tissue (magenta) are automatically identified and used to quantify extent of inflammation.

This routine is presently being used to directly assess the effects of the anti-inflammatory treatment administered during Aim 3 experiments. All synovial histology sections have been generated and digitized. The Visiomorph analysis routine is being applied to the 120 resulting histology slides (30 animals x 2 limbs x 2 sections/limb). The final results will be compared between the different treatment groups and reported in the final manuscript detailing the results of the NAC/GZ treatment.

3.5.b Synovial Fluid Cytokine Concentrations

A second measure of the effectiveness of antioxidant treatment in the minipig model was evaluation of synovial fluid cytokine concentrations. From the work in Task 3, we accumulated a substantial database of normal/pre-operative cytokine concentrations, and we found that while there was substantial animal-to-animal variation, the pre-operative values from the right and left limbs of the same animal were very similar. Therefore, pre-operatively, synovial fluid was drawn from only the non-operated contralateral hock. At the time of animal sacrifice and tissue harvest, the synovial fluid was drawn from both the fractured hock and the intact contralateral. The same porcine-specific multiplex cytokine array (Raybiotech, Norcross GA) was used to measure concentrations of ten cytokines (IL1β, IL4, IL6, IL8, IL10, IL12, GMCSF, INFγ, TNF and TGFβ) from the synovial fluid.

Once again, concentrations of IL6 and IL8 were significantly increased 1 week after IAF. Administration of the NAC/GZ treatment was able to decrease the spikes in IL6 and IL8 concentrations at that one week time-point. While this treatment was unable to return the cytokine levels to pre-operative or contralateral values, proving efficacy of this particular treatment was not the primary goal of this work. Rather, these data show that the minipig hock is a suitable environment in which to evaluate these types of biological treatment. As with the cytokine concentrations measured in Task 3, the standard deviations were very large in some of the cytokines investigated, and IL6 and IL8 were the most responsive cytokines.

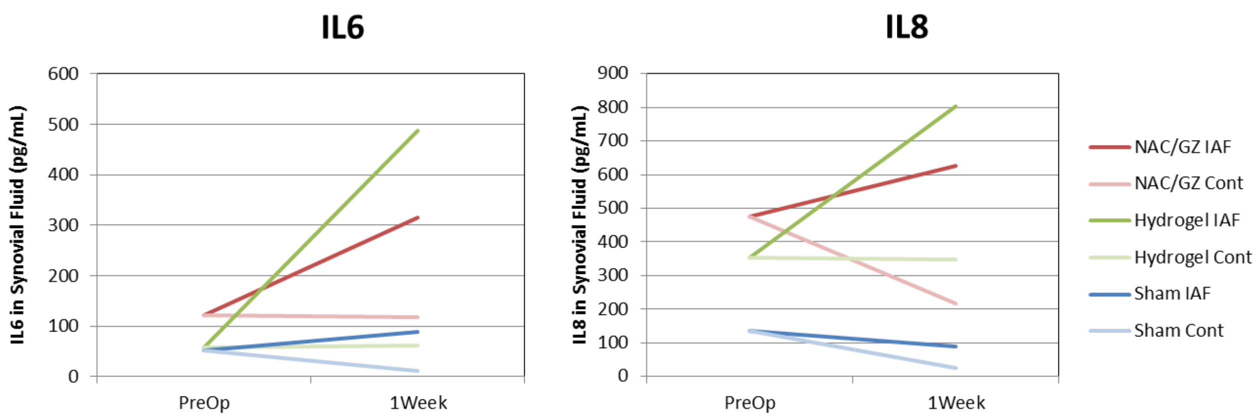

Figure 14. Concentrations of IL6 and IL8 in minipig hock synovial fluid one week after IAF. Administration of the NAC/GZ treatment was able to decrease the significant increase in both inflammatory cytokines one week after IAF, although not to pre-operative or to contralateral joint levels.

3.5.c Oxidative Stress Measurement

The antioxidant N-acetylcysteine (NAC) freely crosses plasma membranes to enter cells where it is rapidly de-acetylated to form cysteine. This additional cysteine is capable of modest operation as an antioxidant on its own but primarily supplements glutathione (GSH) production by the cell.[9] Glutathione is a tripeptide thiol, which acts as the primary redox buffer of the cell. The ratio of GSH to its oxidized counterpart, glutathione disulfide (GSSG), is a well-recognized indicator of cellular oxidative stress and unstressed cells are known to maintain this ratio at specific, homeostatic values. In cases of oxidative stress, the ratio of GSSG/total GSH will increase because reduction of GSSG to GSH requires consumption of cellular energy (NADPH), a mechanism that will fall further and further behind with increasing levels of oxidative stress. Because intra-articular fracture introduces a large amount of molecular oxygen and iron, classic contributors to oxidative stress, into the joint (primarily via blood entering the joint) and because NAC is capable of decreasing oxidative stress which damages cartilage, measurement of this ratio was of interest in the Aim 3 experimental animals.

Immediately after sacrifice and prior to fixation for histological analysis, a small cartilage sample was excised from the joint surface for analysis of the GSSG/GSH content via the method of Griffith.[10] It was found that an IAF significantly ($p < 0.0001$) increased the total GSH content over the normal levels seen in the intact contralateral (Figure 15). As expected given the intracellular conversion of NAC to GSH, the administration of NAC/GLZ further increased total GSH levels in the fractured hocks ($p= 0.0362$). This indicated that NAC was being absorbed intracellularly. Untreated (hydrogel) fractured hocks demonstrated a statistically significant increase in oxidized GSH (%GSSG) relative to controls (Figure 16). Administration of the NAC/GLZ treatment was able to return levels of oxidized glutathione to normal (contralateral) levels. This work indicates that NAC/GLZ was able to be absorbed by the chondrocytes, converted to GSH, and subsequently protect the injured chondrocytes from oxidative stress.

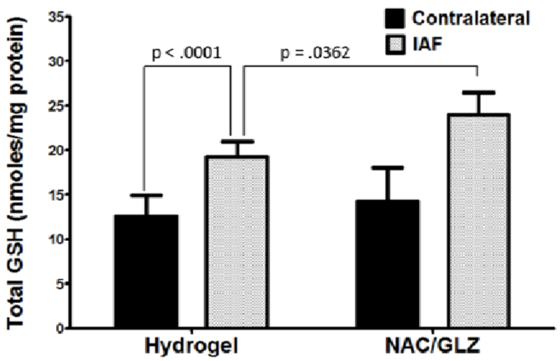

Figure 15. Injection of NAC/GZ augments increases in cartilage total GSH after an IAF.

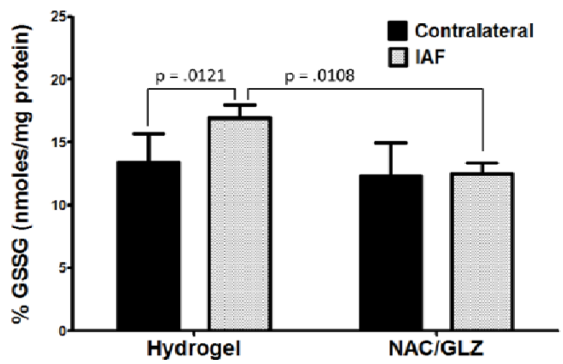

Figure 16. IAF increased oxidation of glutathione, and NAC/GZ administration returned levels to the baseline level.

3.5.d Mitochondrial Metabolic Function

Emerging evidence has suggested that mitochondrial function plays an integral role in cartilage homeostasis, altering inflammatory responses and contributing to loss of chondrocyte anabolic function in response to injury and other insults. In work conducted in rabbit and bovine models, it has been found that chondrocyte mitochondrial damage and losses in mitochondrial respiration precede development of tissue-level pathology (manuscript in preparation). Further, mitochondria are a common target of oxidative damage. Thus, mitochondrial metabolism was measured to evaluate the effects of IAF on the chondrocyte homeostasis in the hock as well as to determine if the NAC/GZ treatment cocktail was able to alter that behavior through redox pathways related to the mitochondria.

A small piece of the articular cartilage harvested from each hock was digested in 0.25 mg/mL collagenase/pronase and extracted chondrocytes were plated and cultured for a maximum of 5 days to ensure that chondrocyte phenotypes remained stable. Chondrocytes were analyzed on the Seahorse XF-96 Extracellular Flux Analyzer (Seahorse Bioscience, North Billerica, MA). This sophisticated instrument measures the oxygen consumption rate (OCR) within individual culture wells in response to a series of chemical injections. Normalizing the OCR to the number of cells in the well, determined via hemocytometer, provides a precise measure of the oxygen consumed per cell per unit time, i.e. cellular respiration. By sequentially injecting oligomycin to block ATP synthase, an uncoupling agent (carbonyl cyanide 4-trifluoromethoxy phenylhydrazone) to allow maximal respiration, and a combination of antimycin A and rotenone to halt mitochondrial respiration entirely (thus leaving only "non-mitochondrial respiration"), specific mitochondrial performance parameters can be obtained (Figure 17). Of particular interest are 1) basal respiration = uninhibited OCR – non-mitochondrial OCR, 2) maximal respiration = uncoupled OCR – non-mitochondrial OCR, 3) spare respiratory capacity = basal respiration – maximum respiration, and 4) proton leakage = oligomycin inhibited OCR – non-mitochondrial OCR. Basal respiration correlates to the normal anabolic activity of the chondrocytes. We believe maximal respiration is descriptive of the maximal metabolic response a chondrocyte is capable of in response to stimulus, and the difference between those two quantities (spare respiratory capacity) is representative of the ability of the chondrocyte to respond to increases in metabolic demand. The final quantity, proton leakage, is indicative of the health of the mitochondrial membrane and known to be an early casualty during oxidative stress where lipid peroxidation is occurring. Interestingly, proton leakage has also been demonstrated to be increased in chondrocytes from arthritic knees (5).

IAF was associated with a slightly elevated basal respiration rate, a slightly decreased maximum respiration rate, and therefore a decreased spare respiratory capacity relative to the non-injured contralateral limbs (Figure 18). Administration of NAC/GZ did not appear to significantly alter these trends. Hydrogel IAF hocks showed an increased amount of proton leakage relative to contralateral hocks, indicating damage to the mitochondrial membranes of these chondrocytes (Figure 19). This damage was not present in those hocks receiving NAC/GLZ, further supporting the hypothesis that NAC/GLZ is capable of preventing cellular oxidative stress.

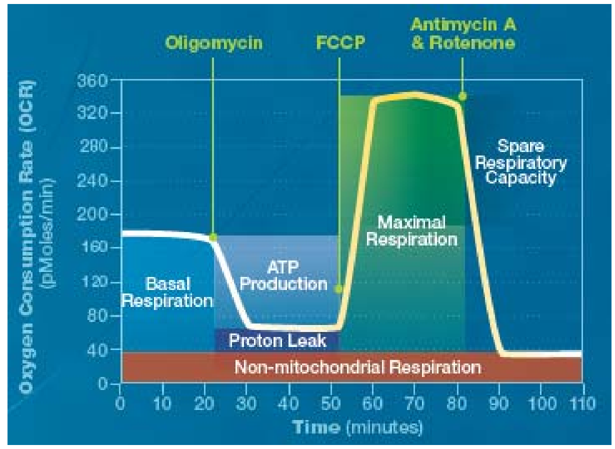

Figure 17. Illustration of Seahorse analysis. http://www.seahorsebio.com/resources/pdfs/brochure-XFe-2012.pdf. The different chemical injections are shown across the top, and the mitochondrial respiration measures derived from the oxygen consumption rate are shown on the plot.

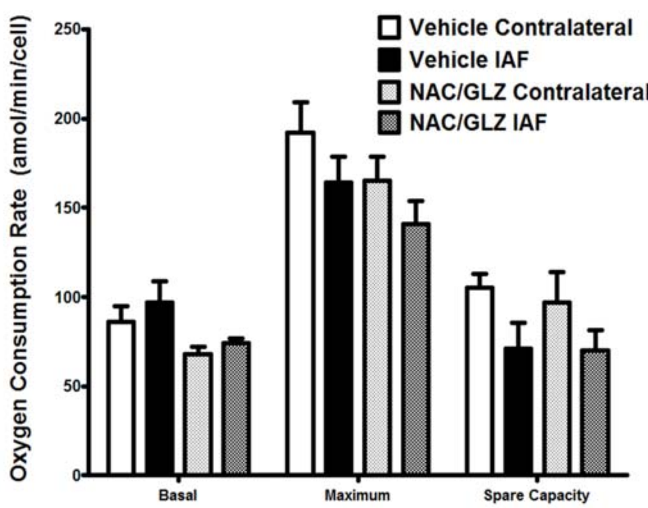

Figure 18. Three measures of mitochondrial health: 1.) Basal respiration (left), 2.) Maximum respiration (middle), and 3.) Spare respiratory capacity (right). N=12 for each group.

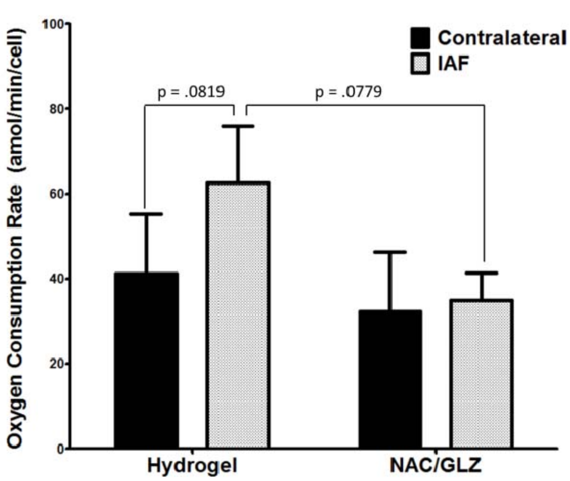

Figure 19. IAF induces increases in proton leakage from chondrocyte mitochondria. This is indicative of increases in mitochondrial membrane damage as a result of oxidative stress. This damage to chondrocyte mitochondria was alleviated with the administration of NAC/GLZ, suggesting that augmentation of cellular GSH pathways can protect chondrocyte mitochondria during oxidative stress.

Upon completion of the histological grading of synovial inflammation, an fourth full-length manuscript detailing the outcome of Aim 3 will be prepared. The combination of the analysis of the anti-inflammatory and the anti-oxidant effects of the applied treatment cocktail are of scientific interest. However, the main strength of the work conducted to complete Aim 3/Task4 is demonstrating that the minipig hock is a useful research tool for investigating promising biological treatment options. The model was able to show uptake and effects of the treatment, and the effects were similar to what was anticipated based on the known function of the treatment compounds.

4. Key Research Accomplishments

Completion of methodological development

- Established final surgical and impact fracture creation protocols
- Established post-operative animal treatment protocols
- Validated metric for measuring impact energy associated with fracture

Completion of 12-week survival experimental series (n=22)

- Confirmation of radiographic fracture healing in a time course very consistent with the post-injury time course of human clinical IAFs
- Confirmation of gradual recovery of experimental joint loading
- Confirmation of an inflammatory cytokine response following joint injury similar to that seen in human joint injury
- Confirmation of cartilage histological findings consistent with human post-traumatic OA
- Application of a CT-based image analysis technique enabling quantitative evaluation of joint incongruity in the fractured experimental joints

Completion of 1-week survival experimental series (n=30)

- Indications of anti-inflammatory treatment decreasing the joint inflammatory response following and intra-articular fracture
- Direct measurement of treatment delivery and associated decreases in oxidative stress via glutathione assay
- Direct measurement of mitochondrial respiration measures confirm decreases in oxidative stress via Seahorse analysis

5. Conclusion

The goal of this project was to develop a large animal model of post-traumatic osteoarthritis after an intra-articular fracture and to demonstrate the utility of this new model for the investigation of biological treatment. The first step in this work was to establish the definitive experimental and animal treatment protocols. That work resulted in the completion of a Master's thesis and two full length peer-reviewed papers. The next step was to document the natural history of an IAF in the minipig hock, specifically focusing on bone healing and the development of PTOA. That work has resulted in a third full-length manuscript that is currently undergoing revision. And finally, the resultant model was used to investigate the short-term effects of a promising anti-inflammatory/anti-oxidant cocktail. That work is in the final stages of analysis and is currently being formatted into a 4th full-length manuscript that will be submitted for peer review in the next few months. This body of work details the development and the utility of a large animal model of PTOA after an IAF, which fills a critical gap in translating promising treatments from the benchtop or small animal models into human treatment protocols. Future work will include using this model as a preclinical tool to evaluate treatment biological, mechanical, or surgical treatment options focused on reducing the burden of PTOA.

6. PUBLICATIONS, ABSTRACTS AND PRESENTATIONS

6.1 Peer-reviewed Papers

- Tochigi Y, Buckwalter JA, Martin JA, Hillis SL, Zhang P, Vaseenon T, Lehman AD, Brown TD. *Distribution and progression of chondrocyte damage in a whole-organ model of human intra-articular fracture.* J Bone Joint Surg Am. 2011 Mar;93(6):533-9. PMID:21411703, PMC3052703.
- Tochigi, Y; Zhang, P; Rudert, MJ; Baer, TE; Martin, JA; Hillis, SL; Brown, TD. *A novel impaction technique for modeling intra-articular fracture in large animal joints.* Osteoarthritis Cartilage 2013; 21(1): 200-8. PMID:23069855, PMC3538937.
- Diestelmeier BW, Rudert MJ, Tochigi Y, Baer TE, Fredericks DC, Brown TD. *An instrumented pendulum system for measuring energy absorption during fracture insult to large animal joints in vivo.* J Biomech Eng. 2014 Jun;136(6):064502. PMID:24760051.
- Goetz JE, Fredericks DC, Petersen E, Rudert MJ, Baer TE, Swanson E, Roberts NH, Martin JA, Tochigi Y. *A clinically realistic large animal model of intra-articular fracture that progresses to post-traumatic osteoarthritis.* Osteoarthritis Cartilage (In revision).

6.2 Meeting Abstracts/Presentations

- Diestelmeier, BW; Rudert, MJ; Tochigi, Y; Baer, TE; Fredericks, DC; Brown, TD. *Quantification impaction system for a large animal survival model of intraarticular fracture.* 36th Annual Meeting of the American Society of Biomechanics, August 15–18, 2012, Gainesville, Florida.
- Tochigi, Y; Diestelmeier, BW; Rudert, MJ; Baer, TE.; Fredericks, DC.; Arunakul, M; Brown, TD. *A clinically-realistic large animal survival model of human intra-articular fracture.* 2013 Annual Meeting of the Orthopaedic Research Society, January 26–29, 2013, San Antonio, Texas. Paper #0138, Session 023:
- Swanson, E; Goetz, JE; Tochigi Y. *Evaluation of articular surface geometry deviation and cartilage damage in a porcine model of intra-articular fracture.* 2013 Annual Meeting of the Orthopaedic Research Society, January 26–29, 2013, San Antonio, Texas. Poster #PS1-056.
- Roberts N, Martin JA, Fredericks DC, Tochigi Y, Goetz JE. Fluctuation of synovial fluid inflammatory cytokine concentrations in an animal model of intra-articular fracture. 2014 Annual Meeting of the Orthopaedic Research Society, March 15-18, 2014, New Orleans, LA. Poster #PS1-0342.
- Goetz JE, Martin JA, Rudert MJ, Roberts NH, Fredericks DC, Tochigi Y. Natural history of post-traumatic osteoarthritis in a large animal model of intra-articular fracture. *Extremity War Injuries Symposium IX.* February 10-12, 2014, Washington DC. Poster 10.

- Coleman MC, Martin JA, Fredericks DC, Bergh MS, Goetz JE. *Intraarticular administration of n-acetylcysteine and glycyrrhizin alleviates acute oxidative stress following intraarticular fracture.* 2015 Annual Meeting of the Orthopaedic Research Society, March 25-31, 2015, Las Vegas NV. (submitted)

7. Inventions, Patents and Licenses

Nothing to report

8. Reportable outcomes

Nothing to report

9. Other Achievements

9.1 Degrees Obtained

- *Design and application of an instrumented pendulum device for measuring energy absorption during fracture insult in large animal joints in vivo.* M.S. thesis, Bryce W. Diestelmeier, Department of Biomedical Engineering, The University of Iowa, 2012.

9.2 Research Grants

- US Department of Defense (Department of Army) CDMRP-PRMRP
  Technology/Therapeutic Development Award W81XWH-11-1-0583
  Mitochondrial Based Treatments that Prevent Posttraumatic Osteoarthritis in a Translational Large Animal Intraarticular Fracture Survival Model
  (PI: Todd O. McKinley, MD/James A. Martin PhD) - Funded
- NIH/NIAM CORT Grant 5 P50 AR055533
  Innovations to Assess and Forestall Post-Traumatic Osteoarthritis
  (Program Director: Joseph A. Buckwalter, MD)
  Project-2: Establishing Treatments and Diagnostic Tools for Post-Traumatic OA In Vivo.
  (Project PI: Yuki Tochigi, MD, PhD/Douglas Pedersen PhD) - Funded
- Orthopaedic Research Society/Orthopaedic Research and Education Foundation
  Postdoctoral Fellowship Grant Application
  Probing the Origin of Mitochondrial Dysfunction Associated with Osteoarthritis Following Intra-articular Fracture
  (PI: Mitchell C. Coleman) - Pending

10. References

1. Diestelmeier, BW. 2012. Design and application of an instrumented pendulum device for measuring energy absorption during fracture insult in large animal joints in vivo. M.S. thesis, Department of Biomedical Engineering, The University of Iowa, 2012.
2. Tochigi, Y; Zhang, P; Rudert, MJ; Baer, TE; Martin, JA; Hillis, SL; Brown, TD. A novel impaction technique for modeling intra-articular fracture in large animal joints. Osteoarthritis and Cartilage 2013; 21(1): 200-8.

3. Cameron ML, Fu FH, Paessler HH, Schneider M, Evans CH. Synovial fluid cytokine concentrations as possible prognostic indicators in the ACL-deficient knee. Knee Surg, Sports Traumatol, Arthroscopy. 1994; 2: 38-44.

4. Swärd P, Frobell R, Englund M, Roos H, Struglics A. Cartilage and bone markers and inflammatory cytokines are increased in synovial fluid in the acute phase of knee injury (hemarthrosis) - a cross-sectional analysis". Osteoarthritis and Cartilage, 2012; 20(11): 1302-8.

5. Pritzker KP, Gay S, Jimenez SA, Ostergaard K, Pelletier JP, Revell PA, Salter D, van den Berg WB. Osteoarthritis cartilage histopathology: grading and staging. Osteoarthritis and Cartilage. 2006; 14(1): 13-29.

6. Moussavi-Harami SF, Pedersen DR, Martin JA, Hillis SL, Brown TD. Automated objective scoring of histologically apparent cartilage degeration using a custom image analysis program. J Orthop Res. 2009; 27(4): 522-8.

7. Doige C, Horowitz A. A study of articular surfaces and synovial fossae of the pectoral limb of swine. Canadian journal of comparative medicine. 1975;39:7-16.

8. Wegener KM, Heje NI, Aarestrup FM, et al. The morphology of synovial grooves (Fossae synoviales) in joints of cattle of different age groups. Zentralblatt fur Veterinarmedizin Reihe A. 1993;40: 359-370.

9. De Flora S, Bennicelli C, Camoirano A, Serra D, Romano M, Rossi GA, Morelli A, De Flora A. In vivo effects of N-acetylcysteine on glutathione metabolism and on the biotransformation of carcinogenic and/or mutagenic compounds. Carcinogenesis. 1985;6(12):1735-45.

10. Griffith OW. Determination of glutathione and glutathione disulfide using glutathione reductase and 2-vinylpyridine. Anal Biochem 1980; 106(1): 207-12.

Distribution and Progression of Chondrocyte Damage in a Whole-Organ Model of Human Ankle Intra-Articular Fracture

By Yuki Tochigi, MD, PhD, Joseph A. Buckwalter, MS, MD, James A. Martin, PhD, Stephen L. Hillis, PhD, Peng Zhang, MD, Tanawat Vaseenon, MD, Abigail D. Lehman, BS, and Thomas D. Brown, PhD

Investigation performed at The University of Iowa, Iowa City, Iowa

Background: Despite the best current treatments, intra-articular fractures commonly cause posttraumatic osteoarthritis. In this disorder, death and dysfunction of chondrocytes associated with acute cartilage injury presumably plays an important role in triggering the pathomechanical cascade that eventually leads to whole-joint degeneration. Information regarding this cell-level cartilage injury, particularly at the whole-organ level in actual human joints, has been lacking. In this study, the distribution and progression of fracture-associated cell-level cartilage damage were assessed using a novel whole-organ model of human ankle intra-articular fracture.

Methods: Seven normal human ankles harvested immediately following amputation were subjected to a transarticular compressive impaction insult that mimicked an injury mechanism typical of tibial plafond fractures. For each ankle, site-specific, time-dependent changes in chondrocyte viability in the fractured tibial surface were studied by means of live-dead assay, using a confocal laser-scanning microscope. Fractional chondrocyte death was measured at several time points, in the superficial zone of the cartilage in ''fracture-edge'' regions within 1 mm of the fracture lines, as well as in ''non-fracture'' regions more than 3 mm centrally away from the fracture lines.

Results: All seven experimental fractures morphologically replicated tibial plafond fractures. Immediately post-fracture, superficial-zone chondrocyte death was significantly greater ($p = 0.001$) in fracture-edge regions (fractional cell death = 7.6%) than in non-fracture regions (1.6%). Progression of cell death over the next forty-eight hours was significantly faster in fracture-edge regions ($p = 0.007$), with the fractional cell death reaching 25.9%, which was again significantly higher ($p < 0.001$) than in non-fracture regions (8.6%).

Conclusions: Cell-level cartilage damage in human intra-articular fractures was characterized by acute chondrocyte death that predominated along fracture lines and that spontaneously progressed in the forty-eight hours following injury.

Clinical Relevance: Progressive chondrocyte damage along fracture lines appears to be a reasonable target of therapeutic treatment to preserve the whole-joint cartilage metabolism in intra-articular fractures, eventually to mitigate the risk of posttraumatic osteoarthritis.

Intra-articular fractures commonly cause posttraumatic osteoarthritis (OA), despite current treatments that effectively reduce and stabilize the fractured surfaces. Clinical series of tibial plafond fractures[1-4] have shown that more than half of patients treated by surgical reconstruction of the joint nevertheless develop posttraumatic OA, often within two years of injury. To develop novel treatment strategies that effectively mitigate the risk of posttraumatic OA, there is a clear need to advance the understanding of the pathogenesis of progressive joint degeneration following injury.

There are several factors that presumably contribute to cartilage degeneration in fracture-injured joints[5,6]. These factors include acute mechanical articular cartilage damage at the instant of the injury event, biological stimuli associated with joint bleeding and/or inflammatory responses, and chronic cartilage overloading resulting from incongruity, instability,

Disclosure: In support of their research for or preparation of this work, one or more of the authors received, in any one year, outside funding or grants in excess of $10,000 from the University of Iowa Biological Science Funding Program, the Orthopaedic Trauma Association (a research grant), and the National Institutes of Health (Grant P50 AR055533). Neither they nor a member of their immediate families received payments or other benefits or a commitment or agreement to provide such benefits from a commercial entity.

and malalignment. Recently, chondrocyte damage involved in human intra-articular fractures has been receiving increasing attention[7-9]. Death or dysfunction of chondrocytes in fracture-damaged joints necessarily impacts cartilage metabolism, presumably triggering a pathological cascade that eventually leads to whole-joint degeneration. Cell-level cartilage injury appears to be an important pathological process to target for new orthopaedic treatment(s) to forestall the development of OA following intra-articular fractures.

Previous studies documented that chondrocyte damage accompanying fracture-associated articular cartilage injury in humans was distributed near the edges of fracture fragments, particularly in the superficial zone[7,8]. Unfortunately, in these studies, the use of tissue material obtained at the time of definitive fracture surgery precluded exploration of the characteristics of cell-level cartilage damage occurring in the early acute phase, due to probable post-injury damage progression. In addition, chondrocyte viability in non-fracture regions could not be assessed.

The aim of the present study was to document the distribution and progression of chondrocyte damage in fracture-injured human articular surfaces, at the whole-organ level. The joint of interest was the ankle, in which a relatively high prevalence of intra-articular fractures and predictable OA development had been clinically well documented[1-4]. A unique model of human distal tibial intra-articular fracture was developed to study site-specific, time-dependent changes in chondrocyte death in fractured cartilage in the early acute phase. It was hypothesized that acute chondrocyte damage in human intra-articular fractures would be concentrated along fracture lines and that this chondrocyte damage would progress in the forty-eight hours after injury.

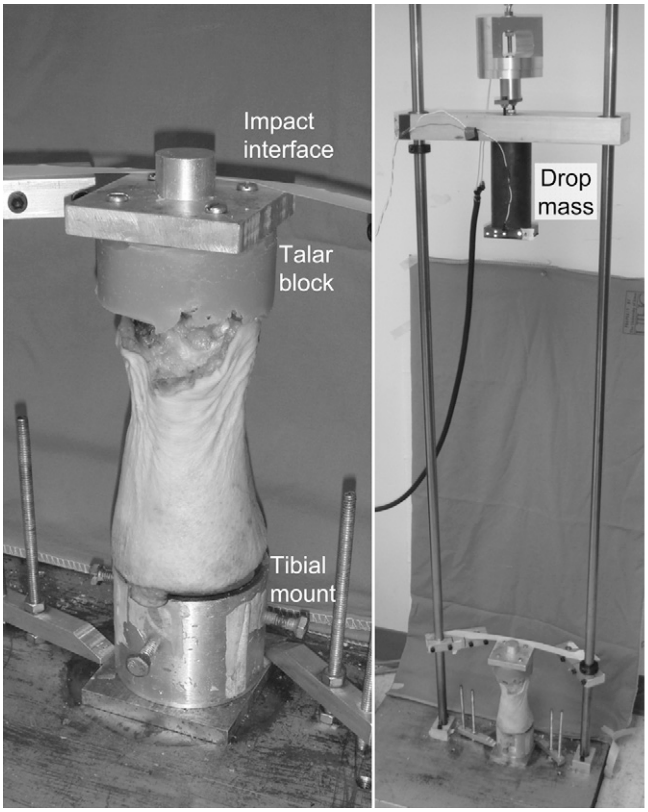

Fig. 1

A human ankle whole-joint specimen prepared for the fracture-impaction insult (left), and the custom drop-tower system to deliver a fracture-impaction insult (right). An electromagnet holds and releases the drop-mass from a prescribed height.

Materials and Methods

Seven normal human ankles obtained immediately (<4 hours) following surgical amputation, from patients (four men and three women, twenty-nine to seventy-one years old) who had a malignant tumor near or proximal to the knee, were utilized. In every case, the specimen was harvested from discarded tissue after pathological examination, with the only information collected being the age and sex of the patient. The tibial shaft, sectioned at the mid-diaphysis, was potted perpendicularly into a poly(methyl-methacrylate) (PMMA) block, leaving 10 cm of the distal part intact (Fig. 1). The subtalar joint was disarticulated, and the bottom of the talus was potted into another PMMA block. During this potting procedure, the ankle was held in the neutral position. Special attention was paid to align the center of the ankle to both potting blocks. The proximal fibular shaft (sectioned 9 cm above the ankle) and the lateral malleolar tip were kept away from the potting blocks. The skin and subcutaneous soft tissue surrounding the ankle were left intact.

These ankles were subjected to an impaction insult that mimicked an injury mechanism typical of clinical tibial plafond fractures. Specifically, the ankle was subjected to a high-energy trans-articular compressive force pulse delivered by a custom drop-tower impaction system (Fig. 1). In this device, each specimen was mounted with the tibial side down, and an aluminum impact interface was attached to the upper face of the talar potting block. The specimen was aligned carefully with the axis of mass fall, and secured to the massive base plate, with the talar impact interface held horizontal. A 6.55-kg mass was then dropped from a 78-cm height, delivering approximately 50 J of kinetic energy to the specimen.

Immediately after impaction, each ankle was disarticulated, and the distal tibial articular surface was digitally photographed (Fig. 2) to record the fracture morphology. Next, under sterile conditions, major osteoarticular fragments were sampled, with juxta-articular bone being trimmed away, while leaving approximately a 5-mm thickness of cancellous bone beneath the cartilage layer (the typical volume per specimen was 1 to 2 cm^3). Each osteoarticular fragment was then secured to a specimen holder, such that the articular surface near the fracture edge was held nearly horizontal, by potting in a biocompatible polymer (Polycaprolactone; Sigma-Aldrich, St. Louis, Missouri). The specimens were then immersed in culture medium (approximately 80 mL per specimen), which was comprised of 45% Ham F-12 Nutrient Mixture, 45% high-glucose Dulbecco modified Eagle medium, and 10% fetal bovine serum (all from Invitrogen, Carlsbad, California), with a 1% antibacterial-antifungal mixture of penicillin-streptomycin (Invitrogen) and amphotericin B (Thermo Scientific HyClone, Logan, Utah), in an incubator maintained at 37°C in an atmosphere of 5% CO_2 in air.

Chondrocyte death in these osteoarticular fragments was assessed with use of calcein AM for labeling live cells and ethidium homodimer-2 for labeling dead cells (Invitrogen). Prior to analysis, the fragments were soaked in culture medium with these fluorescence stains (at a concentration of 1.0 μM each) for approximately one hour at 37°C. After labeling, chondrocytes in the superficial zone, from the cartilage surface to a depth of up to 200 μm (typically 100 to 150 μm), were scanned at 20-μm intervals, using a confocal microscopy system (MRC-1024; Bio-Rad Laboratories, Hercules, California), with the specimen kept immersed in the regular medium during scanning (at room temperature, one to two hours per specimen). After each scanning session, the specimens were washed with Hank's balanced salt solution (#14170; Gibco-Invitrogen, Grand Island, New York) containing 1% of the above-described antibacterial-antifungal mixture and placed into fresh culture media.

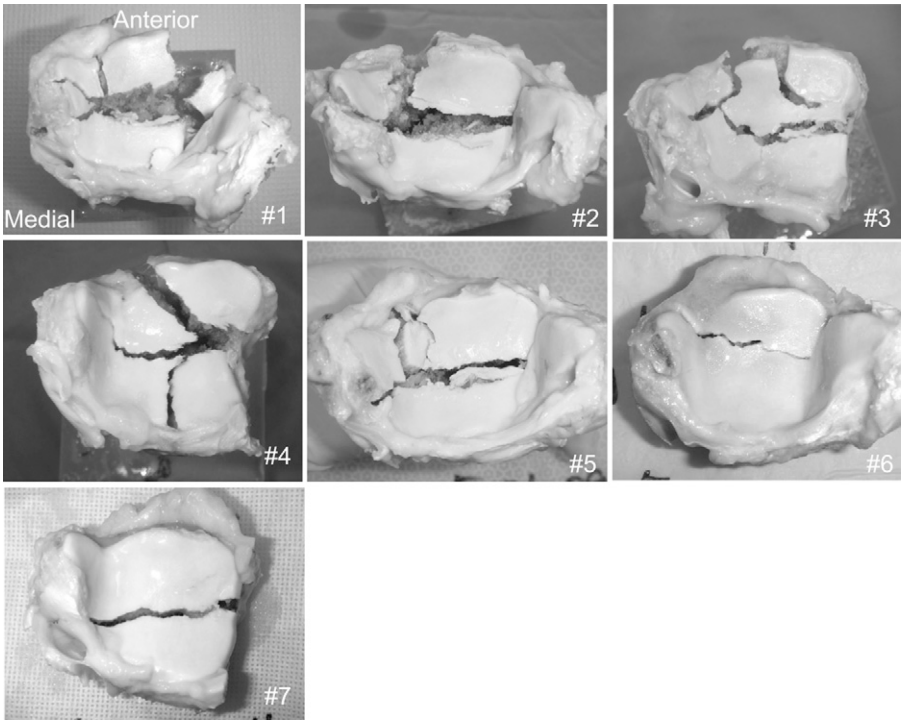

Fig. 2

Distal tibial intra-articular fractures created in the seven human ankle specimens immediately following surgical amputation.

The first two ankles were scanned for cell viability from six to eight hours after the fracture insult. For these ankles, scans were executed at several sites along the primary fracture lines within 1 mm of the fragment edges (fracture-edge regions) and in the regions at least 3 mm centrally (in a direction perpendicular to the fragment edge) away from the fragment edges (non-fracture regions), with use of a ×10 objective lens that allowed scanning of an approximately 1080 × 1080-μm square field per site. The third ankle fracture was scanned after two days of culture. For this ankle, prior to scanning, five representative sites along the primary fracture lines were selected in fracture-edge regions. For each of these sites, two contiguous 540 × 540-μm fields (one including a fracture edge and the next centrally adjacent image field) were scanned with use of a ×20 objective lens (Fig. 3). Scans in non-fracture regions were performed at two nonadjacent sites selected near each fracture-edge scan site but at least 3 mm centrally away from the fragment edges. Scanning at any sites with macroscopically identifiable structural damage (e.g., visible superficial cracks) was avoided. The remaining four ankles were scanned at three time points: immediately (scans completed within six hours), at one day, and at two days post-fracture, in a manner analogous with the third ankle. Prior to the immediate scanning, four to six sets of scanning sites were selected with use of the above-described protocol, and the x-y coordinate information was recorded. Based on this coordinate information, scans at the later time points were repeated at the identical sites, with use of a custom-built programmable microscope x-y axis stage driver (positioning reproducibility, <25 μm).

The scanned images were analyzed with use of ImageJ software (National Institutes of Health, Bethesda, Maryland). Image data for each site and time point consisted of two sets of multi-slice images, one for live cells labeled by green fluorescence and the other for dead cells labeled by red fluorescence. The images, originally in grayscale, were converted to a binary format, allowing fluorescent-labeled cells to be counted with use of the software's particle analysis function. For every image set for live cells, the image intensity threshold for the binary conversion was adjusted such that all plausibly labeled cells were counted, while paying attention to avoid counting the same cells over neighboring multiple

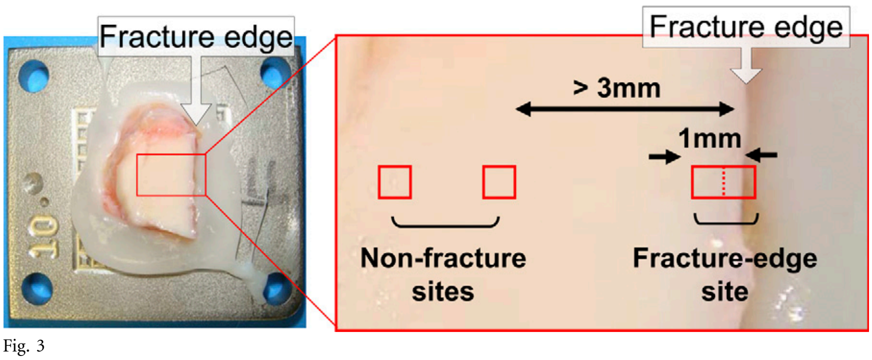

Fig. 3

An osteoarticular fragment mounted in the stage-driver system (left), and an example of scan site selection (right).

TABLE I Individual Specimen Information and Fractional Cell-Death Data

Case (Age, Sex)	Number of Fragments Harvested	Number of Scan Sites	Fracture-Edge Region: Mean Fractional Cell Death (Range) (%) Day 0	Day 1	Day 2
#1 (in 40s, M)	2	3	4.9 (0.0 to 14.5)	—	—
#2 (in 50s, M)	2	2	1.2 (0.1 to 2.2)	—	—
#3 (57, F)	5	5	—	—	13.6 (2.8 to 28.9)
#4 (29, F)	4	5	11.5 (4.7 to 29.6)	20.3 (0.8 to 41.8)	25.5 (4.6 to 58.1)
#5 (71, F)	3	5	6.1 (1.3 to 15.8)	9.4 (3.5 to 15.6)	40.7 (30.8 to 62.4)
#6 (57, M)	3	6	12.2 (3.7 to 18.4)	26.7 (10.4 to 47.9)	34.0 (14.0 to 58.7)
#7 (68, M)	2	4	6.2 (3.5 to 10.0)	7.4 (3.1 to 11.5)	14.0 (10.0 to 18.8)

slices. The identical binary conversion threshold was utilized for cell counting for the corresponding dead-cell image set. The minimum particle size thresholds for automated cell counting were 50 and 20 μm^2 for live and dead cells, respectively. For each site and time point, live and dead cells were counted separately, and the fraction of dead cells among total cells was computed.

In statistical analysis, to account for the repeated-measures and unbalanced-design characteristics of the data, a repeated-measures analysis of variance was performed by fitting a general linear mixed-effects model with use of the SAS PROC MIXED procedure (SAS 9.1.3; SAS Institute, Cary, North Carolina). This estimation approach allowed for unbalanced data. Specifically, each specimen could have a different number of observations at each time point and/or could have no observations at one or more time points[10]. The MIXED approach also afforded flexibility in the specification of the variance-covariance structure. Variances for each location/day combination were allowed to differ. Covariance within specimens (i.e., for a pair of observations from the same specimen, but from different location/day combinations) was modeled by including a random subject effect, which resulted in the same within-specimen covariance between two location/day combinations. Since the variances were allowed to differ, the within-specimen correlations differed although the within-specimen covariance was constant. (Note: the [adjusted] means and 95% confidence intervals reported in the Results section are based on this model; these adjusted means are not conventional arithmetic means of the subject-level observations, but rather are weighted optimally by the MIXED procedure to take into account correlations, variance differences, and sample-size differences.) All tests were performed with a significance level of alpha set at 0.05. For descriptive purposes, the interquartile ranges (IQRs) in the form (25th percentile, 75th percentile) based on the raw data (i.e., the percentiles are computed as though the data values are independent) were also reported.

Source of Funding

This research was supported by the University of Iowa Biological Science Funding Program, by an Orthopaedic Trauma Association Research Grant, and by NIH Grant P50 AR055533.

Results

In all seven of these human ankles, comminuted fractures at the distal tibial surface occurred with the single impaction insult, with the fracture morphology (Fig. 2) being consistent with clinical tibial plafond fractures. Prior examination of these joints revealed no appreciable cartilage degeneration or synovitis in any of the specimens.

Fractional chondrocyte death immediately post-fracture impaction was measured at twenty-four fracture-edge sites and at forty-five non-fracture sites across six ankles. Cell death ranged from 0.0% to 29.6% (IQR: 2.9% to 12.4%) in fracture-edge regions and from 0.0% to 34.2% (IQR: 0.0% to 2.8%) in non-fracture regions, variable across both sites and ankles (Table I). However, the mean value in fracture-edge regions (7.6%, confidence interval [CI]: 4.0% to 11.3%, Fig. 4) was significantly higher ($p = 0.001$) than in non-fracture regions (1.6%, CI: 0.0% to 4.7%). Cell death at two days post-fracture was assessed at twenty-five fracture-edge sites and at forty-seven non-fracture sites, across five ankles. Cell death ranged from 2.8% to 62.4% (IQR: 12.4% to 38.6%) in fracture-edge regions and from 0.0% to 68.8% (IQR: 0.8% to 11.5%) in non-fracture regions. Again, the mean value in fracture-edge regions (25.9%, CI: 18.7% to

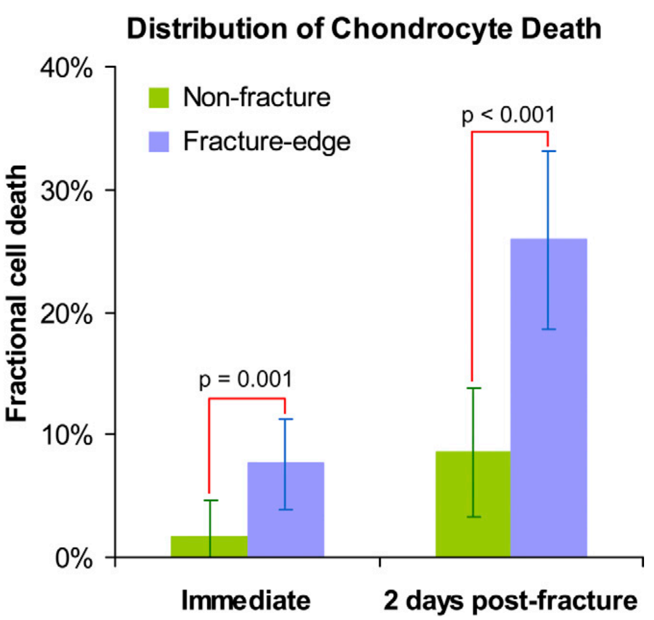

Fig. 4

Chondrocyte viability in fracture-edge regions vs. non-fracture regions, immediately and at two days post-fracture. The values of percent fractional cell death are given as (adjusted) means calculated in the MIXED procedure. The dispersion bars indicate 95% confidence intervals.

TABLE I (*continued*)

	Non-Fracture Region		
	Mean Fractional Cell Death (Range) *(%)*		
Number of Scan Sites	Day 0	Day 1	Day 2
2	0.1 (0.1 to 0.2)	—	—
2	1.3 (0.0 to 2.6)	—	—
10	—	—	7.5 (0.2 to 32.8)
8	0.8 (0.0 to 5.6)	0.5 (0.0 to 1.2)	4.8 (0.0 to 25.0)
15	0.9 (0.0 to 3.1)	2.4 (0.0 to 11.8)	11.3 (0.0 to 37.6)
12	5.4 (0.2 to 34.2)	13.6 (0.6 to 55.6)	14.9 (1.1 to 68.8)
8	2.0 (0.0 to 4.4)	1.7 (0.0 to 6.2)	1.2 (0.0 to 5.9)

33.1%) was significantly higher ($p < 0.001$) than it was in non-fracture regions (8.6%, CI: 3.4% to 13.8%).

The three-time-point chondrocyte death analysis was performed at twenty fracture-edge sites and at forty-one non-fracture sites across the last four of the tested seven ankles. Cell death in fracture-edge regions, whose mean was 9.1% (CI: 4.0% to 14.2%) immediately post-fracture, increased to 16.6% (CI: 9.4% to 23.8%) at one day post-fracture ($p = 0.040$, vs. immediately post-fracture), and further increased to 29.2% (CI: 20.6% to 37.9%) at two days post-fracture ($p = 0.015$, vs. one day post-fracture) as shown in Figures 5 and 6. Although cell death in non-fracture regions also increased from immediately to two days post-fracture ($p = 0.014$), the fractions remained relatively low, below 10% throughout the test period in the majority (76%) of the non-fracture scan sites, and neither of the one-day comparisons (one day vs. immediately post-fracture and two days vs. one day) attained significance. The result of repeated-measures two-way analysis of variance revealed that progression of chondrocyte death from immediate to two days post-fracture in fracture-edge regions was significantly faster than in non-fracture regions ($p = 0.007$), with the near-fracture mean change at 20.1% (CI: 11.6% to 28.7%) and the non-fracture change at 6.3% (CI: 1.3% to 11.3%).

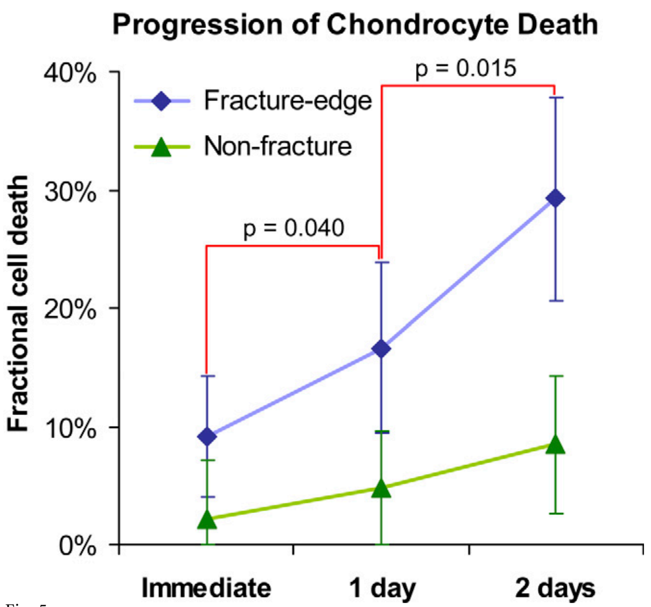

Fig. 5

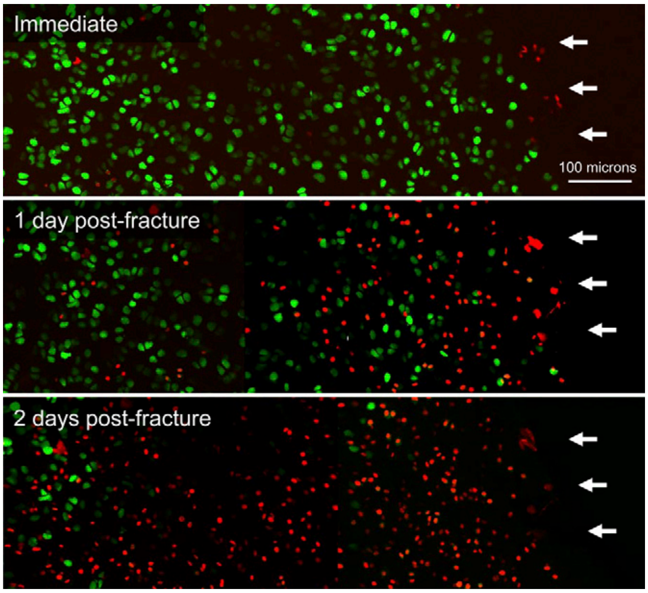

Fig. 6

Fig. 5 Time-dependent changes in human chondrocyte viability at fracture-edge regions and non-fracture regions. The values of percent fractional cell death are given as (adjusted) means calculated in the MIXED procedure. The dispersion bars indicate 95% confidence intervals. **Fig. 6** Confocal microscope images of human superficial chondrocyte viability at a representative fracture-edge scan site, at the immediate, one day, and two days post-fracture time points. Live cells are labeled by green fluorescence, while dead cells are labeled by red fluorescence. White arrows indicate the edge of cartilage on the fracture line.

Discussion

To the best of our knowledge, this is the first study of the distribution and progression of whole-joint chondrocyte death in human intra-articular fractures, in which both specimens and an insult method have closely replicated conditions in human clinical intra-articular fractures. Specifically, fracture-associated articular cartilage pathology was modeled in fresh human cartilage in an anatomical location that clinically frequently sustains intra-articular fracture. For every ankle tested, the fracture insult was delivered within four hours after surgical amputation, and with the joint capsule having been kept closed. Given that articular cartilage is avascular, the consequence of this relatively short duration of blood supply disruption on chondrocyte biological activities was minimal, as confirmed by the immediate low fractional chondrocyte death in the non-fracture regions. It therefore seems reasonable to regard these experimental conditions, under which articular cartilage in these joints was fractured, as approximating those in closed human intra-articular fractures in vivo. Nevertheless, a limitation of this study is the post-fracture conditions, including the lack of blood supply and synovial and cellular reaction the injury. These otherwise may contribute to subsequent progression of chondrocyte death. However, an advantage of the lack of these “extrinsic” biological influences following injury is that it was possible to study the isolated effect of mechanical insult to the articular surface. Another potential limitation is that, since the ankles utilized were from patients who had malignant tumor, these joints may have been load-protected for a certain period prior to amputation. Systemic chemotherapy before surgery also might have influenced chondrocyte activity. However, cells in non-fracture regions retained high fractional viability at most sites even at two days post-fracture, suggesting that the articular cartilage in these joints was initially reasonably healthy. Similarly, the potential adverse effects of ex vivo experimentation on chondrocyte viability were also presumed to be noncritical. A strength of this study was that the insult methodology utilized to produce the fractures in these joints mimicked an injury mechanism typical of clinical tibial plafond fractures. Given that the fractures introduced were morphologically consistent with this type of fracture as seen clinically, the physiologic clinical injury mechanism arguably was appropriately replicated in this model.

The appreciable chondrocyte death identified along fracture lines in the present study is consistent with observations in previous studies that explored fracture-associated cartilage pathology in small osteoarticular fragments during surgery for intra-articular fracture fixation[7-9]. The low fractions of cell death across non-fracture regions, documented in our study, indicate that chondrocyte death in fractured human joints occurs predominantly near fracture lines. Chondrocyte damage in intra-articular fractures appears to be closely associated with structural damage of the articular surface, just as suggested by cartilage blunt-impact experiments[11,12] and by blunt-wounding experiments[13,14] (in which blunt wounding introduced more severe chondrocyte damage than a sharp scalpel cut). Assuming that the majority of chondrocyte damage occurs along fracture lines, the degree of whole-joint chondrocyte dysfunction would presumably be correlated with the total length of fracture lines, which in turn correlates with mechanical energy absorption during the fracture event[15,16]. This observation supports the concept that joints with more severely comminuted articular surfaces sustain a greater insult to cartilage metabolism, and therefore are at a greater risk of posttraumatic OA.

The measured time-dependent increase of cell death in fracture-edge regions indicates that chondrocyte damage in these fractures propagates spontaneously with time. The chondrocyte death identified immediately post-fracture was presumably cell necrosis, due to excessive acute mechanical stresses from the fracture. These physical stresses might have caused delayed apoptosis, which would have contributed to the acute-phase propagation of chondrocyte damage identified at the later observation times. Another possible contributing factor is the cytotoxic effect of biochemical mediators released from damaged chondrocytes and/or from the disrupted extracellular matrix, similar to that observed in cartilage-explant blunt-impact studies[17-19]. In intra-articular fractures in vivo, acutely damaged cartilage is also subsequently subjected to biological stimuli associated with joint bleeding and/or inflammatory responses, including factors known to accelerate cartilage degeneration, such as reactive oxygen species, matrix-damaging enzymes, inflammatory cells, and inflammatory cytokines[20-25]. Arguably, chondrocyte damage in fractured joints is therefore not fully established at the instant of injury event. There may be a certain window of time during which biological treatment may be able to inhibit progression of chondrocyte damage in the early acute phase, potentially moderating the pathological cascade that leads to posttraumatic OA.

Chondrocyte death that predominated along fracture lines in this study suggests that whole-organ cell-level cartilage damage in a fractured human ankle joint is dependent on the total fracture line length and is therefore closely associated with the initial injury severity. Progression of chondrocyte death during the two days of cartilage culture suggests that the fracture-associated cell-level cartilage damage propagates spontaneously with time during the early acute phase. In the somewhat analogous situations of acute myocardial infarction and ischemic stroke, early thrombolytic therapy to minimize progressive cell death has led to dramatic improvement of clinical outcomes[26,27]. A similar concept may apply to treatment of intra-articular fracture. Arguably, the most effective treatment to mitigate the risk of posttraumatic OA would not only treat macroscopic damage with anatomical fracture reduction and fixation but would also seek to preserve viable, metabolically effective chondrocytes. ■

Yuki Tochigi, MD, PhD
Tanawat Vaseenon, MD
Thomas D. Brown, PhD
Department of Orthopaedics and Rehabilitation (Y.T., T.V., and T.D.B.)

and Department of Biomedical Engineering (T.D.B.),
The University of Iowa,
2181 Westlawn,
Iowa City, IA 52242.
E-mail address for Y. Tochigi: yuki-tochigi@uiowa.edu

Joseph A. Buckwalter, MS, MD
Department of Orthopaedics and Rehabilitation,
The University of Iowa,
200 Hawkins Drive,
Iowa City, IA 52242

James A. Martin, PhD
Peng Zhang, MD
Abigail D. Lehman, BS
Department of Orthopaedics and Rehabilitation,
The University of Iowa,
1182 ML, Iowa City, IA 52242

Stephen L. Hillis, PhD
The Center for Research in the Implementation of Innovative Strategies
in Practice (CRIISP), VA Iowa City Medical Center, 152 VA,
Iowa City, IA 52242

References

1. Etter C, Ganz R. Long-term results of tibial plafond fractures treated with open reduction and internal fixation. Arch Orthop Trauma Surg. 1991;110:277-83.

2. Marsh JL, Weigel DP, Dirschl DR. Tibial plafond fractures. How do these ankles function over time? J Bone Joint Surg Am. 2003;85:287-95.

3. Ovadia DN, Beals RK. Fractures of the tibial plafond. J Bone Joint Surg Am. 1986;68:543-51.

4. Teeny SM, Wiss DA. Open reduction and internal fixation of tibial plafond fractures. Variables contributing to poor results and complications. Clin Orthop Relat Res. 1993;292:108-17.

5. Buckwalter JA, Brown TD. Joint injury, repair, and remodeling: roles in post-traumatic osteoarthritis. Clin Orthop Relat Res. 2004;423:7-16.

6. Furman BD, Olson SA, Guilak F. The development of posttraumatic arthritis after articular fracture. J Orthop Trauma. 2006;20:719-25.

7. Hembree WC, Ward BD, Furman BD, Zura RD, Nichols LA, Guilak F, Olson SA. Viability and apoptosis of human chondrocytes in osteochondral fragments following joint trauma. J Bone Joint Surg Br. 2007;89:1388-95.

8. Kim HT, Lo MY, Pillarisetty R. Chondrocyte apoptosis following intraarticular fracture in humans. Osteoarthritis Cartilage. 2002;10:747-9.

9. Murray MM, Zurakowski D, Vrahas MS. The death of articular chondrocytes after intra-articular fracture in humans. J Trauma. 2004;56:128-31.

10. Verbeke G, Molenberghs G. Linear mixed models for longitudinal data. New York: Springer; 2000. p 41-99.

11. Ewers BJ, Dvoracek-Driksna D, Orth MW, Haut RC. The extent of matrix damage and chondrocyte death in mechanically traumatized articular cartilage explants depends on rate of loading. J Orthop Res. 2001;19:779-84.

12. Lewis JL, Deloria LB, Oyen-Tiesma M, Thompson RC Jr, Ericson M, Oegema TR Jr. Cell death after cartilage impact occurs around matrix cracks. J Orthop Res. 2003;21:881-7.

13. Tew SR, Kwan AP, Hann A, Thomson BM, Archer CW. The reactions of articular cartilage to experimental wounding: role of apoptosis. Arthritis Rheum. 2000;43:215-25.

14. Redman SN, Dowthwaite GP, Thomson BM, Archer CW. The cellular responses of articular cartilage to sharp and blunt trauma. Osteoarthritis Cartilage. 2004;12:106-16.

15. Beardsley CL, Anderson DD, Marsh JL, Brown TD. Interfragmentary surface area as an index of comminution severity in cortical bone impact. J Orthop Res. 2005;23:686-90.

16. Anderson DD, Mosqueda T, Thomas T, Hermanson EL, Brown TD, Marsh JL. Quantifying tibial plafond fracture severity: absorbed energy and fragment displacement agree with clinical rank ordering. J Orthop Res. 2008;26:1046-52.

17. Clements KM, Burton-Wurster N, Lust G. The spread of cell death from impact damaged cartilage: lack of evidence for the role of nitric oxide and caspases. Osteoarthritis Cartilage. 2004;12:577-85.

18. Levin A, Burton-Wurster N, Chen CT, Lust G. Intercellular signaling as a cause of cell death in cyclically impacted cartilage explants. Osteoarthritis Cartilage. 2001;9:702-11.

19. Goodwin W, McCabe D, Sauter E, Reese E, Walter M, Buckwalter JA, Martin JA. Rotenone prevents impact-induced chondrocyte death. J Orthop Res. 2010;28:1057-63.

20. Goldring SR, Goldring MB. The role of cytokines in cartilage matrix degeneration in osteoarthritis. Clin Orthop Relat Res. 2004;427 Suppl:S27-36.

21. Hedbom E, Häuselmann HJ. Molecular aspects of pathogenesis in osteoarthritis: the role of inflammation. Cell Mol Life Sc. 2002;59:45-53.

22. Henrotin Y, Kurz B, Aigner T. Oxygen and reactive oxygen species in cartilage degradation: friends or foes? Osteoarthritis Cartilage. 2005;13:643-54.

23. Hooiveld M, Roosendaal G, Wenting M, van den Berg M, Bijlsma J, Lafeber F. Short-term exposure of cartilage to blood results in chondrocyte apoptosis. Am J Pathol. 2003;162:943-51.

24. John T, Stahel PF, Morgan SJ, Schulze-Tanzil G. Impact of the complement cascade on posttraumatic cartilage inflammation and degradation. Histol Histopathol. 2007;22:781-90.

25. Martin JA, McCabe D, Walter M, Buckwalter JA, McKinley TO. N-acetylcysteine inhibits post-impact chondrocyte death in osteochondral explants. J Bone Joint Surg Am. 2009;91:1890-7.

26. Indications for fibrinolytic therapy in suspected acute myocardial infarction: collaborative overview of early mortality and major morbidity results from all randomised trials of more than 1000 patients. Fibrinolytic Therapy Trialists' (FTT) Collaborative Group. Lancet. 1994;343:311-22.

27. Wardlaw JM, Zoppo G, Yamaguchi T, Berge E. Thrombolysis for acute ischaemic stroke. Cochrane Database Syst Rev. 2003;3:CD000213.

Osteoarthritis and Cartilage 21 (2013) 200–208

Osteoarthritis and Cartilage

OSTEOARTHRITIS RESEARCH SOCIETY INTERNATIONAL

A novel impaction technique to create experimental articular fractures in large animal joints

Y. Tochigi †*, P. Zhang †‡, M.J. Rudert †, T.E. Baer †, J.A. Martin †, S.L. Hillis §||, T.D. Brown †¶

† *Department of Orthopaedics and Rehabilitation, University of Iowa, United States*
‡ *Department of Orthopaedics, Affiliated Hospital of Shan Dong University of Traditional Chinese Medicine, China*
§ *Department of Biostatistics, University of Iowa, United States*
|| *Center for Research in the Implementation of Innovative Strategies in Practice (CRIISP), VA Iowa City Medical Center, United States*
¶ *Department of Biomedical Engineering, University of Iowa, United States*

ARTICLE INFO

Article history:
Received 14 March 2012
Accepted 4 October 2012

Keywords:
Intra-articular fracture
Animal modeling
Mechanical insult
Cartilage injury
Chondrocyte death

SUMMARY

Objective: A novel impaction fracture insult technique, developed for modeling post-traumatic osteoarthritis in porcine hocks *in vivo*, was tested to determine the extent to which it could replicate the cell-level cartilage pathology in human clinical intra-articular fractures.
Design: Eight fresh porcine hocks (whole-joint specimens with fully viable chondrocytes) were subjected to fracture insult. From the fractured distal tibial surfaces, osteoarticular fragments were immediately sampled and cultured *in vitro* for 48 h. These samples were analyzed for the distribution and progression of chondrocyte death, using the Live/Dead assay. Five control joints, in which “fractures” were simulated by means of surgical osteotomy, were also similarly analyzed.
Results: In the impaction-fractured joints, chondrocyte death was concentrated in regions adjacent to fracture lines (near-fracture regions), as evidenced by fractional cell death significantly higher ($P < 0.0001$) than in central non-fracture (control) regions. Although nominally similar spatial distribution patterns were identified in the osteotomized joints, fractional cell death in the near-osteotomy regions was nine-fold lower ($P < 0.0001$) than in the near-fracture regions. Cell death in the near-fracture regions increased monotonically during 48 h after impaction, dominantly within 1 mm from the fracture lines.
Conclusion: The impaction-fractured joints exhibited chondrocyte death characteristics reasonably consistent with those in human intra-articular fractures, but were strikingly different from those in “fractures” simulated by surgical osteotomy. These observations support promise of this new impaction fracture technique as a mechanical insult modality to replicate the pathophysiology of human intra-articular fractures in large animal joints *in vivo*.

Introduction

Intra-articular fractures are a leading cause of post-traumatic osteoarthritis (OA)[1]. Recently, the acute cell-level cartilage damage involved in intra-articular fractures has been receiving increasing attention[2–8]. Death or dysfunction of chondrocytes necessarily affects cartilage metabolism in injured joints, presumably triggering a pathological cascade that eventually leads to OA. Therapeutic treatments that amend this disease process (as adjuncts to current surgical treatment) hold potential to mitigate the risk of OA development following intra-articular fractures. Several types of biologic treatments have proven capable of preserving the viability and/or function of chondrocytes in cartilage explants after mechanical or biochemical insult[3,9,11,14–16]. However, progress in translation of these scientific developments into clinical practice has been limited by the lack of a large animal survival model that physiologically mimics human intra-articular fractures, and that is in a size range compatible with surgical procedures utilized in human clinical settings.

For an animal disease model to be scientifically valid, pathophysiological realism is crucial. In the case of intra-articular fracture, this is presumably achievable by fracturing animal joints using

* Address correspondence and reprint requests to: Y. Tochigi, University of Iowa Orthopaedic Biomechanics Laboratory, 2181 Westlawn, Iowa City, IA 52242-1100, United States. Tel: 1-319-335-7547; Fax: 1-319-335-7530.

E-mail addresses: yuki-tochigi@uiowa.edu (Y. Tochigi), pengzhang.med@gmail.com (P. Zhang), jim-rudert@uiowa.edu (M.J. Rudert), thomas-baer@uiowa.edu (T.E. Baer), james-martin@uiowa.edu (J.A. Martin), steve-hillis@uiowa.edu (S.L. Hillis), tom-brown@uiowa.edu (T.D. Brown).

1063-4584/$ – see front matter
http://dx.doi.org/10.1016/j.joca.2012.10.004

a mechanical insult modality that reasonably replicates the injury mechanism of human clinical intra-articular fractures. For this purpose, a new fracture insult technique is here reported, that replicates the typical mechanism of human distal tibial plafond (pilon) fractures. In this technique, the porcine hock joint (human ankle analog) is subjected to an injurious transarticular compressive force pulse, causing impaction fracture.

The objective of the present study was to determine the extent to which this new insult modality was capable of replicating the pathophysiological reality of human intra-articular fractures. For this purpose, two hypotheses were tested. First, we tested whether experimental joints insulted using the new impaction fracture technique would exhibit cell-level cartilage damage consistent with that in human intra-articular fractures[2–4,7,9]. Specifically, this involved cell-level cartilage damage in the fracture-insulted joints being characterized by chondrocyte death concentrated near fracture lines. Second, we tested whether fractional chondrocyte death in these fracture-insulted joints would be significantly higher than that in “fractures” simulated by means of surgical osteotomy, as often has been used experimentally[10–12]. In addition, the temporal and spatial progression of cell death was evaluated for intervals up to 48 h post-impaction.

Methods

Thirteen fresh hock joints from agricultural pigs (age 9–12 months, weight 120–150 kg) were obtained from a local abattoir. These specimens, harvested from animal bodies chilled overnight after euthanasia (following the United States Department of Agriculture regulations), were insulted within 24 h of animal death. Soft tissue surrounding the joint was removed, while leaving the joint capsule and major ligaments intact. Eight specimens were subjected to the impaction fracture insult, while the remaining five were subjected to surgical osteotomy (i.e., fracture simulation control).

For the impaction fracture insult, the joint was mounted in a custom bone anchorage system [Fig. 1(A)]. In this system, an aluminum impact interface was connected to the talus, using three external fixator pins (6-mm diameter, Orthofix Inc., Lewisville, Texas, USA) arrayed in a tripod configuration. Two of these tripod pins were inserted directly into the talus, from inferomedially, toward the talar body. The third pin was inserted from the calcaneus to the talus, though the talocalcaneal joint. The tibia was restrained by a leg holder device, which consisted of a distal tibial plate and a solid rod. A ball-in-socket joint between the plate and the rod provided rotational adjustability, allowing the joint to be aligned appropriately relative to the impact force direction. This tibial plate was secured to the anterior distal tibial surface by two pegs on the plate, and by a cortical screw. An external fixator pin connected the rod to the proximal tibia, in order to maintain predetermined inclination of the tibial shaft (approximately 45°). This tibial inclination created an “offset” condition, by means of which a force pulse applied to the joint caused sudden elevation of vertical shear stresses in the anterior tibial juxta-articular bone. A stress-rising sawcut was used to guide the location and orientation of fracture, to create fractures morphologically similar to human ankle anterior malleolar fractures. This cut was made on the anterior distal tibial cortex, 2–3 mm distal to the distal tibia plate, using a bone oscillator (HALL® oscillator, ConMed Corp., Largo, Florida, USA), typically stopping 5–7 mm short of the undersurface of the subchondral plate.

Thus anchored, the specimen was then mounted in a custom drop-tower device [Fig. 1(B)], with the tibial side down, and with the distal impact face carefully aligned with the axis of mass fall. The tibial potting block was secured to a massive base plate. The distal impact face was lightly held (using masking tape) as horizontal as possible. A 6.55-kg mass was then dropped from 47-cm height, delivering approximately 30 J of kinetic energy to the specimen. (Note: In pilot work, impaction insult in a no-stress-riser condition at 80 J of energy delivery resulted in morphologically inconsistent distal tibial fractures, including highly comminuted fractures inadequate for survival animal modeling.) In the five control specimens, simulated “fractures” at the distal tibia were created, morphologically similar to those from the drop-tower impactions. In these control specimens, anterior tibial sawcuts were similarly made, but the simulated “fractures” were finished using a surgical osteotome, instead of by a falling mass.

Immediately after fracture creation, the joints were disarticulated, and the distal tibial articular surfaces were digitally photographed to record the fracture morphology. Next, using sterile technique, major osteoarticular fragments were sampled for chondrocyte death measurement. Due to the complicated

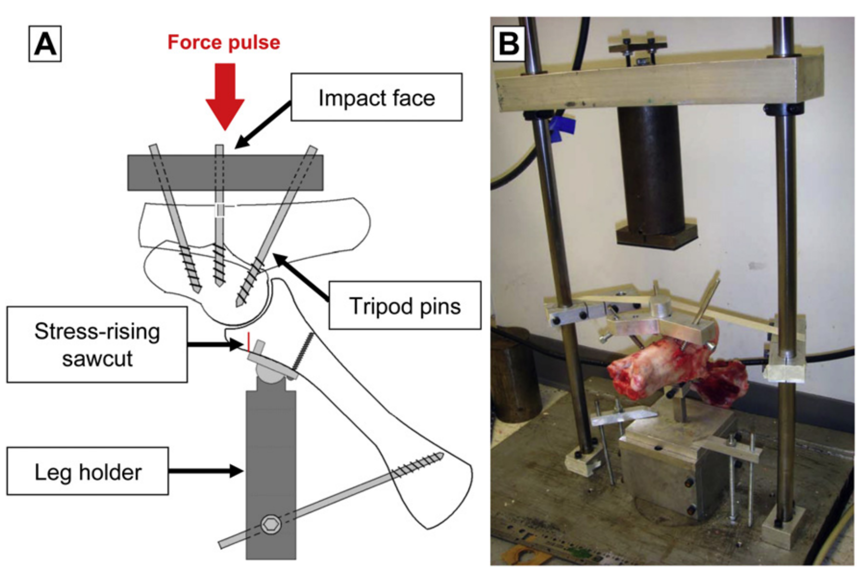

Fig. 1. (A) Schematic of the tripod bone anchorage system for the “offset” fracture impaction technique. (B) A porcine hock specimen mounted using the anchorage system, in the custom drop-tower system for delivering a fracture impaction force pulse.

geometry of the porcine distal tibial articular surface, to facilitate mircoscopy of the cartilage surface, large osteoarticular fragments were dissected into small pieces, with juxta-articular bone being trimmed away, leaving approximately a 5-mm thickness of cancellous bone beneath the cartilage layer. From each joint, three to five osteoarticular fragments were sampled, with a typical volume per specimen of approximately 1 cm^3. Each osteoarticular fragment was then secured to a specimen holder [Fig. 2(A and B)], such that the articular surface near the fracture edge was held nearly horizontal, by potting in a non-exothermic biocompatible polymer (Polycaprolactone, Sigma–Aldrich, Inc., St. Louis, Missouri, USA). The potted specimen was then immersed in culture medium (approximately 80 mL per specimen), comprised 45% Ham's F-12 Nutrient Mixture, 45% high glucose Dulbecco's Modified Eagle Medium, and 10% fetal bovine serum (all from Invitrogen Co., Carlsbad, California, USA), with 1% anti-bacterial/-fungal mixture of pencicillin–streptomycin (Invitrogen) and amphotericin B (Thermo Scientific HyClone, Logan, Utah, USA), in an incubator maintained at 37°C under 5% CO_2.

After 48 h of culture, chondrocyte death in these osteoarticular fragments was assessed using calcein AM for labeling live cells and ethidium homodimer-2 for labeling dead cells (again, both from Invitrogen Co.). Prior to analysis, the fragments were soaked in culture medium with these fluorescent stains (at a concentration of 1.0 μM each) for approximately 1 h at 37°C. For each joint, scans of $540 \times 540\ \mu^2$ fields were executed at several sites adjacent to the primary fracture (or osteotomy) line (designated as the near-edge region), as well as at several sites centrally away from fragment edges in non-fracture areas (designated as the central region). For these central-region scans, any sites with macroscopically identifiable structural damage (e.g., visible superficial cracks) were avoided. For every near-edge or central site, cartilage in the superficial zone (i.e., from the articular surface to a depth of typically 100–150 μ) was scanned at 20-μ intervals, using a confocal microscopy system (MRC-1024, Bio-Rad Laboratories, Hercules, California, USA). During scanning (which required 1–2 h), the specimens were kept immersed in the regular medium at room temperature.

Of the eight impaction-fractured joints, three were scanned at multiple time points. From each of these three joints, three osteoarticular fragments were selected that included a relatively uniform primary fracture line. At the initial scanning time point (within 2 h post-impact), for each fragment, two neighboring sites along the primary fracture line [Fig. 2(C)] were selected, separated by 1 mm. For all of these paired fracture-edge sites, three contiguous 540×540 μ fields (one including the fracture line, along with the two next-centrally-adjacent image fields) were scanned. Typically, this allowed scanning out to 1.4 mm away from the fracture line. For each near-fracture site, two central-region sites at least 3 mm away from the fracture line were also scanned. Of these two groups of scan sites established for each fragment, one was subjected to follow-up scanning at 6 and 12 h post-fracture, and the other at 24 and 48 h post-fracture. The x–y coordinate information at the initial scanning was recorded. Based on this coordinate information, scans at the later time points were repeated at the identical sites, using a custom-built programmable microscope x–y axis stage driver (positioning reproducibility < 25 μ). After each scanning session, the specimens were washed with Hanks balanced salt solution (#14170, Gibco-Invitrogen, Grand Island, New York, USA), containing 1% of the above-described anti-bacterial/-fungal mixture, after which they were placed into fresh culture media.

The scanned images were analyzed using ImageJ software (National Institute of Health, Bethesda, Maryland, USA). Image data for each site/time point consisted of two sets of multi-slice images, one for live cells labeled by green fluorescence, and the other for dead cells labeled by red fluorescence. The images, originally in gray scale, were converted to a binary format, allowing fluorescent-labeled cells to be counted using the software's particle analysis

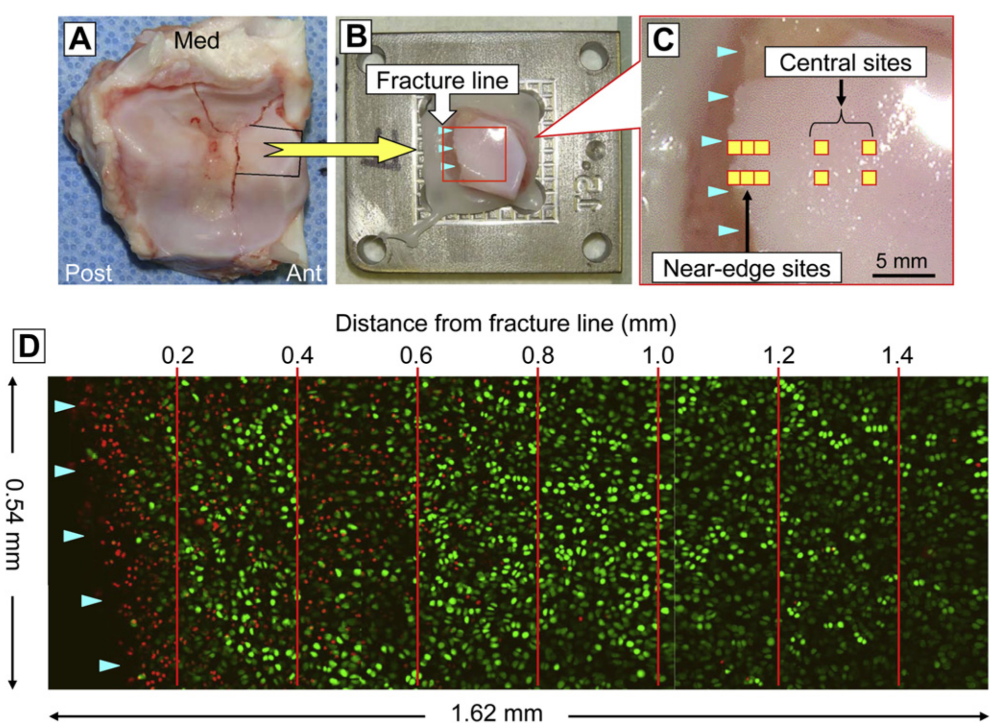

Fig. 2. Chondrocyte viability analysis. (A) Specimen sampling from the fractured distal tibial surface. (B) An osteoarticular sample mounted on the specimen holder. (C) Scanning site selection for the time course analysis. (D) Live/Dead cell counting in the superficial zone (within 100–150 μ of the articular surface), in 0.2-mm intervals in a region neighboring a fracture line.

function. For every image set for live cells, the image intensity threshold for the binary conversion was adjusted such that all plausibly labeled cells were counted, and such that the same cells were not counted over neighboring multiple slices. The identical binary conversion threshold was utilized for cell counting for the corresponding dead-cell image set. The minimum particle size thresholds for automated cell counting were 50 and 20 μ^2 for live and dead cells, respectively. Live and dead cells were counted separately, and the fraction of dead cells among total cells (fractional cell death) in the region of interest was computed. Confocal images from multiple-time-point scans in near-edge regions, consisting of three contiguous scan fields, were parsed into seven zones in 0.2-mm intervals, and fractional cell death was computed separately for each zone [Fig. 2(D)].

Differences in fractional cell death between the near-edge and central regions were analyzed using a logistic regression model with specimen-random effects (also known as a hierarchical generalized linear model or a generalized linear model with random effects), using SAS® (Ver. 9.1.3, SAS Institute Inc., Cary, North Carolina, USA). Specifically, the fractional cell death data were treated as "pseudo-binomial" variables, i.e., the relationship of the mean and variance was assumed to be the same as for a binomial-variable proportion computed from independent trials (Appendix). Inclusion of the random effects accounted for within-specimen correlation, thus allowing conclusions to be generalized to the population of specimens from which the samples were considered representative, rather than being limited only to the specific specimens evaluated. Thus, the model accounted for the dependence of the variance of outputs on the true fractional cell death and on the number of cells, while also accounting for variability in the fractional cell death across specimens. There were four comparisons of interest; using a Bonferroni correction for multiple tests to limit the overall type I error to 0.05, these tests were considered conclusive if $P < 0.05/4 = 0.0125$. Mean values, 95% confidence intervals (CIs), and inter-quartile ranges (IQRs) were reported. For the time-wise analysis, given the small number of specimens ($n = 3$), it was not feasible to use the above specimen-random-effects approach for detecting difference in the time-dependency of cell death between near-edge versus central (control) regions at any given time. Instead, six comparisons were made for each observation time, using two-sample t-tests. These time-wise comparisons were considered conclusive if $P < 0.05/6 = 0.0083$.

Results

At gross morphological inspection, all eight impacted joints were found to have a distal tibial fracture, with the primary fracture line running medially–laterally, typically in the anterior one-third of the distal tibial surface [Fig. 3(A)]. In these impaction-fractured joints, fractional cell death at 48 h post-fracture was measured at 43 near-edge and 72 central sites (total counts across the eight joints). Time-wise changes in cell death were assessed at nine near-edge and 18 central sites across three of the eight joints. Simulated "fractures" in the five osteotomized joints [Fig. 3(B)] also exhibited similar gross morphological characteristics. Cell death in these osteotomized joints was assessed at 36 near-edge and 58 central sites.

In the 48-h scan data for the impaction-fractured joints (Figs. 4 and 5), the local fractional cell death ranged from 0.6 to 97.1% (IQR: 17.8–46.7) in near-edge regions (typically up to 0.3–0.4 mm away from a fracture line), and from 0.0 to 26.0% (IQR: 0.5–5.4) in central regions. The death fraction in near-edge regions (38.1%, CI: 25.7–52.2) was significantly higher ($P < 0.0001$) than that in central regions (4.6%, CI: 2.6–7.9). In the osteotomized specimens, death

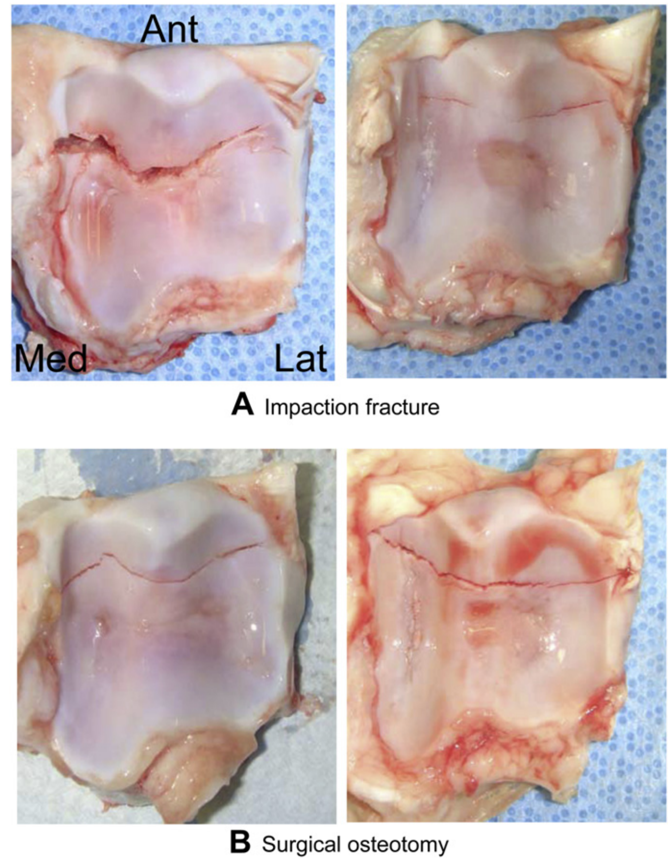

Fig. 3. Examples of (A) experimental porcine distal tibial fractures created using the offset impaction technique and (B) "fractures" conventionally simulated by surgical osteotomy.

fraction ranged from 0.0% to 18.7% (IQR: 1.1–9.9%) in near-edge regions and from 0.0 to 15.9% (IQR: 0.1–1.4%) in central regions. The death fraction in near-edge regions (4.3%, CI: 2.1–8.6) was again significantly higher ($P < 0.0001$) than that in central regions (1.0%, CI: 0.5–2.0). When data were compared regarding the two insult modalities, for both near-edge and central regions, the death fraction in the impaction-fractured specimens was significantly higher (near-edge: $P < 0.0001$; central: $P = 0.0009$) than in the osteotomized specimens.

Regarding time-wise analysis (Fig. 6), at the initial scanning time (within 2 h of fracture), fractional cell death was comparable between near-edge regions (in this dataset, up to 1.4 mm away from a fracture line) and central regions, in both of the 6–12- and 24–48-h datasets ($P = 0.56$ and 0.43, respectively). In both datasets, as cell death progressed with time dominantly in cartilage adjacent to the fracture lines, the difference attained statistical significance at 12 h ($P < 0.001$), and remained so at 24 and 48 h ($P = 0.0002$ and <0.0001, respectively). When distributions of fractional cell death across the seven 0.2 mm-wide zones adjacent to the fracture lines were plotted for individual specimen/site combinations (Fig. 7), distinctly high levels of chondrocyte death (indicated by fractional cell death exceeding the mean plus two standard deviations of the control central-region data) were typically identified within 1.0 mm of the fracture lines.

Discussion

The present study tested a novel mechanical insult modality suitable for modeling human clinical intra-articular fractures in

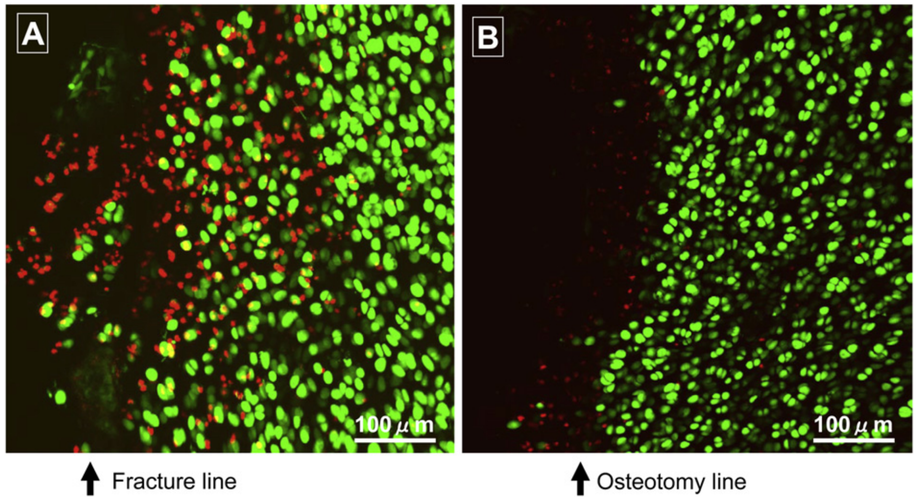

Fig. 4. Confocal microscope images of superficial chondrocyte viability in representative regions adjacent to a fracture line (A) or an osteotomy line (B), at 48 h post-insult. Live cells are labeled by green fluorescence, while dead cells are labeled red.

large animal joints (here, porcine hocks) *in vivo*. This modality, designated as the "offset" impaction technique, was evaluated in a bench-top setting using fresh porcine hock specimens with initially full chondrocyte viability. Osteoarticular samples harvested from these joints were cultured *in vitro* and then subjected to cell death measurement. This *ex vivo* setting of course did not incorporate any effects from injury-associated biological responses, such as intra-articular bleeding and/or synovial inflammation.

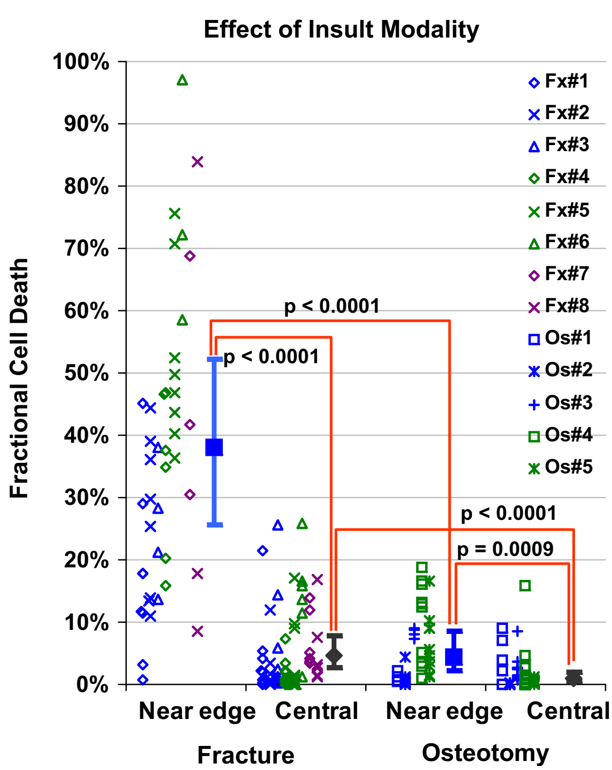

Fig. 5. Chondrocyte viability in the superficial zone, at 48 h after impaction fracture versus osteotomy, in near-edge regions (typically up to 0.3–0.4 mm away from a fracture/osteotomy line) and in central (control) regions. The scatter plots indicate fractional cell death for each specimen/site combination, from the eight impaction-fractured (Fx) and five osteotomized (Os) specimens. The filled squares/diamonds and dispersion bars indicate (estimated) means calculated in the logistic regression analysis, and 95% confidential intervals, respectively.

While this was a limitation in terms of injury realism, the lack of these extrinsic biological influences held the advantage of allowing study of the isolated effects of mechanical insult to articular cartilage. In this culture setting, exposed cancellous bone might have released molecules potentially injurious to cartilage, but any such effects would have been consistent across sites, specimens, and experimental groups. It should be noted that the drop-tower impaction system utilized in the present study was adopted for experimental convenience, but was not suitable for fracture insult to animal joints *in vivo*. Producing similar insults in survival animal surgery requires positioning flexibility for attachment to the joint of interest, while permitting the animal's body to be held in a position appropriate for anesthesia and surgical management. These latter requirements are satisfied by use of a pendulum-based impaction system [Fig. 8(A)], which consistently produces similarly well-controlled fracture patterns in porcine hocks *in vivo* [Fig. 8(B)].

Cell-level acute cartilage damage in the impaction-fractured joints was characterized by chondrocyte death being concentrated along fracture lines. This spatial distribution pattern is analogous to that observed in small (surgical discard) osteoarticular fragments from clinical fracture cases[2–4], as well to as that in previous whole-joint quasi-*in-vivo* models that utilized an insult modality closely replicating the injury mechanisms in human clinical cases to create "true" intra-articular fractures in the human ankle[7] or the porcine stifle[9]. The fractional cell death in cartilage adjacent to fracture lines in the impaction-fractured joints (mean 38.1%, CI: 25.7–52.2) is very consistent with that observed in true human ankle fractures at the same time-point (25.9%, CI: 18.7–33.1) in the quasi-*in-vivo* study[7]. The present insult protocol included placement of a stress riser to guide the location and orientation of fracture. While this stress riser was necessary for reproducible fracture creation (both morphologically and severity-wise), use of the stress riser reduced the magnitude of energy delivery otherwise needed for fracture creation, less than 40% of the magnitude needed in a no-stress-riser condition in pilot work (i.e., 30 vs 80 J; unpublished data). Due to lack of ability to reproducibly create such no-stress-riser fractures, the effects of this energy reduction on cell death characteristics could not be studied. However, given the observations noted above, regardless of the reduced energy delivery, the offset impaction technique proved capable of introducing experimental articular fractures in the porcine hock that share pathophysiological characteristics with human clinical intra-articular fractures.

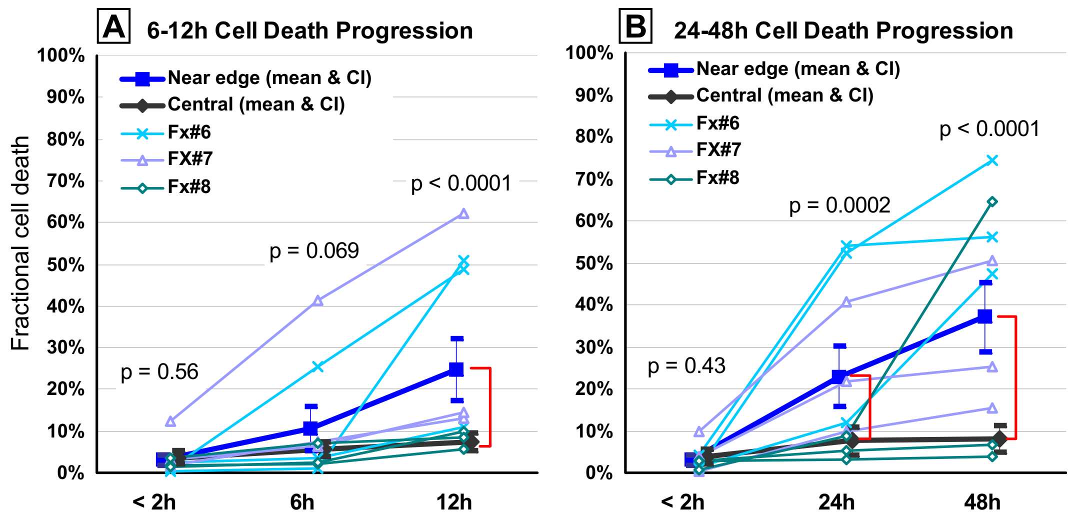

Fig. 6. Time course changes of fractional cell death in the superficial zone, in the 6–12- and 24–48-h datasets. The filled squares indicate the means of fractional cell death in seven 0.2 mm-wide zones in near-edge regions, while the filled diamonds are for those in central regions, both across nine observation sites in three joints The dispersion bars indicate 95% confidential intervals. Near-edge fractional death values for each specimen/site combination (the means across seven 0.2 mm-wide zones) are also individually plotted.

The "fractures" simulated by surgical osteotomy also exhibited cell death preferentially concentrated in regions adjacent to the "fracture" lines. However, the fractional cell death in these regions was much smaller (∼one-ninth) than that observed in corresponding regions in the impaction-fractured porcine joints, or in the above-mentioned human ankle quasi-*in-vivo* model[7]. This striking difference suggests that the physical stress to which chondrocytes were exposed was very different between these two insult modalities. One possible explanation for this difference is the extreme instantaneous cartilage deformation during a fracture event. During impaction, articular cartilage in the contact area would be highly compressed up until the instant when the cartilage–bone complex fractures, thus building up extremely high cartilage internal pressure. Once the articular surface fractures, however, cartilage along fracture lines would abruptly lose buttressing effects from the adjunct cartilage, resulting high stress gradients, leading to abrupt cartilage deformation that would damage chondrocytes.

The time-wise analysis characterized the process of cartilage damage progression in fractured joints. Although fractional cell death was variable across specimens/sites, relatively linear increase of cell death with time was exhibited in regions adjacent to fracture lines. This observation suggests involvement of active factors in contributing to the relatively broad (up to 1 mm) bands of cell death along fracture lines. The cause of this cell death progression might be from delayed apoptosis (resulting directly from physical stress at the instant of fracture), from the cytotoxic effect of biological mediators released from damaged chondrocytes and/or from the disrupted extracellular matrix[13–15], or both. Although the mechanisms of the delayed cell death were not explored in the present study, at the time immediately after injury, some of the dying cells might have been potentially rescuable. Assuming that the process of disease progression is similar in clinical intra-articular fractures, experimental articular fractures created in large animal *in vivo* using the present offset impaction technique would permit piloting new treatment strategies (such as cytoprotective intervention[16–21]) to

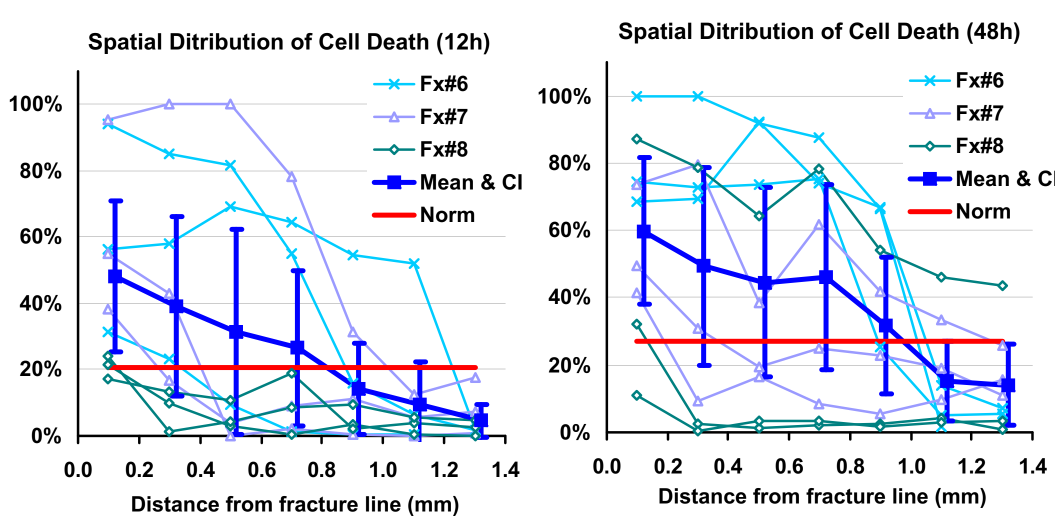

Fig. 7. Spatial distribution of fractional cell death in the superficial zone, at 12 or 48 h post-fracture. The filled squares and dispersion bars indicate the mean values and 95% confidential intervals of fractional cell death measured separately for seven 0.2 mm-wide zones. Data from each specimen/site combination are also individually plotted. The red solid lines indicate the upper limit of normative range (mean plus two standard deviations) of fractional death in central regions, at each observation time.

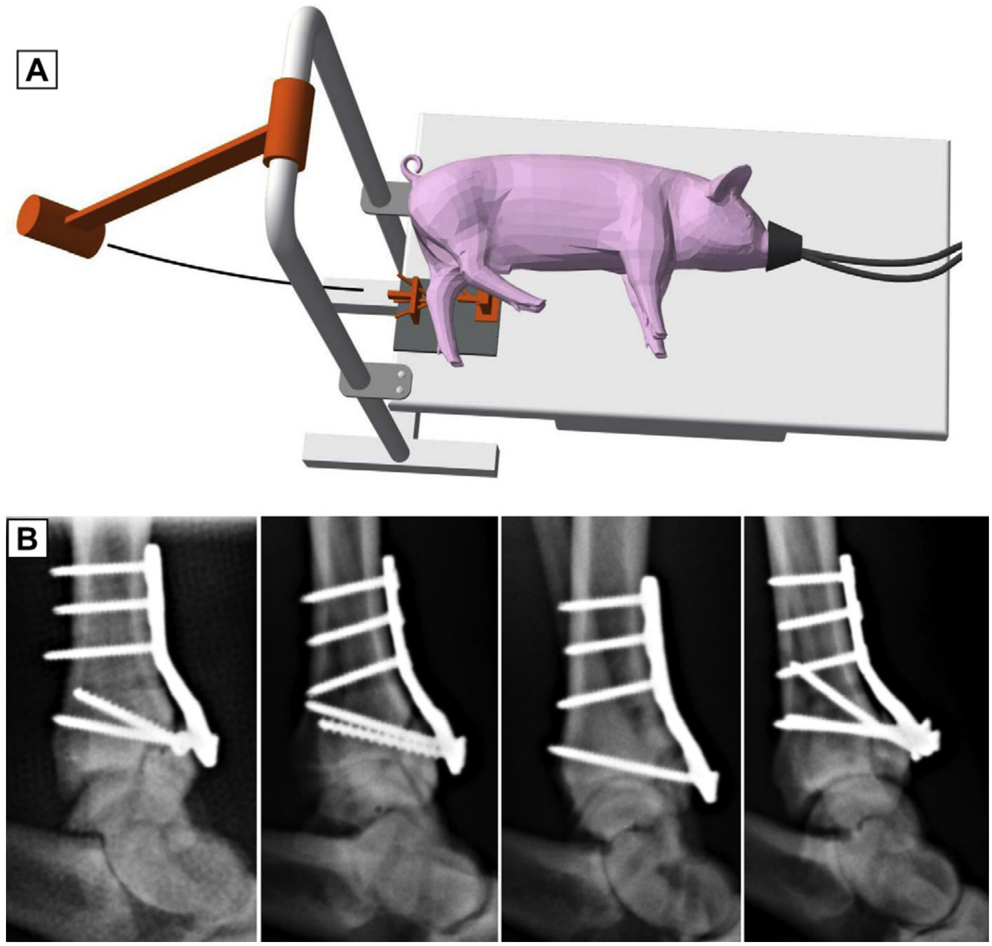

Fig. 8. (A) Schematic diagram of the pendulum impact device for delivering an impaction force pulse in survival animal surgeries. (B) Lateral radiographs of porcine hock experimental fractures created *in vivo*, using the offset impaction technique, in a pilot series ($n = 4$) of an ongoing survival study.

mitigate additional cartilage damage occurring during this period. Given the relatively monotonic increase of cell death with time, the best treatment outcome would be expected if such intervention is applied at the earliest possible time point.

In the present study, the pathology of fracture-associated cartilage injury was assessed in terms of chondrocyte death in the superficial zone, characteristics of which in intra-articular fractures have been well documented in the literature[2,7,9]. Cell viability was assessed only by a single technique, the Live/Dead assay, which did not discriminate the mechanisms of cell death. A major advantage of focusing only on cell death in the superficial zone was that repetitive measurements at the same sites enabled longitudinal observations of changes in the cell death distribution. Unfortunately, as a trade-off, the associated restriction in specimen positioning (due to specimen potting) did not permit assessing cell death on cross sections, and pathological details of fracture-associated cartilage damage in deeper zones could not be explored. In a previous study, Backus *et al.*[9] assessed details of the cross-sectional distribution of cell death in porcine stifle intra-articular fractures created (*ex vivo*) by means of an impaction insult to whole-joint constructs. They found that cell death in regions immediately adjacent to fracture lines (within 100 μ) was distributed across the entire thickness, whereas that in the next-neighboring regions (100–200 μ) was concentrated in the superficial zone. Given the similarities of the fracture insult methodology, similar cross-sectional fractional death distributions presumably occurred in the present study. Additional key observations by Backus *et al.*[9] were that central non-fracture regions on fractured surfaces exhibited a relatively small fraction of cell death, limited to the superficial zone, and that similar cell death characteristics were found in joints after an equivalent magnitude of non-fracturing impaction. These previous observations, along with the relatively small fraction of superficial cell death in central non-fracture regions in the present study, suggest that cartilage-on-cartilage blunt impaction is not a major cause of the cell-level cartilage injury seen for intra-articular fractures.

In conclusion, the offset impaction technique documented in the present study was capable of reproducibly creating morphologically well-controlled experimental articular fractures in porcine hocks. Cartilage damage resulting from fracture-line-controlled impacts was not noticeably different from that in the existing knowledge base of non-fracture-line-controlled impacts (e.g., clinical intra-articular fractures), but strikingly different from that associated with surgical osteotomy. Given that the offset impaction technique is applicable to fracture insult *in vivo*, this novel insult modality holds promise for replicating the pathophysiology of human intra-articular fractures in a large animal survival model.

Author contributions

YT, MJR, and TEB contributed to the conception, design, and fabrication of the impaction fracture system. YT, PZ, and JAM contributed to the validation experiment and interpretation of the data. YT and SLH designed and conducted statistical analysis. TDB oversaw the overall study and contributed to manuscript preparation by providing critical suggestions, particularly for scientific content. All authors gave final approval of the manuscript version submitted.

Role of the funding source

The sponsors listed above were the only funding sources for this research project. None of the above-noted financial sponsors had any involvement in the process of data analysis or manuscript preparation.

Conflict of interest

None.

Acknowledgments

This research was supported by the University of Iowa Biological Sciences Funding Program, by an Orthopaedic Trauma Association Research Grant, by NIH CORT Grant P50 AR055533, and by US Department of Defense CDMRP-PRORP Technology Development Award W81XWH-10-1-0864.

Appendix

Differences in fractional cell death between the near-edge and central regions were studied using a logistic regression model, with specimen-random effects. Inclusion of the random effects accounts for within-specimen correlation, thus allowing conclusions to be generalized to the overall population of specimens of which our sample can be considered representative, rather than being limited only to the specimens used in this particular experiment. Let Y_{ijkl} denote the fraction of dead cells observed at site l in specimen i at location level j ($j = 1$ if near-edge, 2 if central) subjected to insult type k ($k = 1$ if impaction fracture, 2 if osteotomy). For a given specimen, insult type, and location level, the Y_{ijkl} are assumed to be independent across sites with mean P_{ijk} and variance $P_{ijk}[1 - P_{ijk}]/n_{ijkl}$, where n_{ijkl} is the total number of cells corresponding to Y_{ijkl}. Thus we are treating Y_{ijkl} as a "pseudo-binomial" variable, in the sense that we assume the relationship of its mean (i.e., probability of cell death) and variance is similar to that for a binomially-variable proportion. Our motivation for this approach is as follows: Although the fractional deaths are not true binomial variables (because they do not represent the ratio of a count over a total number of independent Bernoulli trials), they are similarly computed and bounded (by 0 and 1). See McCullagh and Nelder[22] for a discussion of this approach.

The P_{ijk} are modeled by the equation

$$\text{logit}\left(p_{ijk}\right) = \mu_{jk} + s_{i(k)};\ \ i = 1,\ldots,n_k;\ j = 1,2;\ k = 1,2$$

where $\text{logit}(P_{jk}) = \log[P_{jk}/(1 - P_{jk})]$, the μ_{jk} are fixed effects, $n_1 = 8$ and $n_2 = 5$ are the number of specimens subjected to impaction fracture and osteotomy, respectively, and the $s_{i(k)}$ are random effects (corresponding to specimens nested within insult type) that are independently and normally distributed with zero mean. This model allows the probability of cell death to depend on region (near-edge vs central) and to vary across specimens, with the population probability of death for location j and impact level k given by $\exp(\mu_{jk})/[1 + \exp(\mu_{jk})]$.

In summary, this model accounts for the dependence of the variance of the fractional cell death on the true proportions and the number of cells, and accounts for variability in the rates across specimens. Other names for this model are hierarchical generalized linear model and generalized linear model with random effects; see Raudenbush and Bryk[23] for a further discussion of such models. We fitted this model using PROC GLIMMIX in SAS® (Ver. 9.1.3, SAS Institute Inc., Cary, North Carolina, USA), with a logit link function and a binomial variance function. Pearson residual plots supported the use of the binomial variance function.

References

1. Brown TD, Johnston RC, Saltzman CL, Marsh JL, Buckwalter JA. Posttraumatic osteoarthritis: a first estimate of incidence, prevalence, and burden of disease. J Orthop Trauma 2006;20:739–44.
2. Hembree WC, Ward BD, Furman BD, Zura RD, Nichols LA, Guilak F, *et al.* Viability and apoptosis of human chondrocytes in osteochondral fragments following joint trauma. J Bone Joint Surg Br 2007;89:1388–95.
3. Kim HT, Lo MY, Pillarisetty R. Chondrocyte apoptosis following intraarticular fracture in humans. Osteoarthritis Cartilage 2002;10:747–9.
4. Murray MM, Zurakowski D, Vrahas MS. The death of articular chondrocytes after intra-articular fracture in humans. J Trauma 2004;56:128–31.
5. Furman BD, Olson SA, Guilak F. The development of posttraumatic arthritis after articular fracture. J Orthop Trauma 2006;20:719–25.
6. Furman BD, Strand J, Hembree WC, Ward BD, Guilak F, Olson SA. Joint degeneration following closed intraarticular fracture in the mouse knee: a model of posttraumatic arthritis. J Orthop Res 2007;25:578–92.
7. Tochigi Y, Buckwalter JA, Martin JA, Hillis SL, Zhang P, Vaseenon T, *et al.* Distribution and progression of chondrocyte damage in a whole-organ model of human ankle intra-articular fracture. J Bone Joint Surg Am 2011;93:533–9.
8. McKinley TO, Borrelli Jr J, D'Lima DD, Furman BD, Giannoudis PV. Basic science of intra-articular fractures and posttraumatic osteoarthritis. J Orthop Trauma 2010;24: 567–70.
9. Backus JD, Furman BD, Swimmer T, Kent CL, McNulty AL, Defrate LE, *et al.* Cartilage viability and catabolism in the intact porcine knee following transarticular impact loading with and without articular fracture. J Orthop Res 2011;29:501–10.
10. Lefkoe TP, Trafton PG, Ehrlich MG, Walsh WR, Dennehy DT, Barrach HJ, *et al.* An experimental model of femoral condylar defect leading to osteoarthrosis. J Orthop Trauma 1993;7: 458–67.
11. Convery FR, Akeson WH, Keown GH. The repair of large osteochondral defects. An experimental study in horses. Clin Orthop Relat Res 1972;82:253–62.
12. Vaseenon T, Tochigi Y, Heiner AD, Goetz JE, Baer TE, Fredericks DC, *et al.* Organ-level histological and biomechanical responses from localized osteoarticular injury in the rabbit knee. J Orthop Res 2011;29:340–6.
13. Clements KM, Burton-Wurster N, Lust G. The spread of cell death from impact damaged cartilage: lack of evidence for the role of nitric oxide and caspases. Osteoarthritis Cartilage 2004;12:577–85.
14. Levin A, Burton-Wurster N, Chen CT, Lust G. Intercellular signaling as a cause of cell death in cyclically impacted cartilage explants. Osteoarthritis Cartilage 2001;9:702–11.
15. Goodwin W, McCabe D, Sauter E, Reese E, Walter M, Buckwalter JA, *et al.* Rotenone prevents impact-induced chondrocyte death. J Orthop Res 2010;28:1057–63.
16. Ramakrishnan P, Hecht BA, Pedersen DR, Lavery MR, Maynard J, Buckwalter JA, *et al.* Oxidant conditioning protects cartilage from mechanically induced damage. J Orthop Res 2010;28:914–20.

17. Martin JA, McCabe D, Walter M, Buckwalter JA, McKinley TO. N-acetylcysteine inhibits post-impact chondrocyte death in osteochondral explants. J Bone Joint Surg Am 2009;91:1890–7.
18. D'Lima D, Hermida J, Hashimoto S, Colwell C, Lotz M. Caspase inhibitors reduce severity of cartilage lesions in experimental osteoarthritis. Arthritis Rheum 2006;54:1814–21.
19. Phillips DM, Haut RC. The use of a non-ionic surfactant (P188) to save chondrocytes from necrosis following impact loading of chondral explants. J Orthop Res 2004;22:1135–42.
20. Rundell SA, Baars DC, Phillips DM, Haut RC. The limitation of acute necrosis in retro-patellar cartilage after a severe blunt impact to the in vivo rabbit patello-femoral joint. J Orthop Res 2005;23:1363–9.
21. Kurz B, Lemke A, Kehn M, Domm C, Patwari P, Frank EH, *et al*. Influence of tissue maturation and antioxidants on the apoptotic response of articular cartilage after injurious compression. Arthritis Rheum 2004;50:123–30.
22. McCullagh P, Nelder JA. Generalized Linear Models. London, UK: Chapman and Hall; 1989. p. 328–32.
23. Raudenbush SW, Bryk AS. Hierarchical Linear Models: Applications and Data Analysis Methods. Thousand Oaks, California, USA: Sage Publications; 2002.

An Instrumented Pendulum System for Measuring Energy Absorption During Fracture Insult to Large Animal Joints in Vivo

B. W. Diestelmeier
Boston Scientific,
St. Paul, MN 55112-5798

M. J. Rudert
Department of Orthopaedics and Rehabilitation,
University of Iowa,
Iowa City, IA 52242-1100

Y. Tochigi
Department of Orthopaedics,
Dokkyo Medical University Koshigaya Hospital,
Saitama 343-8555, Japan

T. E. Baer
Department of Orthopaedics and Rehabilitation,
University of Iowa,
Iowa City, IA 52242-1100

D. C. Fredericks
Department of Orthopaedics and Rehabilitation,
University of Iowa,
Iowa City, IA 52242-1100

T. D. Brown
Department of Orthopaedics and Rehabilitation,
University of Iowa,
Iowa City, IA 52242-1100;
Department of Biomedical Engineering,
University of Iowa,
Iowa City, IA 52242-1527

For systematic laboratory studies of bone fractures in general and intra-articular fractures in particular, it is often necessary to control for injury severity. Quantitatively, a parameter of primary interest in that regard is the energy absorbed during the injury event. For this purpose, a novel technique has been developed to measure energy absorption in experimental impaction. The specific application is for fracture insult to porcine hock (tibiotalar) joints in vivo, for which illustrative intra-operative data are reported. The instrumentation allowed for the measurement of the delivered kinetic energy and of the energy passed through the specimen during impaction. The energy absorbed by the specimen was calculated as the difference between those two values. A foam specimen validation study was first performed to compare the energy absorption measurements from the pendulum instrumentation versus the work of indentation performed by an MTS machine. Following validation, the pendulum apparatus was used to measure the energy absorbed during intra-articular fractures created in 14 minipig hock joints in vivo. The foam validation study showed close correspondence between the pendulum-measured energy absorption and MTS-performed work of indentation. In the survival animal series, the energy delivered ranged from 31.5 to 48.3 Js (41.3 ± 4.0, mean ± s.d.) and the proportion of energy absorbed to energy delivered ranged from 44.2% to 64.7% (53.6% ±4.5%). The foam validation results support the reliability of the energy absorption measure provided by the instrumented pendulum system. Given that a very substantial proportion of delivered energy passed—unabsorbed—through the specimens, the energy absorption measure provided by this novel technique arguably provides better characterization of injury severity than is provided simply by energy delivery.
[DOI: 10.1115/1.4025113]

Introduction

Biomechanical impaction experiments have often been performed to study tissue and organ responses to injury (e.g., Refs. [1–5]). In the field of orthopedic biomechanics, fractures of bone are of particular interest. Clinically, the severity of fractures is often (subjectively) described in terms of the energy of the precipitating injury event [6]. Among fractures of bone, those involving the joint surface (intra-articular fractures (IAFs)) are especially challenging from an orthopedic management standpoint [7]. Besides fostering bony healing, treatment also aims to forestall posttraumatic osteoarthritis (PTOA), joint deterioration that arises from chronic loading abnormality of imprecisely reduced fractures and/or from acute insult of cartilage. To date, IAFs have received relatively little attention in controlled laboratory settings. Rather, most research on IAFs has involved either registry-based clinical studies [8–11] or laboratory animal or cadaveric models, where the insult of interest (e.g., osteotomy [12–15]) bears only limited similarity to an actual physiologic IAF event.

For systematic laboratory studies of bone fractures in general and IAFs in particular, it is necessary to control for injury severity. Quantitatively, a parameter of primary interest in that regard is the energy absorbed during the fracture event [16]. Normally, however, energy assessments in laboratory injury models have involved only the energy delivered to the specimen [1,2], rather than the energy actually absorbed in the injury.

This paper reports novel methodology for measuring the fracture energy absorbed in laboratory biomechanical impaction experiments. The specific implementation is in a testing system used to create IAFs in a large-animal survival model, the porcine hock joint [17]. The underlying concept, however, is generalizable to a wide variety of laboratory impaction experiments.

Methods

Impacts were delivered by a novel instrumented pendulum system (Fig. 1(*a*)), designed for survival animal studies and capable of delivering energy levels sufficient to fracture major weight-bearing joints in large species. The system, shown diagrammatically in Fig. 1(*b*), is compatible with operating room sterile field conditions required for survival studies. Employing the principle of the standard Charpy and Izod impact energy tests [18], energy delivery to the joint is modulated by controlling the release height of a pendulum. When using porcine (minipig) hock joints to model human tibial pilon fractures, the study animal's talus and tibia are suspended in appropriate apposition for creating fractures of the distal tibial articular surface, using a previously described purpose-designed bone-anchoring apparatus (Fig. 1(*c*)). To increase experimental reproducibility of fracture morphology, a subarticular surface stress-rising crack (saw cut) is employed [17]. The apparatus is mounted in series with a sled that can translate horizontally along low-friction linear bearings. Translation of the sled from the impact position is resisted by a linear compression spring placed between the sled and a fixed stop.

The instrumentation for energy absorption measurement is based on the concept that not all of the energy delivered by the

Contributed by the Bioengineering Division of ASME for publication in the Journal of Biomechanical Engineering. Manuscript received March 3, 2013; final manuscript received June 26, 2013; accepted manuscript posted July 30, 2013; published online April 23, 2014. Assoc. Editor: Richard Neptune.

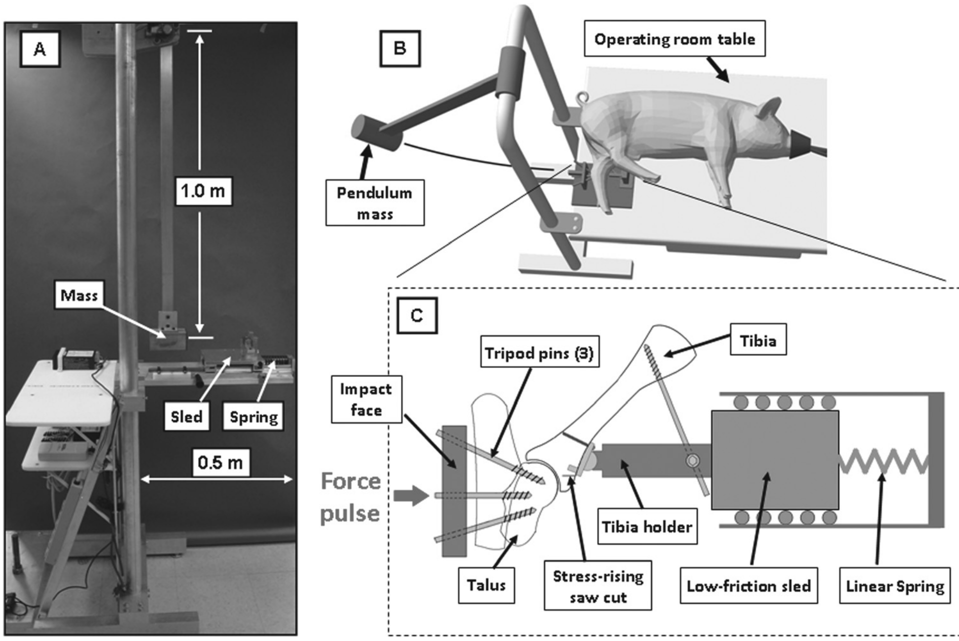

Fig. 1 The instrumented pendulum system is shown in (*a*). (*b*) illustrates its placement relative to the operating room table, such that sterile field conditions are maintained. Energy delivered to the specimen to create a fracture is controlled by the release height of the pendulum mass. (*c*) schematically illustrates a purpose-designed tripod pin fixation system for creating distal tibial articular surface fractures. A subarticular surface stress–rising saw cut is employed to ensure reproducibility of fracture morphology. Energy that passes through the specimen is determined by displacement of the sled.

pendulum mass will be absorbed by the joint during the fracture event [19]. While the pendulum itself would not "swing through" the specimen, as happens in an Izod or Charpy test, nevertheless, a substantial portion of the delivered energy will pass through the specimen and will be absorbed elsewhere, in series, by the overall testing setup. If this through-passed energy could be measured, the difference between the delivered energy and the through-passed energy would correspond to the energy absorbed in the specimen. In the pendulum system, the magnitude of energy delivery ($\mathrm{KE} = {}^1\!/_2 mv^2$) is calculated from the pendulum mass (6.1 kg) and its linear velocity, v, at impact, where linear velocity is derived from the product of angular velocity (measured by a potentiometer at the pendulum pivot) times the length of the pendulum arm. Use of the kinetic energy as the delivered energy, rather than its nominally equivalent potential energy ($\mathrm{PE} = mgh$), corrects for friction losses at the pendulum arm pivot bearing. The mass of the pendulum arm (0.80 kg), distributed uniformly along its 1.0-m length, is neglected; thus, the actual delivered kinetic energy may be slightly greater than the value calculated using the pendulum mass only.

For setup of the system prior to a test, the specimen tripod support is positioned on the sled such that, at impact, the pendulum will be exactly vertical (i.e., KE is maximum), the sled stationary, and the spring uncompressed. The pendulum mass is then raised to a predetermined height and released. The mass impacts the tripod anchor, driving the talus into and fracturing the tibia [17]. During the fracture event, the spring acts to decelerate the sled from its immediate postimpact velocity until bringing it to a stop. A linear potentiometer mounted in parallel with the sled measures the sled's maximum displacement, x, at the instant of stopping. The through-passed energy (i.e., the energy transferred from the specimen to the sled) is calculated by $\mathrm{TE} = {}^1\!/_2 kx^2$, where k is the spring constant. Raw analog voltage signals from the angular (pendulum) and linear (sled) potentiometers are digitized at 15 kHz using LABVIEW and converted into energy data using a custom MATLAB script. The difference between (preimpact) kinetic energy of the pendulum mass and the through-passed energy transferred to the sled is thus, the specimen's absorbed energy (AE), $\mathrm{AE} = \mathrm{KE} - \mathrm{TE}$.

To validate the energy absorption measurements, a polymer foam surrogate for what would otherwise be a minipig hock joint was utilized. A necessary characteristic of this surrogate material was that its energy absorption properties be uniform and measurable. Based on previous empirical experience [16], rigid polyurethane foam (25 lb/ft^3 density, Last-a-Foam, General Plastics Mfg. Co., Tacoma, WA) was chosen. Eighteen identically sized blocks ($5.5 \times 5.5 \times 4.0$ cm) of the foam were cut and impact-tested with the pendulum system. Rather than employ the tripod-mounting fixture used to test animal joints, each foam block rested on the smooth surface of the sled in contact with a rigid, flat-ended cylindrical indenter (11.7 mm diameter), that was in turn rigidly affixed to the sled (Fig. 2). Trial-and-error with different-sized indenters was used to find the largest diameter that would create an easily detected and measured indentation (depth > 0.50 mm) at the lowest impact energy. As with the hock joint fracture tests, the pendulum mass was raised and released for this test configuration, driving the block into the indenter. The digitized linear and rotary potentiometer signals were used to determine the impact duration, that was measured from the initial contact (pendulum vertical) until the time when the pendulum and sled-mounted indenter moved in unison (i.e., when no further penetration of the indenter occurred). For the impacts, durations ranged from approximately 20 ms to 40 ms. Six blocks were tested at each of three different pendulum drop heights (input KE), corresponding to 20 deg, 40 deg, and 60 deg pendulum release angles, and the absorbed energy (AE) was calculated for each test. The depth of indenter penetration for each impact was subsequently measured using a digital caliper (± 0.01 mm).

To provide a "gold standard" independent measurement of energy absorption of the foam, the same indenter (removed from the pendulum system sled) was mounted to an MTS servohydraulic test machine's actuator. Each of the 18 previously pendulum-impacted blocks was supported on the MTS load cell, and the indenter was driven into the block at a site adjacent to that of the pendulum impact. The actuator was displacement-control programmed to nominally apply similar penetration depths as

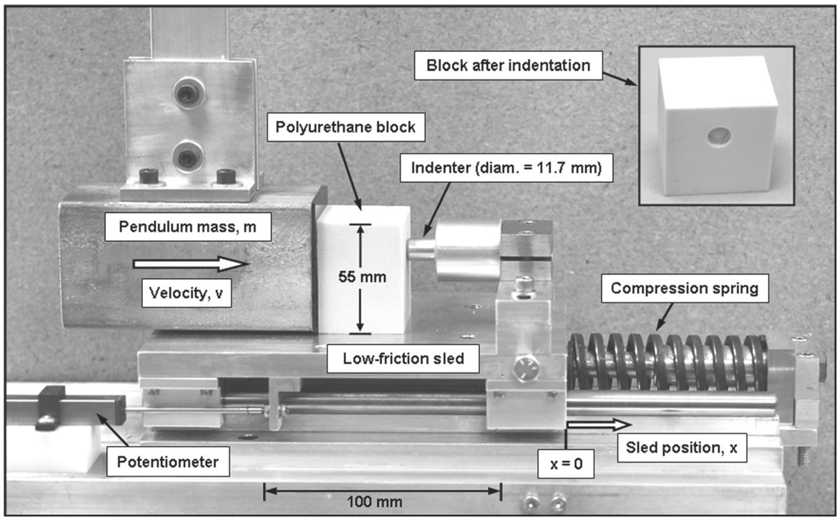

Fig. 2 The pendulum system configured to measure energy absorbed in indentation of a rigid polyurethane foam block. At impact, the pendulum drives the block into the indenter, which is rigidly mounted on the low-friction sled. As the block is driven into the indenter, the sled moves to the right, resisted by an initially uncompressed spring. The energy absorbed by the block equals the difference between the kinetic energy of the mass and the energy through-passed to the spring. The spring constant (36.7 N/mm) had been determined by empirical measurement.

those obtained with the pendulum. The full penetration depth was reached via a 50-ms linear ramp in all tests, the maximum rate obtainable while maintaining closed-loop stability. Although this was slightly longer than the pendulum impact durations, experimentation at other rates showed no evidence of significant rate dependency. All indentation depths were directly caliper-measured, and absorbed energies were determined via integration of the MTS load-displacement curves.

Following the system validation tests, a preliminary series of cadaveric hock specimen experiments was conducted to determine appropriate parameters (e.g., pendulum mass, drop height, and length and stiffness of the compression spring) required to achieve bone fracture. Four representative tibial plateau fractures from the cadaver series are shown in Fig. 3. They exhibit the general clinical appearance of human fractures—the primary fracture lines are medial-lateral and an intact anterior fragment of less than one-half of the total articular surface area is minimally displaced. After the parameters were established, the pendulum impaction system was used in an institutionally approved (IACCUC #1007141) survival animal study, in which experimental IAFs were created in 14 minipig hocks in vivo (approximate age 2 years and weight 90 kg).

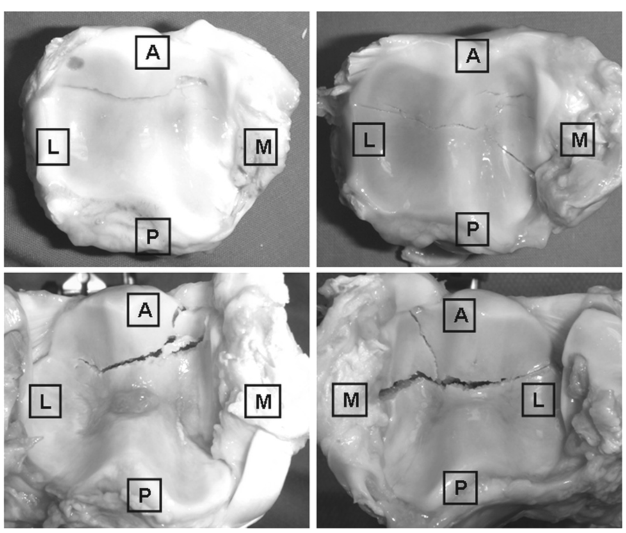

Fig. 3 Pendulum-created porcine cadaver distal tibia fractures produced during experiments to establish the appropriate system parameters for subsequent use in live-animal tests. The fractures exhibit the general clinical appearance of human fractures: the fracture lines are predominately medial-lateral and an anterior fragment is minimally displaced. (A = anterior, P = posterior, L = lateral, M = medial).

Results

Results of the foam surrogate tests for 18 blocks are summarized in Table 1. They were pendulum-impacted, six blocks at each of three release heights, absorbed energies were calculated, and the penetration depths were caliper-measured after each test. The blocks were then MTS-impacted under displacement control, with the target penetration depth for each group set to the average depth obtained in the pendulum impacts—the actual penetration depths reached were directly caliper measured. Absorbed impact energies for both impact types were plotted versus penetration depths, and linear regressions showed strong correlations (Fig. 4). Pendulum impact–absorbed energy versus MTS impact–absorbed energy is plotted in Fig. 5.

Pendulum system energy results for the 14 individual live-animal hock joint fractures are reported in Table 2. Energy delivered (KE) ranged from 31.5 to 48.3 Js (41.3 ± 4.0, mean $\pm$ s.d.). The low delivered energy for animal number one (31.5 J) was due

Table 1 Pendulum-determined versus MTS-determined absorbed energies for impacts of 18 identical polyurethane foam blocks

Pendulum-applied impacts Three drop heights ($n = 6$)		MTS-applied impacts Three target penetration depths ($n = 6$)	
Absorbed energy avg. (s.d.) (J)	Penetration depth avg. (s.d.) (mm)	Absorbed energy avg. (s.d.) (J)	Penetration depth avg. (s.d.) (mm)
0.80 (0.09)	0.67 (0.11)	0.82 (0.08)	0.74 (0.08)
3.82 (0.11)	3.29 (0.14)	4.01 (0.11)	3.52 (0.11)
9.21 (0.33)	6.92 (0.17)	7.63 (0.16)	6.55 (0.12)

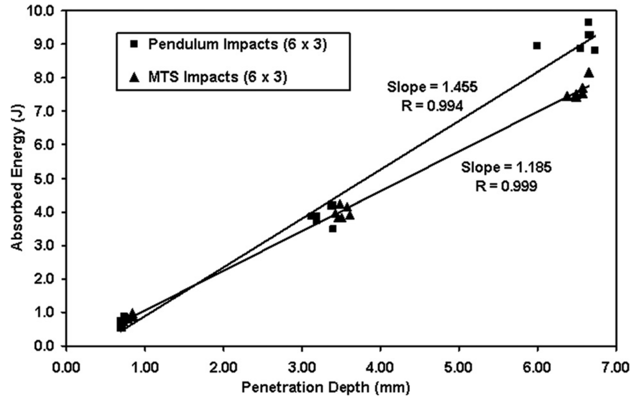

Fig. 4 Absorbed energy (J) versus penetration depth (mm) for pendulum and MTS impacts of 18 identical foam surrogate blocks

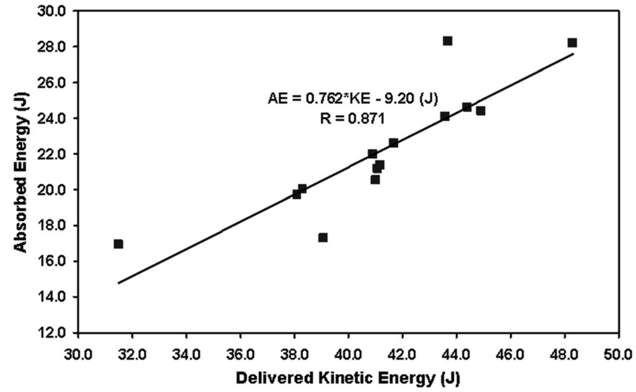

Fig. 6 Absorbed energy (J) versus delivered kinetic energy (J) for 14 survival-animal hock joint fractures produced by the pendulum device

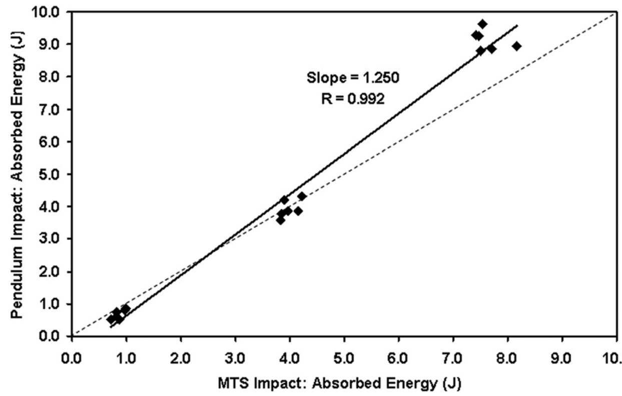

Fig. 5 Pendulum-impact absorbed energy (J) versus MTS-impact absorbed energy for 18 foam surrogate blocks

Table 2 Survival-animal hock joint fracture energy test results for 14 minipigs. AE/KE is the proportion of absorbed energy to pendulum-delivered kinetic energy.

Animal #	Kinetic energy KE (J)	Through-passed energy TE (J)	Absorbed energy AE = KE − TE (J)	AE/KE (%)
1	31.5	14.7	16.9	53.5
2	43.7	15.4	28.3	64.7
3	41.2	19.8	21.4	51.9
4	38.1	18.4	19.7	51.6
5	41.1	19.9	21.2	51.6
6	38.3	18.3	20.0	52.2
7	41.7	19.1	22.6	54.2
8	41.0	20.6	20.5	49.9
9	39.1	21.8	17.3	44.2
10	40.9	18.9	22.0	53.9
11	43.6	19.5	24.1	55.2
12	44.9	20.5	24.4	54.4
13	48.3	20.0	28.2	58.4
14	44.4	19.8	24.6	55.3
Average (s.d.)	**41.3 (4.0)**	**19.0 (1.9)**	**22.2 (3.5)**	**53.6 (4.5)**

to a lower pendulum drop height used for that specimen only. Through-passed energy (TE) ranged from 14.7 to 21.8 Js (19.0 ± 1.9), and absorbed energy (AE) ranged from 16.9 to 28.3 Js (22.2 ± 3.5). The proportion of absorbed energy to energy delivered ranged from 44.2% to 64.7% (53.6% ± 4.5%). Absorbed energy versus delivered energy is plotted in Fig. 6.

Discussion

The instrumented pendulum impaction system documented in the present study measures the magnitude of energy absorption during experimental impaction in terms of the difference between the delivered and through-passed energy magnitudes. To our best knowledge, this system is the first to enable energy absorption measurement in biomechanical impaction settings.

For the foam surrogate validation study, pendulum-absorbed energies were slightly greater than MTS-absorbed energies for similar penetration depths, particularly at the highest delivered energy (Table 1 and Fig. 5). This was not unexpected, as the pendulum device accounts for energy absorbed by the entire system, including penetration, friction, and deflection or vibration of the (nonspring) components of the pendulum device itself, whereas the MTS test isolates the energy expended only in penetration. The nonpenetration absorbed energy effects in the pendulum device may become larger with higher delivered energies. However, the generally good agreement between the pendulum-determined absorption energy and the MTS-determined absorption energy suggests that such energy losses are minor.

As is apparent from the results of the survival-animal pendulum-induced fractures (Table 2), only a portion (53.6%) of the delivered energy was absorbed in creating the experimental injury, while a significant amount (46.4%) passed through the hock specimen, subsequently being absorbed in spring compression. The relationship between absorbed and applied energy is linear (Fig. 6). However, caution is urged in applying this relationship to other fracture studies. In the present fracture impaction setting, there can be a variety of factors that contribute to energy absorption during an impaction event, including nonbone-fracture factors, such as soft tissue damage/deformation. The current technique does not permit discriminating the energy absorption directly associated with bony fracture versus these nonfracture factors. (Imaging techniques for estimating bone-fracture energy from computed tomography–based assessment of de novo interfragmentary-free surface area have recently been developed [20] but are outside the scope of the present study.) However, the present survival experiment results indicate that, at least in this range of impaction parameters for this particular surgical preparation, delivered energy is clearly not a sufficient measure of the energy actually absorbed in creating tissue injury.

Presumably, the degree of discrepancy between delivered versus absorbed energy in any given impaction experiment would be specific to considerations such as specimen type, support fixation arrangement, impaction parameters, etc. Nevertheless, the substantial disparity (46.4%) apparent in this particular experimental setting, seemingly at least generally representative of many laboratory biomechanical impaction experiments, serves to vividly illustrate the fallacy of presuming that delivered energy is necessarily representative of the energy actually involved in causing specimen tissue damage. The sled-spring arrangement used in this particular experimental setting arose as an outgrowth of an already-in-use impaction system. Obviously, however, a wide variety of similarly conceived instrumentation designs might well be used to implement the same underlying concept in other specific study designs.

While it might be possible to design/perform experiments where absorbed energy much more closely approximates delivered energy (based on empirical trials), biologic variability is such that many such trials might fail to produce bony fracture, thus, requiring (biologically confounding) repeat impactions. So, for practical purposes, it is desirable to deliver kinetic energy levels that are amply large to reliably achieve fracture, which in turn presumes that through-passed energy levels will, in general, be nonnegligible.

Acknowledgment

This research was supported by NIH CORT grant P50 AR055533 and DOD grants W81XWH-10-1-0864 and W81XWH-11-1-0583.

References

[1] Backus, J. D., Furman, B. D., Swimmer, T., Kent, C. L., McNulty, A. L., Defrate, L. E., Guilak, F., and Olson, S. A., 2011, "Cartilage Viability and Catabolism in the Intact Porcine Knee Following Transarticular Impact Loading With and Without Articular Fracture," Orthop Res. **29**(4), pp. 501–510.

[2] Tochigi, Y., Buckwalter, J. A., Martin, J. A., Hillis, S. L., Zhang, P., Vaseenon, T., Lehman, A. D., and Brown, T. D., 2011, "Distribution and Progression of Chondrocyte Damage in a Whole-Organ Model of Human Ankle Intra-articular Fracture," J. Bone Joint Surg. Am., **93**(6), pp. 533–539.

[3] Borrelli, J. Jr., Burns, M. E., Ricci, W. M., and Silva, M. J., 2002, "A Method for Delivering Variable Impact Stresses to the Articular Cartilage of Rabbit Knees," J. Orthop. Trauma, **16**(3), pp. 182–188.

[4] Isaac, D. I., Meyer, E. G., and Haut, R. C., 2008, "Chondrocyte Damage and Contact Pressures Following Impact on the Rabbit Tibiofemoral Joint," ASME J. Biomech. Eng., **130**(4), p. 041018.

[5] Rundell, S. A., Baars, D. C., Phillips, D. M., and Haut, R. C., 2005, "The Limitation of Acute Necrosis in Retro-Patellar Cartilage After a Severe Blunt Impact to the in Vivo Rabbit Patello-Femoral Joint," J. Orthop. Res., **23**(6), pp. 1363–1369.

[6] Marsh, J. L., Slongo, T. F., Agel, J., Broderick, J. S., Creevey, W., DeCoster, T. A., Prokuski, L., Sirkin, M. S., Ziran, B., Henley, B., and Audigé, L., 2007, "Fracture and Dislocation Classification Compendium—2007: Orthopaedic Trauma Association Classification, Database and Outcomes Committee," J. Orthop. Trauma, **21**(suppl), pp. S1–S133.

[7] McKinley, T. O., Borrelli, J. Jr., D'Lima, D. D., Furman, B. D., and Giannoudis, P. V., 2010, "Basic Science of Intra-Articular Fractures and Posttraumatic Osteoarthritis," J. Orthop. Trauma, **24**(9), pp. 567–570.

[8] Saterbak, A. M., Marsh, J. L., Nepola, J. V., Brandser, E. A., and Turbett, T., 2000, "Clinical Failure After Posterior Wall Acetabular Fractures: The Influence of Initial Fracture Patterns," J. Orthop. Trauma, **14**(4), pp. 230–237.

[9] Lansinger, O., Bergman, B., Körner, L., and Andersson, G. B., 1986, "Tibial Condylar Fractures. A Twenty-Year Follow-Up," J. Bone Joint Surg. Am., **68**(1), pp. 13–19.

[10] Stevens, D. G., Beharry, R., McKee, M. D., Waddell, J. P., and Schemitsch, E. H., 2001, "The Long-Term Functional Outcome of Operatively Treated Tibial Plateau Fractures," J. Orthop. Trauma, **15**(5), pp. 312–320.

[11] Marsh, J. L., Weigel, D. P., and Dirschl, D. R., 2003, "Tibial Plafond Fractures. How Do These Ankles Function Over Time?" J. Bone Joint Surg. Am., **85-A**(2), pp. 287–295.

[12] Trumble, T., and Verheyden, J., 2004, "Remodeling of Articular Defects in an Animal Model," Clin. Orthop. Relat. Res., **423**, pp. 59–63.

[13] McKinley, T. O., Tochigi, Y., Rudert, M. J., and Brown, T. D., 2008, "Instability-Associated Changes in Contact Stress and Contact Stress Rates Near a Step-Off Incongruity," J. Bone Joint Surg. Am., **90**(2), pp. 375–383.

[14] Lefkoe, T. P., Trafton, P. G., Ehrlich, M. G., Walsh, W. R., Dennehy, D. T., Barrach, H. J., and Akelman, E., 1993, "An Experimental Model of Femoral Condylar Defect Leading to Osteoarthrosis," J. Orthop. Trauma, **7**(5), pp. 458–467.

[15] Vaseenon, T., Tochigi, Y., Heiner, A. D., Goetz, J. E., Baer, T. E., Fredericks, D. C., Martin, J. A., Rudert, M. J., Hillis, S. L., Brown, T. D., and McKinley, T. O., 2011, "Organ-Level Histological and Biomechanical Responses From Localized Osteoarticular Injury in the Rabbit Knee," J. Orthop. Res., **29**(3), pp. 340–346.

[16] Beardsley, C. L., Anderson, D. D., Marsh, J. L., and Brown, T. D., 2005, "Interfragmentary Surface Area as an Index of Comminution Severity in Cortical Bone Impact," J. Orthop. Res., **23**(3), pp. 686–690.

[17] Tochigi, Y., Zhang, P., Rudert, M. J., Baer, T. E., Martin, J. A., Hillis, S. L., and Brown, T. D., 2013, "A Novel Impaction Technique to Create Experimental Articular Fractures in Large Animal Joints," Osteoarthritis Cartilage, **21**(1), pp. 200–208.

[18] Callister, W. D. J., 1994, *Materials Science and Engineering: An Introduction*, Wiley, New York.

[19] Abdel-Wahab, A. A., and Silberschmidt, V. V., 2012, "Experimental and Numerical Analysis of Izod Impact Test of Cortical Bone Tissue," Eur. Phys. J. Spec. Top., **206**, pp. 41–50.

[20] Thomas, T. P., Anderson, D. D., Mosqueda, T. V., Van Hofwegen, C. J., Hillis, S. L., Marsh, J. L., and Brown, T. D., 2010, "Objective CT-Based Metrics of Articular Fracture Severity to Assess Risk for Post-Traumatic Osteoarthritis," J. Orthop. Trauma, **24**(12), pp. 764–769.

A Clinically Realistic Large Animal Model of Intra-Articular Fracture that Progresses to Post-Traumatic Osteoarthritis

Running Title: PTOA Following Minipig Hock Fracture

Jessica E. Goetz*+, Douglas Fredericks*, Emily Petersen*, M. James Rudert*, Thomas Baer*, Eric Swanson°, Nathaniel Roberts*, James Martin*+, Yuki Tochigi§

*Department of Orthopaedics & Rehabilitation, University of Iowa, Iowa City, IA, USA
+Department of Biomedical Engineering, University of Iowa, Iowa City, IA, USA
°Department of Bioengineering, University of Washington, Seattle, WA, USA
§Department of Orthopaedics, Dokkyo Medical University Koshigaya Hospital, Saitama, Japan

August 20, 2014

A Research Paper for submission to *Osteoarthritis & Cartilage*

Corresponding Author:

Jessica E. Goetz, Ph.D.
Orthopaedic Biomechanics Lab
2180 Westlawn Building
Iowa City, IA 52242-1100
Phone: (319) 384-4275
Fax: (319) 335-7530
Email: jessica-goetz@uiowa.edu

Abstract

Objective: Translation of promising treatments for post-traumatic osteoarthritis to patients with intra-articular fracture has been limited by the lack of a realistic large animal model. To address this issue we developed a large animal model of intra-articular fracture in the distal tibia of Yucatan minipigs.

Design: Twenty-two fractures were treated using open reduction and internal fixation with either an anatomic reduction or an intentional 2-mm step-off. Pre-operatively and 3 days, 1, 2, 4, 8, and 12 weeks post-operatively, animals were sedated for synovial fluid draws and radiographs. Limb loading was monitored at the same time points using a Tekscan Walkway. Animals were sacrificed at 12 weeks and the limbs were harvested for histological evaluation.

Results: All animals achieved bony union by 12 weeks, facilitating nearly complete recovery of the initial 60% decrease in limb loading. TNFα, IL1β, IL6, and IL8 concentrations in the fractured limbs were elevated during the two weeks after fracture. Histological cartilage degeneration was more severe in the step-off group than in the anatomic reconstruction group.

Conclusions: This model replicated key features of a human IAF, including surgical stabilization, inflammatory responses, and progression to post-traumatic osteoarthritis, thereby providing a potentially useful model for translating promising treatment options to clinical practice.

Key Words: Post-traumatic Osteoarthritis, Closed Fracture, Intra-articular Fracture, Yucatan Minipig

Introduction

Post-traumatic osteoarthritis (PTOA) is a common and potentially devastating complication following joint injuries. It has been estimated that capsular or ligamentous injury can increase the risk of subsequent osteoarthritis (OA) by 10-fold, and an intra-articular fracture (IAF) can increase the risk of subsequent OA more than 20-fold.[1] In the general population, PTOA accounts for approximately 12% of all symptomatic OA, affecting approximately 5.6 million patients at a cost of more than $3 billion annually.[2] The burden of PTOA has been shown to be dramatically increased in the military population, with a prevalence of PTOA more than double that of the general population, and 94.4% of OA cases resulting in a designation of unfit for duty being attributable to a traumatic joint injury.[3] Patients from the general population presenting with PTOA are typically 9 – 14 years younger than those patients presenting for primary OA,[2] and patients presenting with PTOA in a military population are frequently in their late 20's and early 30's.[4; 5] This young and highly disabled patient population is at a much higher risk for implant failure requiring revision in joints treated with arthroplasty, and at a higher risk for development of OA in adjacent joints if treated with a joint fusion.

It is believed that accurate anatomic reconstruction of the joint surface is the best way to prevent PTOA after an IAF. This belief has been supported by numerous clinical studies in which more accurate articular surface reconstruction resulted in better clinical and functional outcomes in patients with tibial plafond[6; 7] and acetabular fractures.[8] Furthermore, finite element models of contact stress in fractured and repaired tibial plafond fractures have demonstrated that abnormal cartilage stress distributions[9] and greater degrees of joint incongruity correlate with the development of PTOA two years after IAF.[10] However, with the exception of arthroscopically assisted reduction, which has shown some promise to improve surgical reduction,[11] there has been very little advancement in the ability of a surgeon to accurately reconstruct IAFs. Perhaps more importantly, even with the emphasis on improved articular reduction, there has been very little change in the overall incidence of PTOA after IAF over the past 40 years.[12]

These data would indicate that anatomic reduction is not the only factor contributing to PTOA, and the impact injury sustained by the cartilage plus the whole-joint biological response (including inflammation) are significant factors contributing to the development of PTOA after an IAF.[13] Work in explant models has shown that cartilage impact in isolation induces different patterns of chondrocyte death and biological response compared to the combination of impact plus an osteochondral fracture.[14] Chondrocytes can remain viable for a longer period of time before apoptosing in highly strained cartilage when the tissue remains intact. However, with an IAF, chondrocyte viability decreases dramatically along the fracture edges,[15] and over time chondrocyte death propagates away from the fracture lines into previously viable cartilage.[16] The different mechanisms of cell death (apoptosis in highly strained cartilage vs. necrosis in fractured cartilage) each induce inflammatory responses in the joint which can actively degrade the cartilage.[13; 14; 17; 18] Potential mechanisms for blocking cell death and inflammatory response to IAF are being studied in many benchtop and small animal models. An explant system, however, does not allow replication of a full inflammatory response, and most *in vivo* cartilage impacts reported in the literature involve opening the joint and impacting the cartilage with a non-physiologic metallic surface. Translation of promising treatment methods for PTOA from the benchtop into clinical practice necessitates animal models that replicate the full spectrum of joint reaction to IAF and eventual degradation to late-stage PTOA.

A mouse model of closed IAF has recently been developed and used to investigate several natural history features and potential treatment targets for preventing PTOA. In that model, an IAF is created in the proximal tibia of the mouse using a materials testing machine to control an indenter applied outside of the joint. The result is a proximal tibia fracture that is created without opening the joint and subjecting the system to the additional and non-physiologic complications associated with disrupting the joint capsule.[19] This quasi-physiologic mouse model has been successfully used to demonstrate that chondrocyte death was associated with IAF in a closed setting, that synovitis scores increase in joints with higher energy fractures,[20] PTOA severity increases in the context of obesity,[21] and that decreasing particular inflammatory cytokines limits PTOA development.[22-24] The main drawback of this model is that the mouse knee is extremely small, which precludes the ability to replicate human-like treatment of the IAF, which typically includes open reduction and internal fixation. Additionally, mice are an extremely resilient species, and often heal injuries and defects much faster than other species.

The objective of this work was to develop a large animal model of closed IAF and to document the progression from initial injury to development of PTOA. It was hypothesized that the Yucatan minipig would reliably model the natural history of a distal tibia IAF while allowing human-like fracture treatment. This large animal model would fill the gap between small animal model studies and clinical implementation of candidate therapies for PTOA treatment.

Methods

Intra-articular fracture creation

With IACUC approval (1007141 and 1307140), unilateral intra-articular fractures were created in the left distal tibia of twenty-two male Yucatan minipigs. Under general anesthesia, an antero-medial approach was used to expose the anterior tibial surface, and a secondary posterior-medial approach was used to expose the distal talus. Special attention was paid to preservation of the integrity of the peri-articular soft tissues, including the ligaments and the joint capsule. With fluoroscopic visualization, a custom tripod device was attached to the talus using three 4-mm to 5-mm tapered conical external fixator pins (Electro Biology Inc., Parsippany NJ).[25] A stress-rising saw cut was made across the full medial/lateral width of the distal tibia stopping 1-2 mm proximal to the subchondral bone, and a small metallic plate with a metallic sphere was press fit into two holes drilled through the anterior tibial cortex immediately proximal to the saw cut.[25] Using a custom-designed pendulum device[26], a 40 J impact was delivered to the talus via the custom tripod device. This impact energy had proven sufficient for inducing tibial fracture during extensive pilot cadaveric testing. The impact to the tripod device drove the talus into the anterior distal tibia, resulting in an intra-articular fracture of the distal tibial near the stress-rising saw cut (Figure 1). Any energy that was not associated with causing the fracture passed through the limb and was measured using the compression of a spring construct mounted on the pendulum.[26] The fracture pattern consisted of a single fragment comprising the anterior one-third to one-half of the tibial plafond (Figure 2).

In twelve animals, the fractures were anatomically reduced and plated using a veterinary-grade 2.7-mm TPLO plate (VP4400.R3-2.7, Synthes, West Chester PA). Bicortical screws were inserted into the three screw holes proximal to the fracture line, and one bicortical screw was inserted into the distal center hole. A supplementary bicortical screw was inserted medial to the plate to prevent rotation of the fracture fragment. In the other ten animals, an intentional 2-mm step-off in the articular surface was created by plating the anterior fragment 2 mm proximal to the anatomic position. The incongruous joints were held in the step-off position using a veterinary-grade 2.7-mm TPLO plate on the anterior aspect of the tibia plus a 2.7-mm L-plate (VP1380.R3-2.7, Synthes, West Chester PA) on the medial aspect of the tibia. All animals were casted for a period of 1 week after fracture and allowed to bear weight as tolerated. Casts were changed on Day 3 when the animals were sedated for radiographs and blood/fluid draws.

Gait analysis

Prior to surgery to create the intra-articular fracture, and again at 1, 2, 4, 8, and 12 weeks post-operatively, limb loading was evaluated using a Tekscan Walkway system (Tekscan, Boston, MA). Each animal walked across the Walkway at a self-selected speed while foot pressure data were captured at 60 frames per second, and a synchronized video was recorded during each walking trial. The standard video and the Walkway software were used to identify each foot in the Walkway pressure map. Peak pressure and peak vertical impulse were determined for each limb of the animal. Five trials were acquired for each animal at each Walkway session, and data from replicate trials were averaged to obtain a single value at each post-operative time point. Differences between loading of the fractured and the intact contralateral limbs were evaluated using paired t-tests with a significance of $p<0.05$.

Imaging & Analysis

Intra-operatively, fracture reduction was evaluated using standard C-arm fluoroscopy. At day 3, and at 1, 2, 4, 8, and 12 weeks post-operatively, the animals were sedated for AP and ML radiographs. Fracture healing was evaluated visually for presence of the fracture line, widening of the fracture gap, and progressive displacement of the fracture fragment.

Prior to surgery, CT scans of both the left and the right hocks of each animal were collected, and the hocks were CT scanned again immediately after sacrifice. Pre- and post-operative CT scans were manually segmented (OsiriX, Pixmeo, Geneva, Switzerland) to isolate the distal tibial articular surface. The resulting point clouds were used to generate surfaces, and the post-operative joint surface was matched to the pre-operative joint surface by aligning the non-articular portions of the distal tibia (Figure 3) with a registration algorithm in Geomagic Studio (3DS, Rock Hill SC). The registered surfaces were exported to Matlab (The Mathworks, Natick, MA) for analysis of articular surface deviation using custom-developed code for identifying maximum step-off height, average surface depression, and percentage of joint surface depressed more than 1 mm.

Synovial Fluid Cytokine Concentrations

At the same time the animals were sedated for post-operative radiographs, synovial fluid was collected from both the fractured and the intact contralateral hocks, and blood was drawn. The synovial fluid was analyzed for concentrations of ten inflammatory cytokines using a porcine-specific array (QAP-CYT-1, RayBiotech, Norcross, GA). The cytokines included in the array were IL1β, IL4, IL6, IL8, IL10, IL12, GM-CSF, IFNγ, TGFβ, and TNF. To account for dilution of the synovial fluid that occurred as a result of joint lavage during the harvest, cytokine values were normalized using the ratio of serum blood urea nitrogen (BUN) to the synovial fluid BUN. A Wilcoxon matched-pairs signed rank test was used to compare cytokine levels between the fractured and the intact contralateral limbs.

Histological Evaluation

Upon sacrifice at 12 weeks, the fractured and the contralateral hocks were harvested for histological analysis. The tibia and the talus were split into medial and lateral compartments, fixed in formalin, decalcified, embedded in paraffin, and cut into 5-μm sagittal sections. Sections were stained with Weigert's H&E, Safranin O, and fast green and digitized on an Olympus VS100 virtual microscopy system using a 20x objective (383 nm/pixel image resolution). Digitized images were analyzed using a porcine-specific automated Mankin scoring routine developed in Matlab.[27-29] The porcine-specific cell density, proteoglycan (PG) density, and zonal thickness values were defined from six normal Yucatan minipig hocks harvested and processed identically to the experimental limbs. An objective Mankin score was assigned every 0.5 mm across the joint surface, and continuous quantitative cell count and PG density data were calculated across the joint surface. Cartilage evaluation in the distal tibia was complicated by the presence of the synovial fossa, which is a naturally occurring depression in the articular surface of many quadruped joints.[30; 31] Any cartilage overlying this feature does not have a normal articular cartilage appearance, and thus cannot be accurately evaluated with the Mankin scale. Therefore, two 5-mm spans of cartilage were evaluated on the tibia (one anterior and one posterior to the fracture and/or the naturally occurring synovial fossa), and a 20-mm span of weightbearing cartilage was evaluated on the talar surfaces. Two-way ANOVA with a Holm-Sidak multiple comparisons test was used to compare Mankin scores between normal, fractured, and contralateral specimens.

Results

Impact Analysis

Of the twenty-two experimental pigs, four were sacrificed early (range: 3 days to 2 weeks post-operatively) as a result of fracture dislocations of the hock or the hip. An additional two animals were omitted from analysis due to intrusion of the intra-articular fixation hardware into the joint. Thus a total of sixteen animals were available for analysis. Nine of these animals had an anatomic reduction of the fracture, and seven animals were given a 2-mm step-off. One of the animals with an anatomic reduction experienced a delayed union and was grouped with the step-off animals for all analyses. The energy that was absorbed and resulted in fracture averaged 21.9 J +/- 4.8 J (range 11.7 J – 30.0 J), which was an average of 54% of the 40 J input energy. The remainder of the impact energy passed through the system and was absorbed by the spring on the pendulum backstop.[26] Early in the study, three animals required a second impact to achieve a fracture. Because that second impact ultimately caused a fracture with energy in the same range as the single-impact fractures, these multiple-impact cases were considered valid trials, and the data were included in all analyses.

Image Analysis

Radiographs were evaluated qualitatively for evidence of loss of fracture fixation as evidenced by subsidence of the anterior fracture fragment or an expanding gap between the fragment and the intact bone. In one of the early animals there was evidence of a delayed union, which did progress to healed bone by the end of the 12 weeks. All other animals appeared to have stable fixation throughout the duration of the study. When the hardware was removed at the completion of the study, the fracture fragment was integrated with the distal tibia in all the animals.

The post-operative joint surface was evaluated for deviation from the intact surface by direct comparison with the pre-operative joint surface. As expected, both the maximum surface deviation and the average surface deviations were higher in the 2-mm step-off group than in the anatomic reconstruction group (Figure 4). The maximum surface deviation was well above 2 mm in both groups, indicating that even with good reduction there were still focal locations of residual incongruity or bone loss along the edge of a fracture line. However, in the anatomic reduction group, there was significantly less total joint surface that was depressed, and nearly all of that depression was less than 1 mm. The 2-mm step-off group obviously had a much higher area of the joint surface that was depressed relative to the intact case, and much of the surface was depressed more than 2 mm (Figure 4).

Gait Analysis

All animals began walking on their fractured and repaired limbs within hours after surgery and continued to at least partially load the fractured limbs over the duration of the study. Peak vertical force in the injured limb one week after fracture was only 45% of the pre-operative value, recovering only to 49% of pre-operative loading two weeks after fracture. These decreases were statistically significant ($p<0.001$). In weeks 4 – 12, peak vertical force progressively increased, returning to near pre-operative values by the end of the 12-week study. There was no statistically significant difference in peak force on the fractured leg 12 weeks after fracture compared to pre-operative values ($p=0.12$). There was no difference in limb loading between animals with an anatomic fracture reduction and animals with a 2-mm step-off at any time point ($0.06<p<.0.7$). Vertical impulse showed a nearly identical trend, decreasing to 46% of pre-operative values at one week, and recovering to near pre-operative values by week 8. Differences in vertical impulse were significantly different from pre-op only through week 4 ($p<0.001$ for weeks 1 and 2, $p=0.013$ for week 4). These data indicate that the animals continued to load the limb over the duration of the study (Figure 5).

Synovial Fluid Cytokine Analysis

The intra-articular fracture resulted in statistically significant ($p<0.05$) elevations of IL6 and IL8 relative to the intact contralateral limb three days and one week after the fracture (Figure 6). Two weeks after fracture, IL6 and IL8 levels were still elevated relative to preoperative values and relative to contralateral limb values. However, by 4 weeks after the fracture, IL6 and IL8 levels had returned to near baseline values, and they remained stable for the remainder of the 12-week study. While only reaching statistical significance at single time points, there was a trend for IL1β and TNF concentrations to be elevated in the acute period after fracture, and to return to contralateral values by approximately 4 weeks after fracture (Figure 6). The other six inflammation-related cytokines measured did not show any strong trends associated with time after fracture. Concentrations of IL4, IL10, IL12, GM-CSF, IFNγ, and TGFβ1 were nearly identical between the fractured hock and the uninjured contralateral (Supplemental Data).

Histological Analysis

On both the medial and the lateral talar cartilage surfaces, the average Mankin scores were higher in the step-off group than in the anatomic fracture reduction group ($p<0.001$ lateral, $p=0.23$ medial), indicating that the cartilage articulating with the step-off degenerated more over the 12-week survival period than the cartilage articulating with an anatomic reduction. While not statistically significant, there was a clear trend for the talar cartilage in the anatomic reconstruction group to have higher Mankin scores than normal cartilage. The talar cartilage from the contralateral limbs also showed elevated Mankin scores relative to normal cartilage, but to a lesser degree than the step-off fracture cases (Figure 7). On the medial and lateral tibial cartilage surfaces, there was a non-statistically significant trend for the fractured and the intact contralateral to have elevated Mankin scores compared to normal cartilage.

Discussion

In this work, a well-controlled intra-articular fracture of the distal tibia in the Yucatan minipig replicated several histological and biological characteristics of PTOA over a 12 week survival period. This progressive joint degeneration occurred after open reduction and internal fixation treatment equivalent to that used in humans with IAF. The original decrease in loading of the injured limb recovered to nearly pre-operative loading levels over the course of the study period, presumably corresponding to bony healing that occurred over a human-relevant time period. While the step-off reduction resulted in more severe histological degeneration of the cartilage, anatomic fracture reconstruction was insufficient to prevent the development of PTOA in the majority of animals and indicated the ability to create PTOA of differing severities for study in future work.

One of the main goals of this work was to create a highly consistent IAF pattern to allow for systematic study, which required the use of moderately invasive hardware fixtures to constrain the bones during impact and a stress-rising saw cut to guide the size and location of the fracture fragment. Given that clinically realistic fracture reduction surgery for rigid internal fixation is similarly invasive, and because only one small incision beyond that needed to reduce and plate the fracture was needed to access the relevant anatomy for fracture creation, it is unlikely that the application of these fixtures substantially affected the local or systemic biological response in this model. The fracture creation methodology resulted in very reproducible IAF fracture locations and very similar impact energies absorbed by the joint during fracture, thereby creating a highly controlled cartilage injury system.

To document the biological reaction to the impact fracture injury, we monitored inflammatory cytokine concentrations. Based on previous work in which the mouse model of IAF did not show any trends in systemic inflammatory cytokine levels or biomarkers,[20] we elected to focus entirely on synovial fluid rather than serum cytokine concentrations. While this did not allow for identification of a minimally invasive biomarker measure of PTOA development and progression, it did allow for comparison with cytokine concentrations in acutely injured human joints. While inflammatory cytokine concentrations have not been well studied in human patients after IAF, it has been shown that IL1β, IL6, IL8, and TNFα are all substantially elevated in the acute period after intra-articular injury such as an ACL tear.[32-34] In both primary OA and in PTOA, these particular cytokines are associated with a prolonged inflammatory response that promotes cartilage breakdown ,[17] which makes replicating such fluctuations in these cytokines in an animal model a crucial feature of a useful model. While the increases in IL1β and TNFα did not maintain statistical significance in the fractured joints relative to the intact contralateral, it is possible that their peak values were not captured at our 3-day and 1-week sampling times. Sward, et al. reported maximum levels of these cytokines in human patients 1 day after knee injury, and concentrations began to decrease towards normal values within 2 – 3 days after injury.[32] The significantly increased IL6 values at our sampling time points may be a result of upregulation caused by previous increases in IL1β that had begun to resolve by 3 days post injury.

The histologically evident cartilage degeneration in the joints with a 2-mm step-off was more severe than in the anatomic reduction joints; however, several of the joints in the anatomic reconstruction group had substantially elevated Mankin scores, indicating PTOA development even after best-case reconstruction. Longer term follow up of this animal model will be important to determine if these histological changes in cartilage continue to progress to fully eroded cartilage and bony changes characteristic of late stage osteoarthritis. The Mankin scores for all joint surfaces were elevated relative to normal cartilage in the contralateral joints as well. While not impacted or fractured, these contralateral joints were also likely damaged to a lesser degree as a result of (1) the sequential synovial fluid draws over the course of the study, and (2) increased joint loading to compensate for the decreased fractured limb loading that occurred at the early post-operative time points.

Unfortunately, the degree of cartilage degeneration on the tibial surfaces was not well-described by an average Mankin score. The Mankin score is not intended for application to repairing articular cartilage or to the tissue in the porcine synovial fossa,[30] and therefore could not be applied to the entire tibial surface. Because so much tibial surface had to be omitted from the averaging (Figure 8), differences in focal changes in cartilage health were less apparent between the different fracture reconstruction groups and the contralaterals. The average tibial cartilage Mankin scores between the two fracture reduction groups, the contralateral groups, and the normal group were not statistically different, despite gross visual assessment of cartilage quality indicating localized areas of degenerated cartilage (Figure 7). In the tibia, the naturally occurring synovial fossa was not scored on the Mankin scale, and large areas of fibrocartilage in the healed fracture gap were also omitted from scoring. This left very small, peripheral spans of cartilage on the tibia for evaluation of PTOA. Based on previous work[16; 25] in which areas of cell death were concentrated around the fracture lines, we would not expect these peripheral areas to be highly damaged. The consistent degeneration of the cartilage on the talar surface, which was subjected to impact and then articulated with a repaired fracture, provides excellent evidence of the development of PTOA in this model, despite the highly focal nature of the degenerated cartilage occurring on the fractured tibial surfaces.

The financial burden of using this large animal species makes it unsuitable for large-scale investigations of all candidate interventions. Rather, this minipig model of PTOA development after IAF is intended to be a vehicle to translate ideas for PTOA treatment that have proven promising in benchtop studies and/or in small animal models into clinical practice. The extremely well-controlled insult methodology and consistency of fracture fragment size and location ensure that future investigations with this model will yield quality preclinical data, and the ability to perform open reduction and internal fixation will confirm that any biological treatments will be applicable within the context of human-like fracture treatment.

Acknowledgements: This work was funded by a grant W81XWH-10-1-0864 from the US Department of Defense. The study sponsor had no influence over the methods, results, or conclusions resulting from this work. The authors wish to acknowledge the hard work of Bryce Diestelmeier, Gail Kurriger, and the staff at the Bone Healing Research Laboratory.

Author Contributions: The study design and several aspects of its execution were primarily performed by JEG and YT. DF and EP were critical for executing all live animal work and live animal data captures. MJR and TB were responsible for mechanical design, YT performed the gait analysis, and ES and JEG performed radiographic image analysis. NR and JM contributed the cytokine analysis, and JEG performed the histological analysis. All authors contributed to data interpretation and have read and approved the final manuscript.

Conflict of Interest: None of the authors have any financial conflict of interest related to this work.

References

1. Anderson DD, Chubinskaya S, Guilak F, et al. 2011. Post-traumatic osteoarthritis: improved understanding and opportunities for early intervention. Journal of orthopaedic research : official publication of the Orthopaedic Research Society 29:802-809.

2. Brown TD, Johnston RC, Saltzman CL, et al. 2006. Posttraumatic osteoarthritis: a first estimate of incidence, prevalence, and burden of disease. J Orthop Trauma 20:739-744.

3. Rivera JC, Wenke JC, Buckwalter JA, et al. 2012. Posttraumatic osteoarthritis caused by battlefield injuries: the primary source of disability in warriors. The Journal of the American Academy of Orthopaedic Surgeons 20 Suppl 1:S64-69.

4. Patzkowski JC, Owens JG, Blanck RV, et al. 2012. Management of posttraumatic osteoarthritis with an integrated orthotic and rehabilitation initiative. The Journal of the American Academy of Orthopaedic Surgeons 20 Suppl 1:S48-53.

5. Cross JD, Ficke JR, Hsu JR, et al. 2011. Battlefield orthopaedic injuries cause the majority of long-term disabilities. The Journal of the American Academy of Orthopaedic Surgeons 19 Suppl 1:S1-7.

6. Ovadia DN, Beals RK. 1986. Fractures of the tibial plafond. J Bone Joint Surg Am 68:543-551.

7. Teeny SM, Wiss DA. 1993. Open reduction and internal fixation of tibial plafond fractures. Variables contributing to poor results and complications. Clinical orthopaedics and related research:108-117.

8. Tannast M, Najibi S, Matta JM. 2012. Two to twenty-year survivorship of the hip in 810 patients with operatively treated acetabular fractures. J Bone Joint Surg Am 94:1559-1567.

9. Li W, Anderson DD, Goldsworthy JK, et al. 2008. Patient-specific finite element analysis of chronic contact stress exposure after intraarticular fracture of the tibial plafond. Journal of orthopaedic research : official publication of the Orthopaedic Research Society 26:1039-1045.

10. Anderson DD, Van Hofwegen C, Marsh JL, et al. 2011. Is elevated contact stress predictive of post-traumatic osteoarthritis for imprecisely reduced tibial plafond fractures? Journal of orthopaedic research : official publication of the Orthopaedic Research Society 29:33-39.

11. Schenker ML, Mauck RL, Ahn J, et al. 2014. Pathogenesis and prevention of posttraumatic osteoarthritis after intra-articular fracture. The Journal of the American Academy of Orthopaedic Surgeons 22:20-28.

12. McKinley TO, Borrelli J, Jr., D'Lima DD, et al. 2010. Basic science of intra-articular fractures and posttraumatic osteoarthritis. J Orthop Trauma 24:567-570.

13. Furman BD, Olson SA, Guilak F. 2006. The development of posttraumatic arthritis after articular fracture. J Orthop Trauma 20:719-725.

14. Stolberg-Stolberg JA, Furman BD, Garrigues NW, et al. 2013. Effects of cartilage impact with and without fracture on chondrocyte viability and the release of inflammatory markers. Journal of orthopaedic research : official publication of the Orthopaedic Research Society 31:1283-1292.

15. Backus JD, Furman BD, Swimmer T, et al. 2011. Cartilage viability and catabolism in the intact porcine knee following transarticular impact loading with and without articular fracture. Journal of orthopaedic research : official publication of the Orthopaedic Research Society 29:501-510.

16. Tochigi Y, Buckwalter JA, Martin JA, et al. 2011. Distribution and progression of chondrocyte damage in a whole-organ model of human ankle intra-articular fracture. J Bone Joint Surg Am 93:533-539.

17. Goldring MB. 2000. Osteoarthritis and cartilage: the role of cytokines. Current rheumatology reports 2:459-465.

18. Fernandes JC, Martel-Pelletier J, Pelletier JP. 2002. The role of cytokines in osteoarthritis pathophysiology. Biorheology 39:237-246.

19. Furman BD, Strand J, Hembree WC, et al. 2007. Joint degeneration following closed intraarticular fracture in the mouse knee: a model of posttraumatic arthritis. Journal of orthopaedic research : official publication of the Orthopaedic Research Society 25:578-592.

20. Lewis JS, Hembree WC, Furman BD, et al. 2011. Acute joint pathology and synovial inflammation is associated with increased intra-articular fracture severity in the mouse knee. Osteoarthritis Cartilage 19:864-873.

21. Louer CR, Furman BD, Huebner JL, et al. 2012. Diet-induced obesity significantly increases the severity of posttraumatic arthritis in mice. Arthritis and rheumatism 64:3220-3230.

22. Ward BD, Furman BD, Huebner JL, et al. 2008. Absence of posttraumatic arthritis following intraarticular fracture in the MRL/MpJ mouse. Arthritis and rheumatism 58:744-753.

23. Lewis JS, Jr., Furman BD, Zeitler E, et al. 2013. Genetic and cellular evidence of decreased inflammation associated with reduced incidence of posttraumatic arthritis in MRL/MpJ mice. Arthritis and rheumatism 65:660-670.

24. Furman BD, Mangiapani DS, Zeitler E, et al. 2014. Targeting pro-inflammatory cytokines following joint injury: acute intra-articular inhibition of interleukin-1 following knee injury prevents post-traumatic arthritis. Arthritis research & therapy 16:R134.

25. Tochigi Y, Zhang P, Rudert MJ, et al. 2013. A novel impaction technique to create experimental articular fractures in large animal joints. Osteoarthritis Cartilage 21:200-208.

26. Diestelmeier BW, Rudert MJ, Tochigi Y, et al. 2014. An instrumented pendulum system for measuring energy absorption during fracture insult to large animal joints in vivo. J Biomech Eng 136.

27. Moussavi-Harami SF, Pedersen DR, Martin JA, et al. 2009. Automated objective scoring of histologically apparent cartilage degeneration using a custom image analysis program. Journal of orthopaedic research : official publication of the Orthopaedic Research Society 27:522-528.

28. Pedersen DR, Goetz JE, Kurriger GL, et al. 2013. Comparative digital cartilage histology for human and common osteoarthritis models. Orthopedic research and reviews 2013:13-20.

29. Arunakul M, Tochigi Y, Goetz JE, et al. 2013. Replication of chronic abnormal cartilage loading by medial meniscus destabilization for modeling osteoarthritis in the rabbit knee in vivo. Journal of orthopaedic research : official publication of the Orthopaedic Research Society 31:1555-1560.

30. Doige C, Horowitz A. 1975. A study of articular surfaces and synovial fossae of the pectoral limb of swine. Canadian journal of comparative medicine Revue canadienne de medecine comparee 39:7-16.

31. Wegener KM, Heje NI, Aarestrup FM, et al. 1993. The morphology of synovial grooves (Fossae synoviales) in joints of cattle of different age groups. Zentralblatt fur Veterinarmedizin Reihe A 40:359-370.

32. Sward P, Frobell R, Englund M, et al. 2012. Cartilage and bone markers and inflammatory cytokines are increased in synovial fluid in the acute phase of knee injury (hemarthrosis)--a cross-sectional analysis. Osteoarthritis Cartilage 20:1302-1308.

33. Cameron ML, Fu FH, Paessler HH, et al. 1994. Synovial fluid cytokine concentrations as possible prognostic indicators in the ACL-deficient knee. Knee surgery, sports traumatology, arthroscopy : official journal of the ESSKA 2:38-44.

34. Olson SA, Horne P, Furman B, et al. 2014. The role of cytokines in posttraumatic arthritis. The Journal of the American Academy of Orthopaedic Surgeons 22:29-37.

Figure 1. Schematics (left) and corresponding intra-operative photographs (right) of the full impaction pendulum and the hardware applied during surgery.

Figure 2. Intra-operative fluoroscopy image of the fracture fragment (left) and the final reduction and fixation (middle). The resulting fracture fragment is approximately one-third of the AP joint width (right). In this inferior to superior view of the distal tibia, the synovial fossa is evident as the darker area in the center of the tibia.

Figure 3. Illustration of the methodology used to calculate residual surface incongruity at the end of the 12-week survival period in a 2-mm step-off animal. The post-operative tibial surface geometry (gray) was matched to the pre-operative surface geometry using the diaphyseal shaft and the intact posterior joint surface. The residual incongruity distances were mapped on the post-operative joint surface geometry and exported for further analysis.

Figure 4. CT-based analysis of articular surface incongruity. The 2-mm step-off group had greater maximum depth of incongruity and a higher percentage of the joint surface that deviated substantially from the intact joint surface. Anatomic reconstruction resulted in much less final surface incongruity; however, even the anatomic reconstruction was unable to completely prevent surface incongruity at the 12-week time point.

Figure 5. Average (black) and individual animal (gray) limb loading following intra-articular fracture. All data are normalized to the individual animal's pre-operative values. One week after fracture and repair, and persisting to two weeks, there was a statistically significant decrease in

limb loading. Limb loading progressively recovered over the 12-week duration and was near pre-operative values 12 weeks after fracture.

Figure 6. Fracture- and time-related changes in synovial fluid cytokine concentrations. Results are shown for fluid harvested pre-operatively (Pre-Op), at 3 days post-operatively (D3), and at subsequent post-operative weeks 1 to 12 (W1-W12). IL6 and IL8 concentrations were consistent throughout the time course in contralateral controls, but fluctuated in fractured joints, increasing significantly (* corresponds to $p<0.05$ in a Wilcoxon matched-pairs signed rank test) at one and two weeks after fracture and returning to contralateral values after four weeks. IL1β and TNF concentrations demonstrated a similar trend; however, that trend only reached statistical significance at single post-operative time points.

Figure 7. Average Mankin score in each compartment of the minipig hock. Mankin scores in the talar cartilage were higher than in the tibial cartilage, and the step-off reconstruction specimens were statistically significantly more severely degenerated than the normal cartilage (* indicates $P<0.05$). In the lateral talus, the contralateral limbs were significantly more degenerated than normal cartilage ($P<0.05$), but the average of all fractured and anatomically reconstructed was not statistically significantly worse than normal cartilage. In the tibia, the trend was for the cartilage on the fractured tibial surfaces to be more degenerated than normal cartilage or the contralateral limb cartilage, but this trend did not reach significance.

Figure 8. Illustration of the synovial fossa and its location relative to the fracture in an intact (far left) and fractured (left) tibial surface. While the synovial fossa does not have the same

appearance as normal articular cartilage, it should not be mistaken for damaged or arthritic cartilage. Images on the right and the associated insets show typical cartilage damage on the talar surface. Sections are the anterior half of the talus with anterior to the right. The region of degenerated cartilage in the talar surface opposing the fractured case corresponds to the location of the fracture line on the tibia. Arthritic changes including PG depletion and extreme hypocellularity are evident in the fractured joint (lower right).

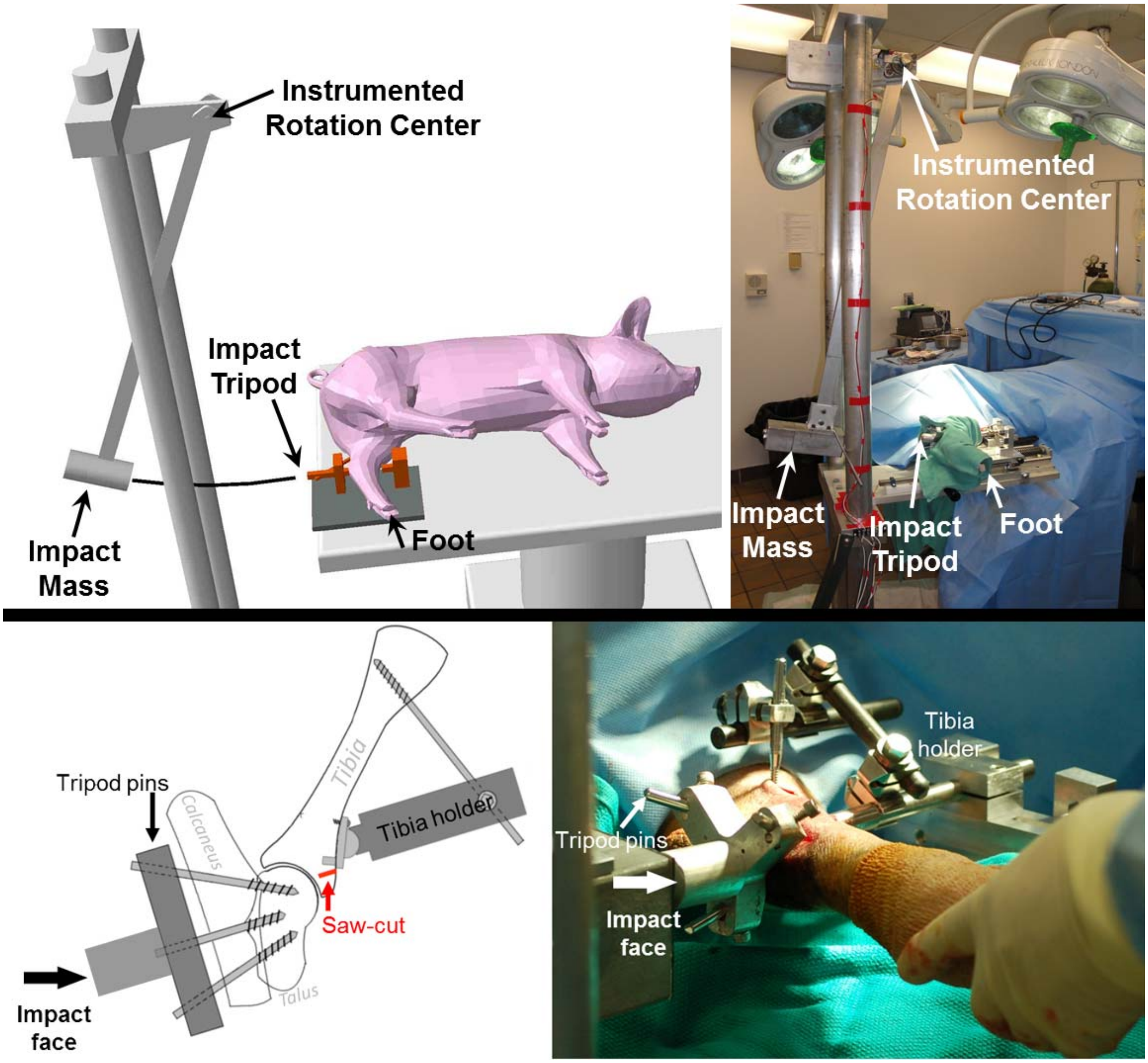

Figure 1. Schematics (left) and corresponding intra-operative photographs (right) of the full impaction pendulum (top) and the hardware applied during surgery (bottom).

Figure 2. Intra-operative fluoroscopy image of the fracture fragment (left) and the final reduction and fixation (middle). The resulting fracture fragment is approximately one-third of the AP joint width (right). In this inferior to superior view of the distal tibia, the synovial fossa is evident as the darker area in the center of the tibia.

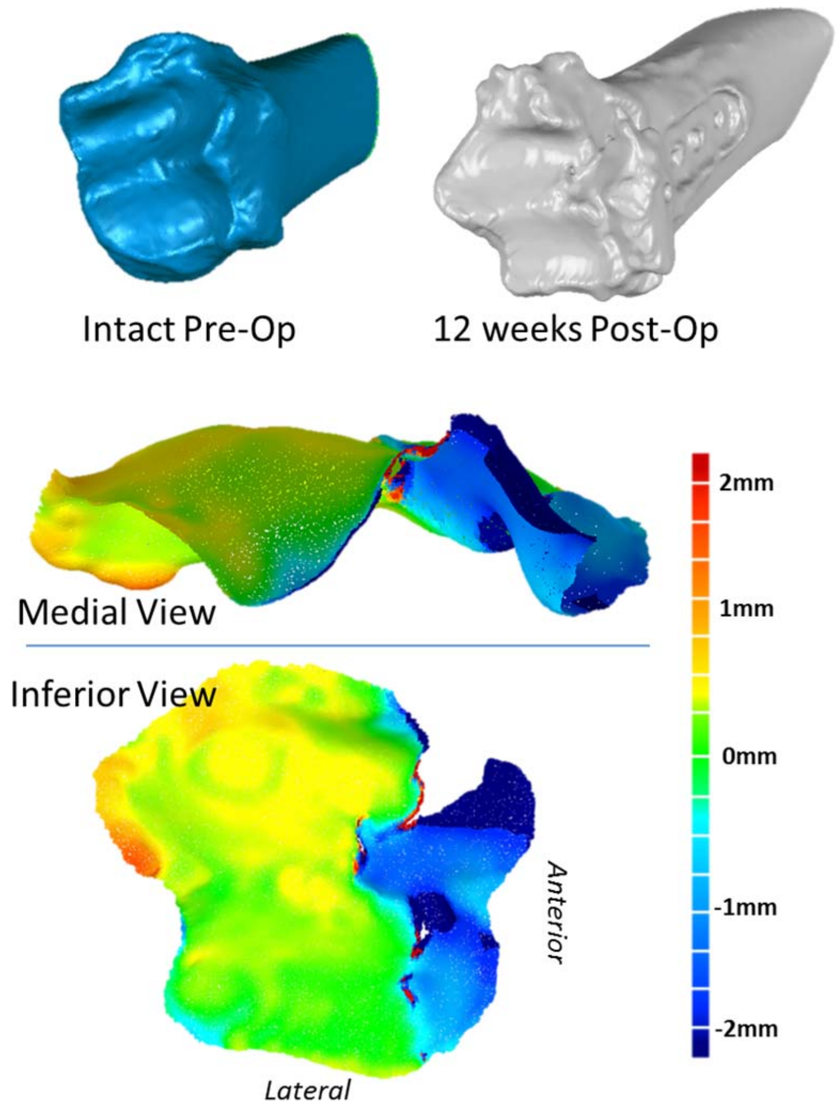

Figure 3. Illustration of the methodology used to calculate residual surface incongruity at the end of the 12 week survival period in a 2-mm step-off animal. The post-operative tibial surface geometry (gray) was matched to the pre-operative surface geometry using the diaphyseal shaft and the intact posterior joint surface. The residual incongruity distances were mapped on the post-operative joint surface geometry and exported for further analysis.

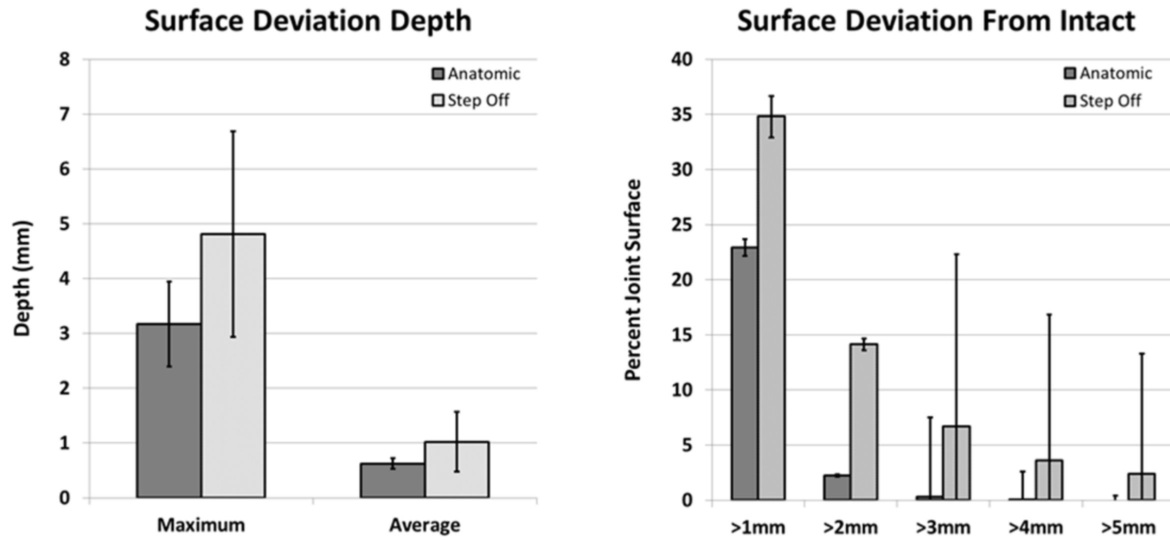

Figure 4. CT-based analysis of articular surface incongruity. The 2-mm step-off group had greater maximum depth of incongruity and a higher percentage of the joint surface that deviated substantially from the intact joint surface. Anatomic reconstruction resulted in much less final surface incongruity, however, even the anatomic reconstruction was unable to completely prevent surface incongruity at the 12-week time point.

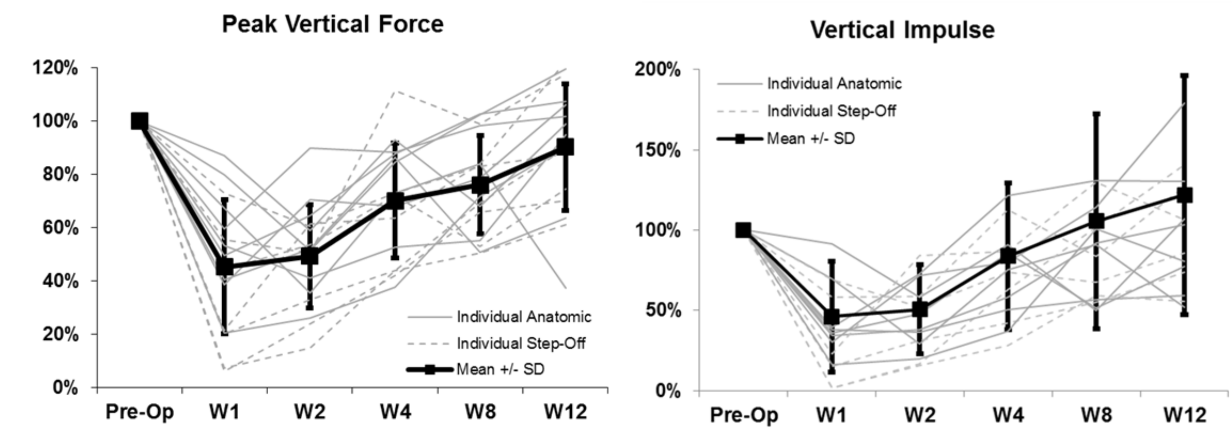

Figure 5. Average (black) and individual animal (gray) limb loading following intra-articular fracture. All data are normalized to the individual animal's pre-operative values. One week after fracture and repair, and persisting to two weeks, there was a statistically significant decrease in limb loading. Limb loading progressively recovered over the 12-week duration and was near pre-operative values 12 weeks after fracture.

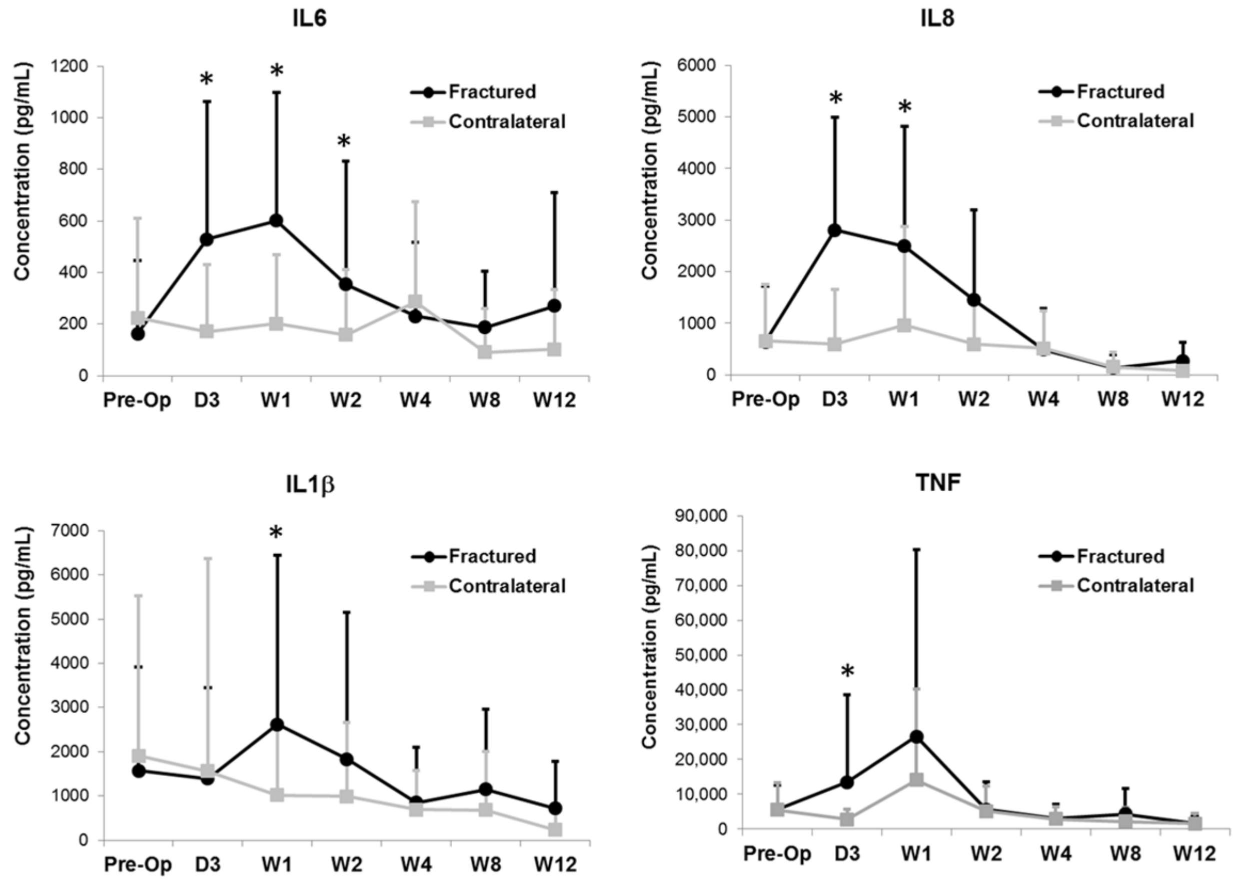

Figure 6. Fracture- and time-related changes in synovial fluid cytokine concentrations. Results are shown for fluid harvested pre-operatively (Pre-Op), at 3 days post-operatively (D3), and at subsequent post-operative weeks 1 to 12 (W1-W12). IL6 and IL8 concentrations were consistent throughout the time course in contralateral controls, but fluctuated in fractured joints, increasing significantly (* corresponds to $p<0.05$ in a Wilcoxon matched-pairs signed rank test) at one and two weeks after fracture and returning to contralateral values after four weeks. IL1β and TNF concentrations demonstrated a similar trend; however, that trend only reached statistical significance at single post-operative time points.

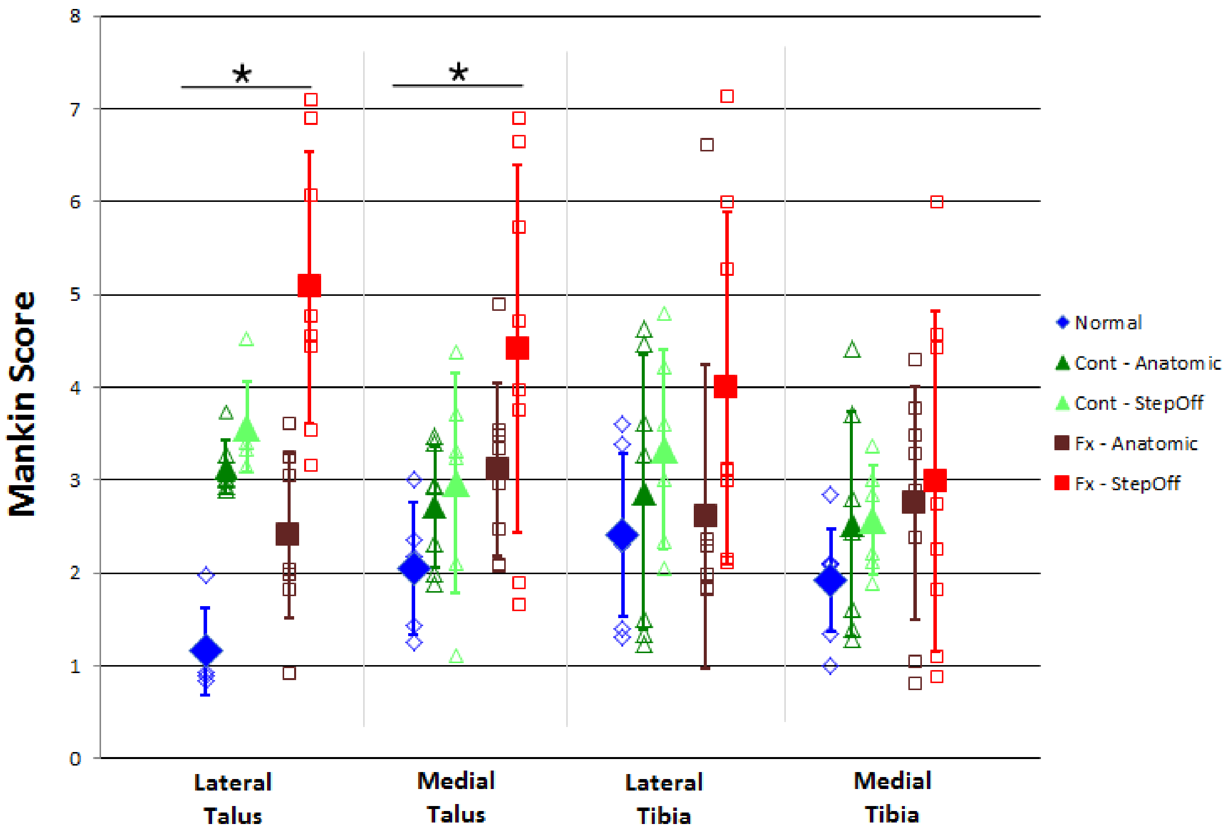

Figure 7. Average Mankin score in each compartment of the minipig hock. Mankin scores in the talar cartilage were higher than in the tibial cartilage, and the step-off reconstruction specimens were statistically significantly more severely degenerated than the normal cartilage (* indicates P<0.05). In the lateral talus, the contralateral limbs were significantly more degenerated than normal cartilage (P<0.05), but the average of all fractured and anatomically reconstructed was not statistically significantly worse than normal cartilage. In the tibia, the trend was for the cartilage on the fractured tibial surfaces to be more degenerated than normal cartilage or the contralateral limb cartilage, but this trend did not reach significance.

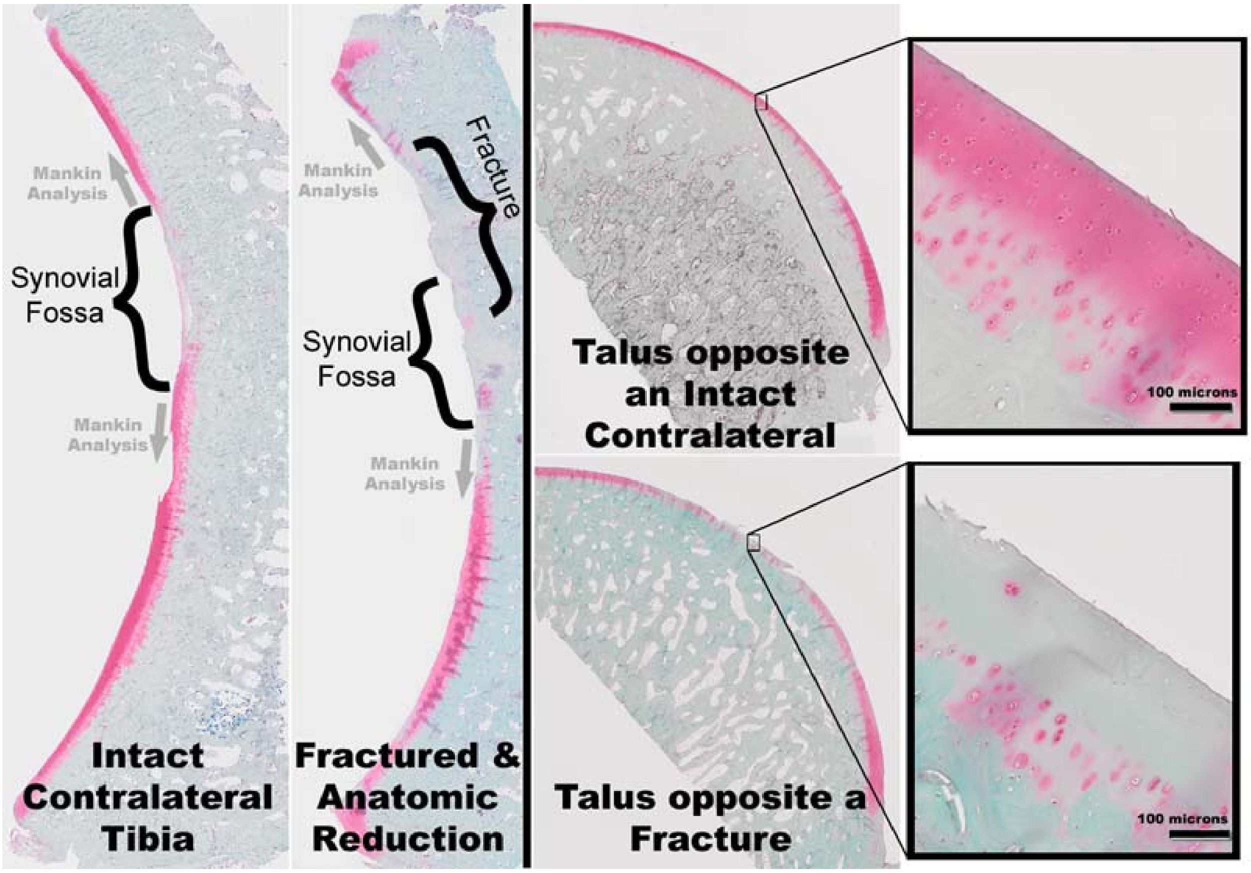

Figure 8. Illustration of the synovial fossa and its location relative to the fracture in an intact (far left) and fractured (left) tibial surface. While the synovial fossa does not have the same appearance as normal articular cartilage, it should not be mistaken for damaged or arthritic cartilage. Images on the right and the associated insets show typical cartilage damage on the talar surface. Sections are the anterior half of the talus with anterior to the right. The region of degenerated cartilage in the talar surface opposing the fractured case corresponds to the location of the fracture line on the tibia. Arthritic changes including PG depletion and extreme hypocellularity are evident in the fractured joint (lower right).

Supplemental Table 1. Average (standard deviation) cytokine concentrations in pg/mg BUN for all pigs from pre-operation until week 12. Week 8 data was similar to week 4 and week 12 data, and was therefore omitted from this table. All values are pg/mL.

		IL-4		IL10		IL-12		GM-CSF		IFN-g		TGFβ	
	pg/mL	*Avg*	*(SD)*	*Avg*	*(SD)*	*Avg*	*(SD)*	*Avg*	*(SD)*	*Avg*	*(SD)*	*Avg*	*(SD)*
Pre-op	All hocks	13,299	*(23,105)*	442	*(795)*	1,481,943	*(4,384,721)*	6,120	*(8,329)*	5,345	*(17,816)*	116,505	*(479,174)*
Day 3	IAF hock	16,447	*(23,013)*	211	*(236)*	1,346,835	*(3,439,662)*	4,386	*(7,100)*	3,485	*(8,266)*	69,320	*(140,155)*
	Contralateral	11,466	*(23,521)*	71	*(155)*	122,126	*(261,195)*	4,459	*(10,281)*	789	*(1,445)*	36,408	*(51,981)*
Week 1	IAF hock	30,099	*(39,026)*	315	*(363)*	1,987,314	*(5,263,418)*	7,464	*(6,919)*	4,738	*(8,772)*	157,765	*(296,125)*
	Contralateral	26,277	*(56,033)*	100	*(110)*	1,270,950	*(2,459,711)*	6,430	*(7,636)*	2,416	*(5,248)*	146,851	*(289,995)*
Week 2	IAF hock	28,862	*(29,049)*	185	*(356)*	1,658,249	*(3,390,504)*	6,960	*(9,368)*	1,566	*(2,497)*	140,156	*(184,737)*
	Contralateral	22,483	*(24,031)*	91	*(139)*	1,249,697	*(2,490,384)*	4,729	*(5,294)*	1,299	*(2,956)*	213,354	*(399,426)*
Week 4	IAF hock	18,415	*(25,626)*	96	*(155)*	1,627,154	*(4,259,270)*	4,883	*(5,421)*	2,182	*(6,510)*	61,645	*(82,091)*
	Contralateral	26,118	*(31,329)*	117	*(185)*	1,272,792	*(3,205,982)*	4,213	*(4,032)*	3,699	*(7,551)*	50,974	*(55,715)*
Week 12	IAF hock	12,995	*(26,037)*	300	*(610)*	299,436	*(483,863)*	4,085	*(5,858)*	3,362	*(7,085)*	18,439	*(24,287)*
	Contralateral	9,194	*(19,785)*	37	*(99)*	91,481	*(189,927)*	1,176	*(1,720)*	531	*(1,302)*	19,434	*(44,384)*

Intraarticular Administration of N-Acetylcysteine and Glycyrrhizin Alleviates Acute Oxidative Stress Following Intraarticular Fracture

Mitchell Coleman, James Martin, Douglas Fredericks, Mary Bergh, Jessica Goetz

Intraarticular fractures (IAFs) have long been associated with poor prognosis and a profoundly increased risk of development of post-traumatic osteoarthritis (PTOA) (1). We have recently developed a new model of IAF in which the tibial surface of the Yucatan mini-pig hock (ankle) joints is reproducibly fractured without surgical disruption of the capsule (2). In order to demonstrate the utility of this model for future study of potential interventions abrogating PTOA development following IAF, a cocktail of pharmaceuticals was administered to injured joints post-fracture. This cocktail contained 10 mM N-acetylcysteine (NAC), an antioxidant, and 100 μM glycyrrhizin (GLZ), an anti-inflammatory agent. This therapy was applied to test the hypothesis that IAF initiates acute oxidative stress in conjunction with increased inflammation in the injured joint, and that blocking these mechanisms may prevent cellular damage and dysfunction associated with PTOA development.

Oxidative stress is expected following IAF given the flood of oxygen and blood into the joint, a physiological setting normally relatively devoid of both. While oxidative stress following IAF has been implicated, it has not been directly assessed *in vivo* following IAF. The antioxidant we have chosen to administer, NAC, operates by freely crossing cellular membranes into the cytosol where it is rapidly deacetylated to form cysteine. This additional cysteine is capable of modest operation as an antioxidant on its own but primarily supplements glutathione (GSH) production by the cell (3). GSH is a tripeptide thiol that acts as the primary redox buffer of the cell, contributing to maintenance of the overall reduced environment of the cell with a concentration in the low millimolar range in most mammalian cells. Oxidation of GSH to glutathione disulfide (GSSG) is rapidly reversible under normal conditions, but requires the consumption of NADPH. Therefore, in cases where a cell is truly under oxidative stress, as opposed to simply oxidatively damaged, GSSG will slowly begin to accumulate and the GSH-GSSG couple with appear more oxidized, i.e. %GSSG or GSSG/total GSH will increase. This is viewed as a standard measure of oxidative stress as distinct from oxidative damage.

In order to test for the presence of oxidative stress following IAF, anesthetized pigs were subjected to a 40 J impact to the distal tibia, producing IAFs which were then anatomically reduced and surgically plated. All surgeries were conducted under IACUC approved protocols. Either 0.5 mL hydrogel vehicle or 0.5 mL hydrogel containing 10 mM NAC and 100 μM GLZ was injected directly into the joint immediately post operatively and again 24 hours later. All operated pigs (n = 12) were casted for one week, at the end of which the animal was sacrificed and cartilage was fresh harvested from the articular surface, homogenized in 5% sulfosalicylic acid to protect against GSH autoxidation, and analyzed for GSH/GSSG content according to the Griffith GSH reductase-recycling method (4). Data were determined as %GSSG (of total GSH) in hocks enduring fractures (left) and the corresponding contralateral, healthy hocks (right). A small piece of articular cartilage from each hock was also digested in 0.25 mg/ml collagenase/pronase and harvested chondrocytes were plated for analysis on the Seahorse XF-96 Extracellular Flux Analyzer. This sophisticated instrument is capable of querying the mitochondrial health of living cells on a per cell basis. By measuring oxygen consumption in the presence of a partial (2 μM oligomycin) and total respiratory blockade (oligomycin, 2 μM rotenone, 5 μM antimycin A), the number of protons displaced and subsequently relaxing back across the mitochondrial membrane without generating ATP, so-called proton leakage, can be determined. This quantity is indicative of the health of the mitochondrial membrane, often an early casualty of oxidative stress. Interestingly, proton leakage has also been demonstrated to be increased in chondrocytes from arthritic knees (5).

Data from vehicle control (ie. hydrogel-injected) IAF hocks demonstrated increases in total GSH in response to injury relative to contralateral hocks from the same animal (Figure 1). This increase was exaggerated with addition of 10 mM NAC and 100 μM GLZ immediately post-fracture, as expected given the intracellular conversion of NAC to GSH. This demonstrates that intraarticular administration of NAC resulted in chondrocyte uptake of NAC which successfully increased cellular GSH pools. Hydrogel IAF hocks also demonstrated a statistically significant increase in GSH oxidation relative to contralateral controls that was prevented with administration of NAC/GLZ (Figure 2). Hydrogel IAF hocks showed an increased amount of proton leakage relative to contralateral hocks which is not present in those hocks receiving NAC/GLZ, further supporting the hypothesis that NAC/GLZ is capable of preventing cellular oxidative stress (Figure 3). In addition to demonstrating the presence of oxidative stress in a large animal model of IAF, these data suggest that NAC/GLZ injections are interrupting joint pathology and the commencement of oxidative stress following IAF. Given recent findings concerning the mitochondrial and redox disruptions present in osteoarthritic chondrocytes, data presented here represent a promising step towards potential cooperative antioxidant/anti-inflammatory interventions targeted at preventing oxidative stress with the intention of slowing PTOA progression. We have not yet determined the specific roles of the antioxidant NAC and the anti-inflammatory GLZ. Further, the impact of these findings upon joint health and early indications of PTOA has not yet been evaluated; however, these data demonstrate that the porcine hock IAF model is capable of distinguishing physiological, biochemical differences among treatment groups following IAF. We believe our data indicate that the Yucatan mini-pig model of IAF can be applied as a powerful tool for advanced testing of pharmaceutical approaches to preventing PTOA after IAF. Funding for this work was provided by the Department of Defense grant #W81XWH-10-1-0864.

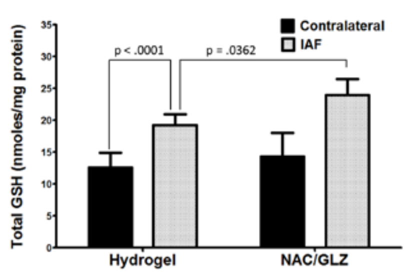

Figure 1. Injection of N-Acetylcysteine/Glycyrrhizin Augments Increases in Cartilage Total Glutathione Content Following Intraarticular Fracture

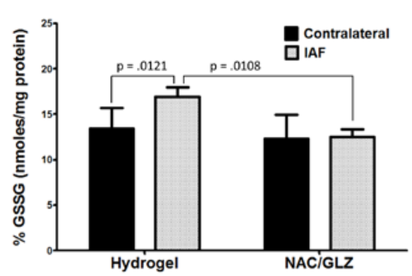

Figure 2. Intraarticular Fracture Induces Increased Oxidation of Glutathione which is Reversed by N-Acetylcysteine/Glycyrrhizin

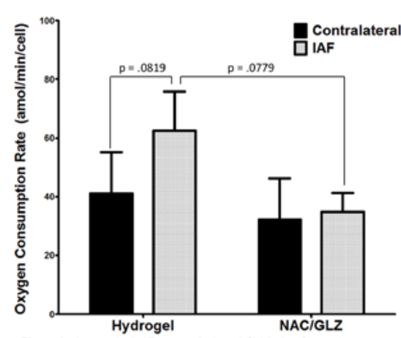

Figure 3. Intraarticular Fracture-Induced Oxidative Stress is Associated with Increases in Mitochondrial Membrane Damage which are Alleviated with addition of N-Acetylcysteine/Glycyrrhizin